CENTRIFUGE STUDIES OF CYCLIC LATERAL LOAD-DISPLACEMENT BEHAVIOR OF SINGLE PILES

Ronald F. Scott

Final Report 1976-1977
Research Program

for

American Petroleum Institute
OSAPR Project 8

Soil Mechanics Laboratory
Division of Engineering and Applied Science
California Institute of Technology
Pasadena, California 91125

TABLE OF CONTENTS

FIGURE CAPTIONS

FIGURE CAPTIONS (CONTINUED)

FIGURE CAPTIONS (CONCLUDED)

1. Introduction

A meeting was held at the California Institute of Technology, February 26, 1976, between a group representing the American Petroleum Institute (API), and Professors K. L. Lee of UCLA and R. F. Scott of Caltech. Problems relating to the dynamic performance of offshore structures were discussed, in particular with respect to their interaction with foundation soils, and the hazards related to the sliding of those soils on modest slopes. Attention was given to both wave- and earthquake-generated forces, especially on pile-supported structures, with particular consideration directed towards the latter. Although the behavior of structures at a wide variety of locations is of concern, current interest centers on those in the Arctic.

The particular point of the discussion regarded current field investigations, laboratory test procedures, determination of soil material properties and behavior under cyclic or dynamic loadings, and analysis including soil-structure interactions. It is felt that improvement is needed in all these areas to improve confidence in the ability of analyses to estimate the performance of offshore structures under design loads. Field data on the performance of full-scale structures under severe loading conditions are urgently required, but are unlikely to be obtained because of the scale of the structures involved and the low probability of having a particular instrumented structure subjected to design loads. Consequently some form of model study seems inevitable to enable alternative design or analysis methods to be checked.

A program of implementing this possibility was suggested. It would consist of a program of laboratory tests, and associated analytical efforts, performed at UCLA under the supervision of Professor Lee, to determine the types of test and analysis best suited to the present problem. This program would be addressed by Professor Lee in a complementary proposal.

In order to provide the equivalent of field tests which can be employed to check the results of analysis, it was proposed that centrifugal model tests be performed at Caltech under the supervision of Professor Scott, in close cooperation with Professor Lee. These would consist of cyclic tests of simplified, but realistic model structures consisting of one-pile or multi-pile arrangements imbedded in saturated soil. The soil would be the same as is to be used at UCLA in the parallel investigation.

The proposal to perform tests on model piles in a centrifuge at Caltech was accepted by the American Petroleum Institute, and work was initiated. Static and cyclic lateral loading tests on model piles in dry and saturated sands and a saturated sandy silt have been performed. This report describes the apparatus, tests, results, and analyses involved in the tests.

2. Centrifugal Model Soil Testing

If the scaling relations required to characterize tests of geotechnical models are established, it is found that, because of the general dependence of the mechanical properties of soil on the ambient stress conditions, and the importance of gravity-induced stresses,

scaling can only be satisfied under special conditions. In the special case of soil, it is inconvenient or impossible to construct a model material, and a real soil is usually employed in model tests. In that case, the scaling conditions require that the soil model be subjected to a higher gravitational acceleration than the prototype. The ratio of the accelerations in model and prototype structures is inversely proportional to the ratio of their linear dimensions; that is to say, a one-hundredth scale soil model must be subjected to one hundred times the earth's gravitational acceleration, and so on. To obtain the necessary accelerations, a centrifuge is required. Considering the size and mass of soil in model experiments, even at 1/100 scale, the centrifuge has to be quite large.

If the ratio of linear prototype dimensions to those of the centrifuge model is h, then the ratio of area is h^2 and volumes h^3. The scaling relations indicate that forces in the prototype are h^2 times those in the model, so that stresses (force per unit area) are unchanged. Deformation in the prototype is h times larger than in the model, but strains (deformation per unit length) are the same. Thus, the presence of the same material in both prototype and model results in identical stresses and strains at homologous points. Where dynamic problems are involved, it turns out that time in the prototype is h times the time in the model. In consequence, model frequencies are higher by the factor h, but velocities are unchanged. Energy in the prototype is h^3 times the energy in the model but energy density (energy per unit volume) is the same. Table 2.1 lists the relations between prototype and model (centrifuge) parameters.

Table 2.1

Scaling Relations

Quantity	Full Scale (Prototype)	Centrifugal Model at n g's
Linear Dimension, Displacement	1	$1/n$
Area	1	$1/n^2$
Volume	1	$1/n^3$
Stress	1	1
Strain	1	1
Force	1	$1/n^2$
Mass	1	$1/n^3$
Acceleration	1	n
Energy	1	$1/n^3$
Density	1	1
Energy Density	1	1
Velocity	1	1
Time		
In Dynamic Terms	1	$1/n$
In Diffusion Cases	1	$1/n^2$
In Viscous Flow Cases	1	1
Frequency in Dynamic Problems	1	n

The attractiveness of the centrifugal method is that the stresses in the model are identical to those in the prototype so that it avoids problems associated with testing, at earth gravity, small soil models involving material with strongly nonlinear behavior. The disadvantages are associated with performing the tests on models which are rotating at rates of 100-to-500 rpm in a centrifuge. Power and signals have to be passed in and out through electrical and hydraulic sliprings. To the present, electrical noise has presented a problem in recording the results of a variety of experiments, especially where strain gauges have been employed. The noise comes from ambient sources, the electric motor driving the centrifuge and from motors used to control the tests. The Caltech centrifuge is shown in Figure 2.1; it is described in detail in Section 4.

A number of centrifuges have been built and used for soil testing. There are three in the United Kingdom, two at Cambridge and one at Manchester, with radii up to 5 meters and acceleration capabilities up to 200g. In Russia, a recent paper (6) refers to the employment of "several dozen" centrifuges for soil testing purposes. So far, only one or two small centrifuges have been used for such tests in the United States, although the technique was apparently originated here (1); the reasons for this limited usage have not been determined. Centrifuges are currently used for geotechnical research in Sweden, Denmark, France, and Japan, apart from the Soviet Union and the United Kingdom. A compilation of references on centrifugal testing, worldwide, extends to more than 150 papers and a number of books.

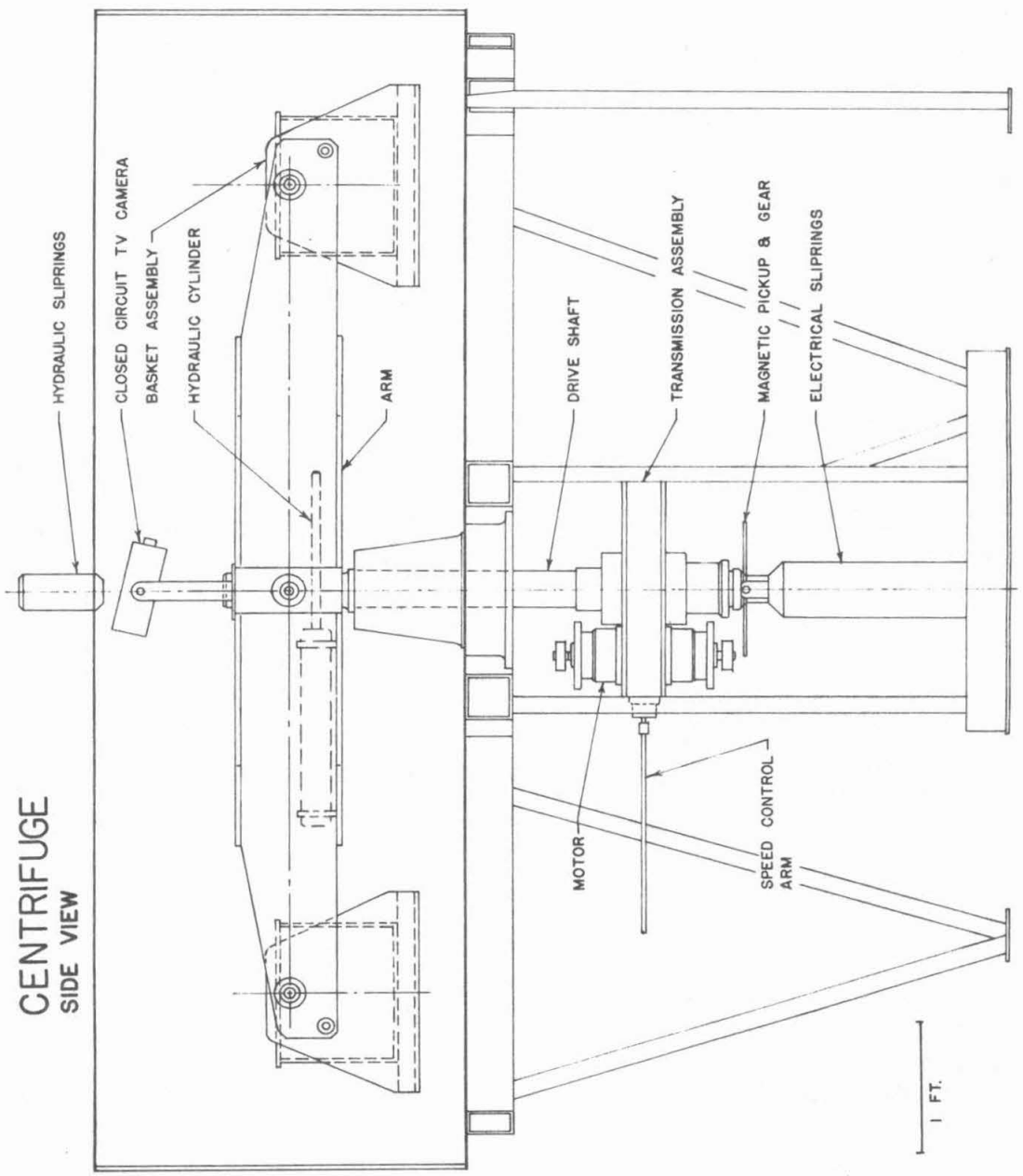

Fig. 2.1. Side View of Centrifuge

In initiating a program of centrifuge testing, the first question to arise concerns the proof or the accuracy of the technique. How well does a model test predict a prototype behavior? Do the scaling relations tell the whole story? In addition, particularly when models of particularly small dimensions such as piles are considered for testing, there is a problem in deciding at what soil grain scale the applicability of continuum and constitutive laws to both model and prototype soils breaks down. For very fine-grained soils, such as clays, many particles span the diameter of both model and prototype pile; on the other hand, in a coarse sand with grains a millimeter or so in diameter, there will be relatively few grains in the model pile diameter. It is likely that gravity scaling will apply to the constitutive laws but not to the grain dimensions in the first example. In the second example, it seems possible that the stress-strain relations of model and prototype may not be the relevant factors, but that the individual grains in the model represent the behavior of boulders in the prototype. Thus, a model pile in coarse sand may not represent the behavior of a prototype pile in the same coarse sand, but that of a pile imbedded in gravel.

Because of the relatively small size of the centrifuge at Caltech, with its limited payload of 100 pounds at 100g, it was necessary to select prototype civil engineering unit systems which would, at approximately 1/100 scale, fit into the machine. The best candidate, for which some prototype quantitative information is also available, is the pile, or small pile group. Various, imperfectly understood aspects of pile behavior can be usefully studied under controlled

conditions in the centrifuge. The pile itself is relatively easy to model and instrument. A number of studies of piles have therefore been initiated.

With so many centrifuges built and operational, and the number of tests performed, it might well be thought that the questions above would have been satisfactorily answered by this time; that many comparisons would have been made between models and prototypes. Study of the accessible literature does not show this to be the case in the quantitative sense, although a fair number of studies show qualitatively similar behavior and mechanisms. Consequently, in the pile tests being performed at Caltech, an effort is being made to duplicate the conditions in actual field tests of piles in order to see how much correspondence exists between predicted and actual performances. However, at the same time, the qualitative behavior of piles subjected to cyclic lateral loading was also the subject of the study. Some pile dynamic vibration studies have already been performed and reported (8).

3. Soils Tested

To date, two different soils have been employed in the centrifuge tests. These were: (1) a relatively uniform fine Ottawa silica sand ("Ottawa sand"); and (2) a sandy clayey silt obtained in soil investigations off the Californian coast in the vicinity of Santa Barbara and supplied by Dames and Moore, San Francisco, through the courtesy of Chevron Oil Research Company, La Habra, California ("Santa Barbara silt"). Grain size distribution curves for these soils are shown in Figure 3.1.

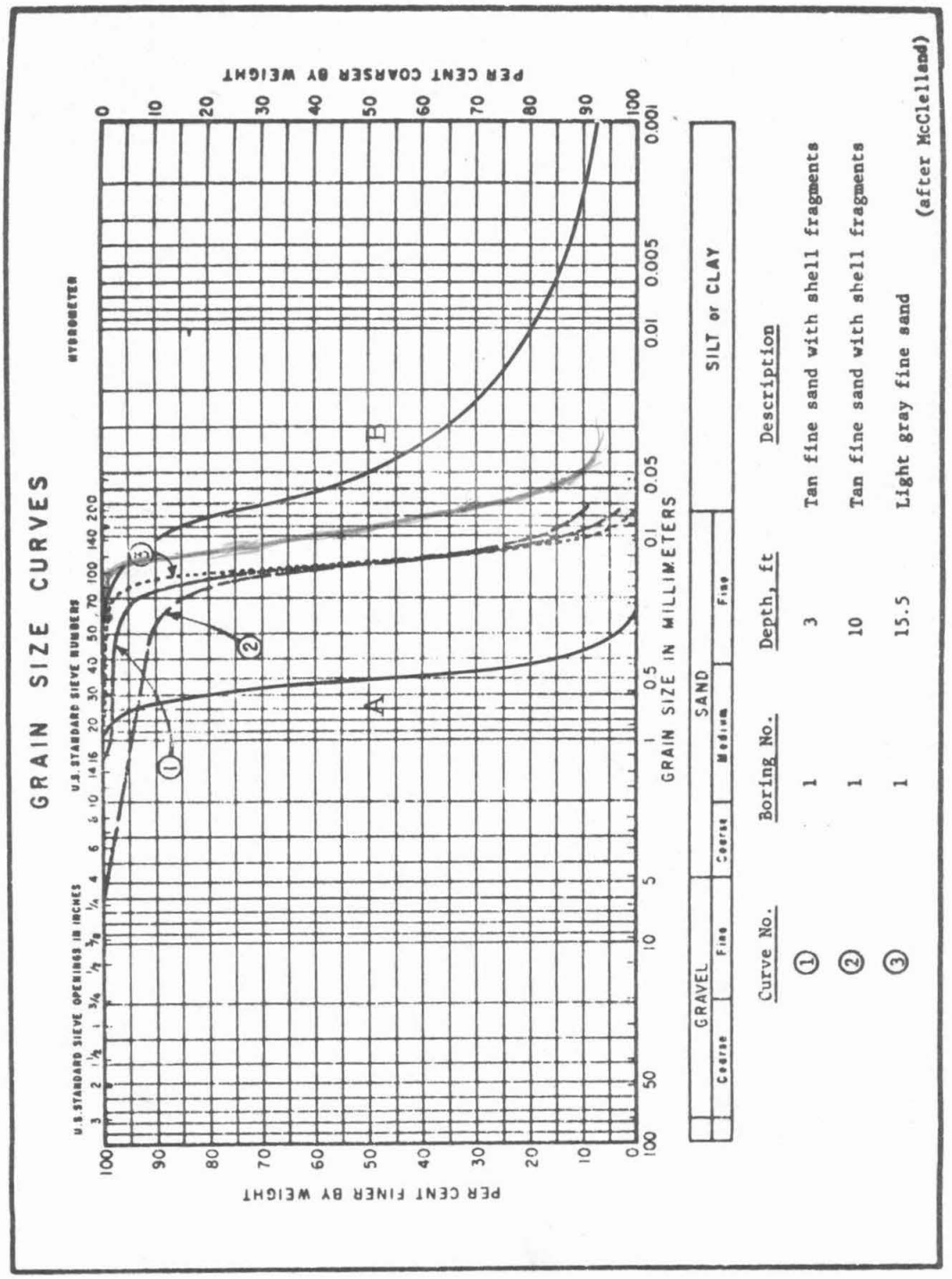

Fig. 3.1. Grain size distribution curves of soils
A. Ottawa sand. B. Santa Barbara silt

The two sands were used in static and cyclic lateral pile tests carried out in both dry and saturated soils for the purpose of comparing the test results both qualitatively and quantitatively with full-scale field pile tests performed in a saturated fine sand at Mustang Island, Texas, as reported by Reese, et al. (7). The grain size distribution of the Mustang Island sand is also shown in Figure 3.1.

Initially, the tests were carried out on the soils in a rectangular container 14.5" by 11.5" by 10" mounted on the centrifuge platform (Figure 3.2); the soil density was measured from the known volume of test sand and the weight required. On the Santa Barbara silt, however, difficulty was encountered in fully consolidating it in a reasonable duration of time in this rectangular container, and some subsequent tests employed a cylindrical vessel 8.5" high by 8.10" in diameter.

The sand specimens were prepared either by pouring the sand loosely into the container, or by placing it in layers with varying degrees of compaction. The saturated sand beds were formed by pouring the sand into water. The unit weight of soil in each test was measured and is reported with the test. The Santa Barbara silt, on the other hand, as initially obtained, was supplied in the form of dried-out chunks of soil, left over from laboratory tests performed by Dames and Moore. Later, extra quantities of this material were received in moist condition in plastic sample tubes, from which the soil was removed by jacking with a piston extractor. It was not convenient or correct in either case, to place the soil in the test containers

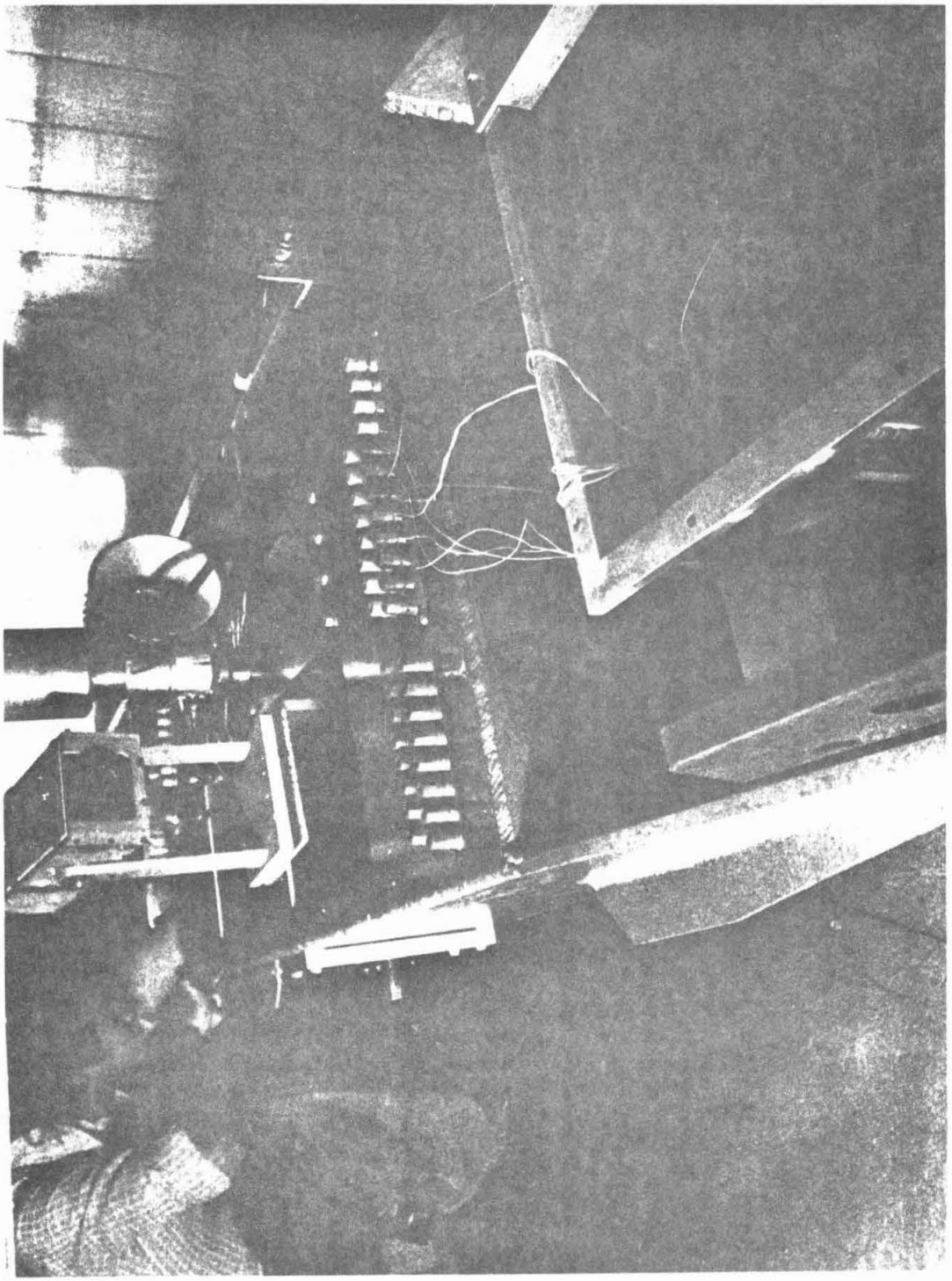

Fig. 3.2. Centrifuge; view of test container with model pile in place in Ottawa sand

in the form in which it was received, since it was desirable to install the pile in normally-consolidated soil to simulate an ocean floor test site. Consequently, both dry and wet as-received samples of Santa Barbara silt were mixed with tap water in a mixing machine until the resulting material was smooth and lump-free at a water content slightly higher than the liquid limit of the soil ($w_L \sim 30\%$).

The soil slurry was then poured into the test container, taking care to avoid the inclusion of air bubbles. To prepare the test specimen the container was centrifuged at 100g, the test acceleration, until it had consolidated. Drainage was facilitated by the presence of a sand layer at the bottom of the container, overlaid by blotting paper to prevent mixing of the silt and sand, and by a layer of blotting paper placed inside the wall of the test container. This procedure was followed for the pile tests reported here, but was modified for the purpose of preparing a consolidated Santa Barbara silt specimen for delivery to Dr. K. L. Lee of UCLA for use in his complementary studies of the soil behavior. In the modified test, the soil slurry specimen was made somewhat thinner, and covered with a layer of blotting paper, on which was placed a sand layer 3.1 inches thick. Then the upper surface of the silt soil was also consolidated by the sand to a firmer consistency than the normally-consolidated samples; this made manipulation and transport of the silt slab easier.

The question of the similarity of the centrifuge test specimen of soil to that of the larger prototype section, and in particular, the identification of the stress paths in model and prototype is complicated. Appendix A has been added giving a comprehensive review of this

problem, together with some illustrative examples. It will be seen there that absolutely similar stress histories and stress paths cannot be obtained during testing, but that a reasonable facsimile can be developed on the centrifuge.

The duration of centrifuging was arrived at by (1) consideration of the consolidation properties of the soil obtained from consolidation tests and (2) by performing miniature vane shear and water content tests on samples from varying depths in the test container. When the soil is fully consolidated, the shear strength profile should increase essentially linearly with depth from almost zero values at the upper surface, and the water content should decrease with depth. Both dry and total unit weight should increase with depth.

Two sets of soil test results from the container in which model piles were loaded are shown in Figures 3.3 and 3.4. The silt occupied the container to a depth of 5 inches, representing a depth of 500 inches or about 42 feet in the prototype. For Figure 3.3, the soil was probed in the center of the container and for Figure 3.4, in one corner. Superimposed on these drawings are soil property results obtained from offshore borings in the material. It is apparent that, although the water content profiles in the centrifuged material diminish steadily from the surface down, the strength does not increase with depth as it should, in the top two inches. Instead, it remains almost uniform with depth to that level, at about 200-300 psf, and then increases markedly at the four inch depth to values of about 1500 psf. It would be expected that the soil in the corner would be better drained than at the center, and this is apparently true in the

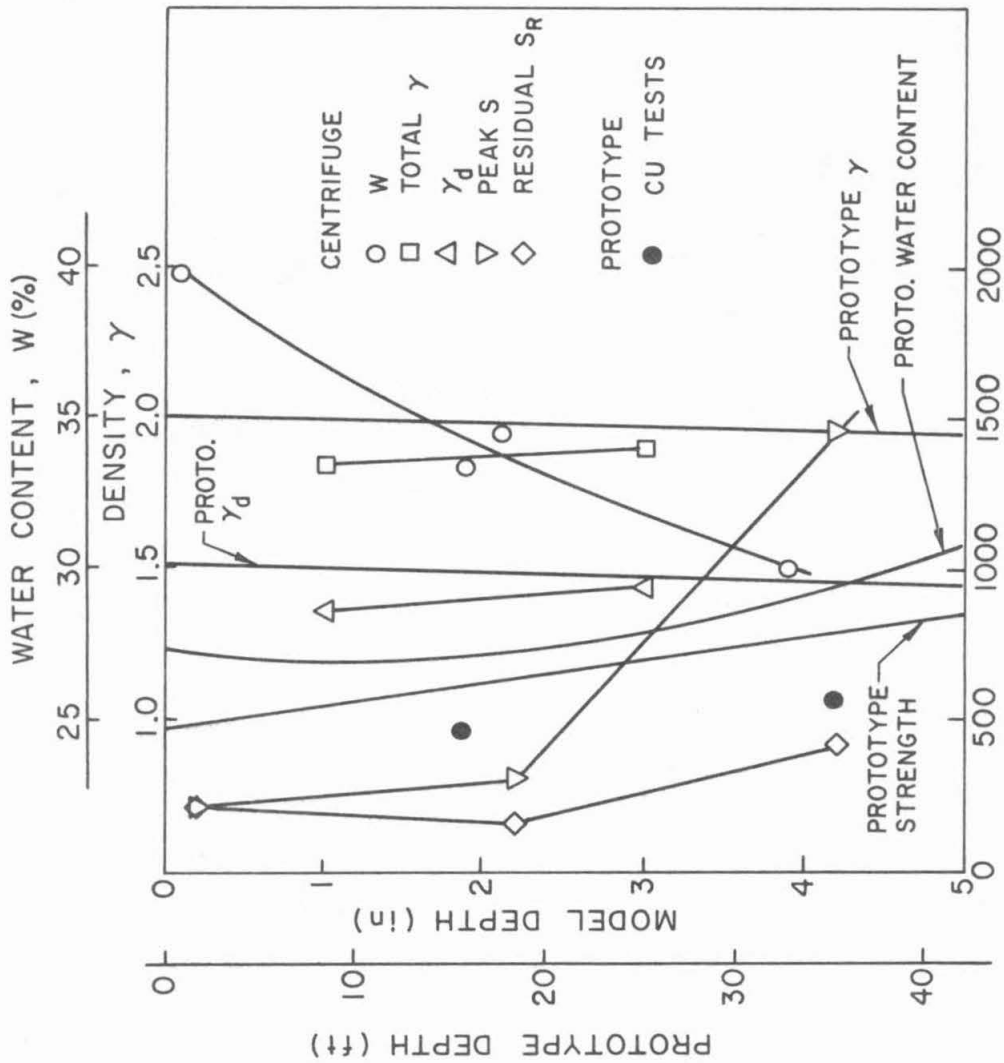

Fig. 3.3. Santa Barbara soil properties near center of test container

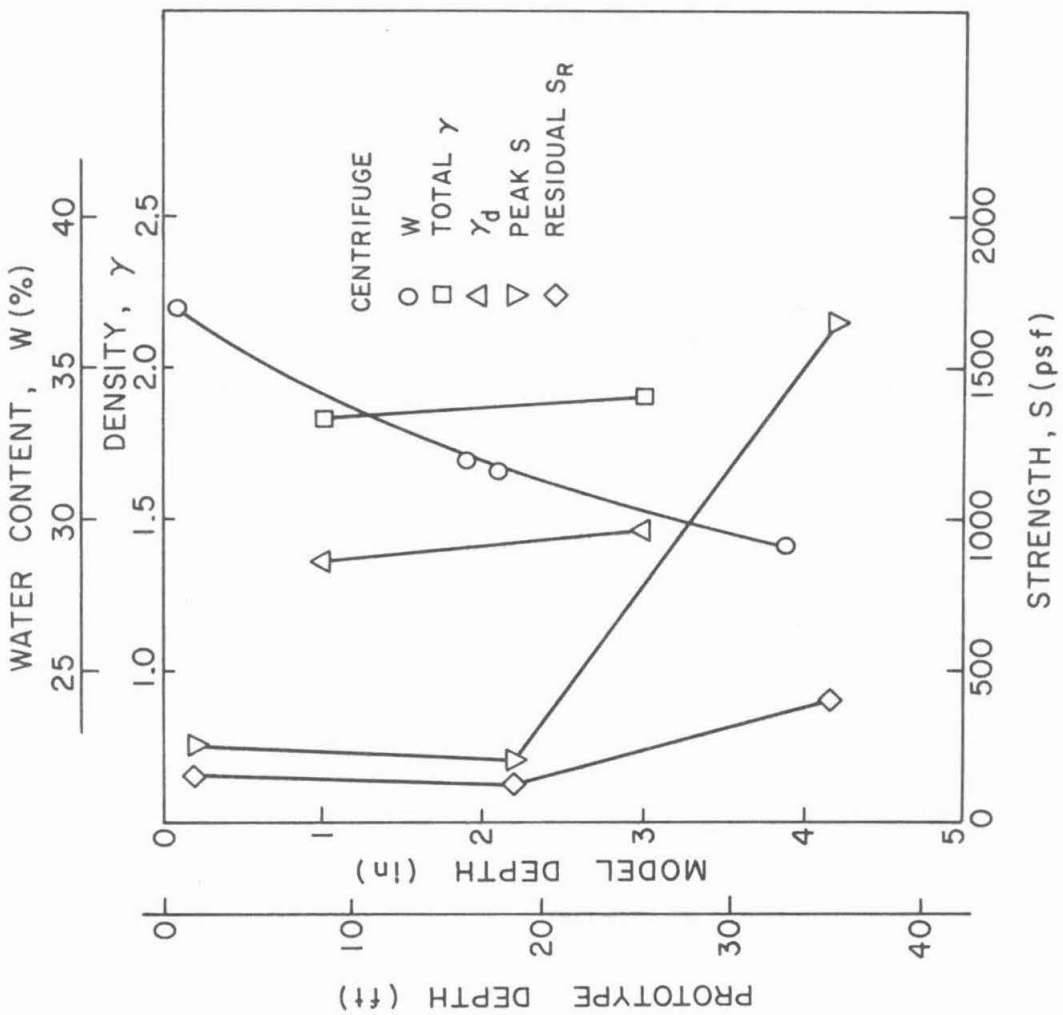

Fig. 3.4. Santa Barbara soil properties in corner of test container

case of the water content in Figure 3.4, but the shearing strengths in Figures 3.3 and 3.4 are similar, and do not, in particular in Figure 3.4 by comparison with Figure 3.3, reflect the usual sensitivity to water content.

The Santa Barbara silt pile tests were performed with the soil in this state, but in future tests, an attempt will be made to achieve better drainage in the test container; it may also be desirable to overconsolidate the soil slightly by covering it with a one inch thick layer of sand during the consolidation phase. The sand would be removed before inserting the pile. This would effect a closer simulation of the real material properties in the field, as is seen from the field profiles from Boreholes 1 and 1A* indicated in Figure 3.3. The soil at the site is slightly overconsolidated, with a field shear strength at the mud line of about 500 psf. The strength increases with depth to a value of close to 1000 psf at a depth of about 40 ft in the prototype, equivalent to 5 inches in the model. The field strength was obtained by performing "Tor-vane" tests on the samples as they were obtained on the deck of the drilling vessel. As such, they are not very precise and depend largely on the local nature of the soil exposed at the end of each sample tube for testing. These shear strength values are similar in magnitude to those of laboratory consolidated-undrained tests.

In the top 35 ft of the real profile, the water content is relatively constant at about 27 to 28%. Below this depth, the water content is

---

*Field investigation performed by Dames & Moore.

higher, around 35% to 40%, reflecting, presumably, an increase in the clay content of the soil. With a few thin layer variations, this latter water content is characteristic of the soil to a depth of 450 ft. Consolidated-undrained laboratory triaxial tests were also performed on the returned soil samples; the results from two of these tests fall within the depth range of interest for the pile tests and are shown in Figure 3.3. The water contents of the two test specimens were about 24%. They generally fall in the range of properties described previously, but the relations between triaxial and vane shear tests have been the subject of a considerable amount of discussion in the geotechnical literature.

4. Equipment and Instrumentation

(a) Centrifuge

The centrifuge used is a Model A1030 Genisco "G-accelerator," which consists of an 80 inch diameter aluminum-alloy arm which rotates in the horizontal plane and is rated at 10,000g-pounds payload capacity. At each end of the arm is located an 18 × 22 inch magnesium mounting basket capable of carrying a 100 pound payload to 100g or 60 pounds to 175g. The acceleration range at the approximately 40 inch radius of the baskets is from 1 to 175g. A variable speed transmission based on the Rouverol ball-galaxy principle allows continuous variation of the acceleration throughout the range. The transmission is driven by a 3 hp 1800 rpm 220V 3-phase double-ended electric drive motor. For accurate determination of the rotational speed, there is located on the main drive shaft a 600 tooth gear wheel,

which via a magnetic pickoff produces 600 pulses per revolution. These pulses are read by an electronic counter which converts them to an LED display of RPM accurate to 0.1 rpm. The drift and wow of the system at any given setting is 0.05%. The acceleration arm is housed in an extruded aluminum enclosure, with all controls and instrumentation, in the interests of safety, located remotely.

Electrical power and signals to and from the rotating arm or basket are conducted through 44 sliprings, of various capacities in the 10 to 30 amp range. Externally generated hydraulic or air pressure is transmitted through either two or four lines by means of rotary unions (hydraulic sliprings). Operations on the centrifuge can be observed by means of a television camera mounted on the rotating arm close to the axis; its signal is conveyed either through the slip-rings mentioned above or through coaxial cable and related, separate sliprings, to a monitor TV in the instrumentation house.

The centrifuge layout is shown in Figure 4.1, with a more detailed view of the arm in the test configuration of this report in Figure 4.2, which will be described below.

(b) Specialized Test Apparatus

In order to apply a constant, controllable peak load to the pile, yet one which could be changed from test to test, an apparatus was constructed which consists of: (1) two bellows (2.1" O.D. × 3.0" obtained from Gardner Bellows Corp.), (2) a carriage assembly suspended and located by 14 0.5" diameter grade 10 steel balls, (3) an aluminum framework locating the preceding parts. This framework

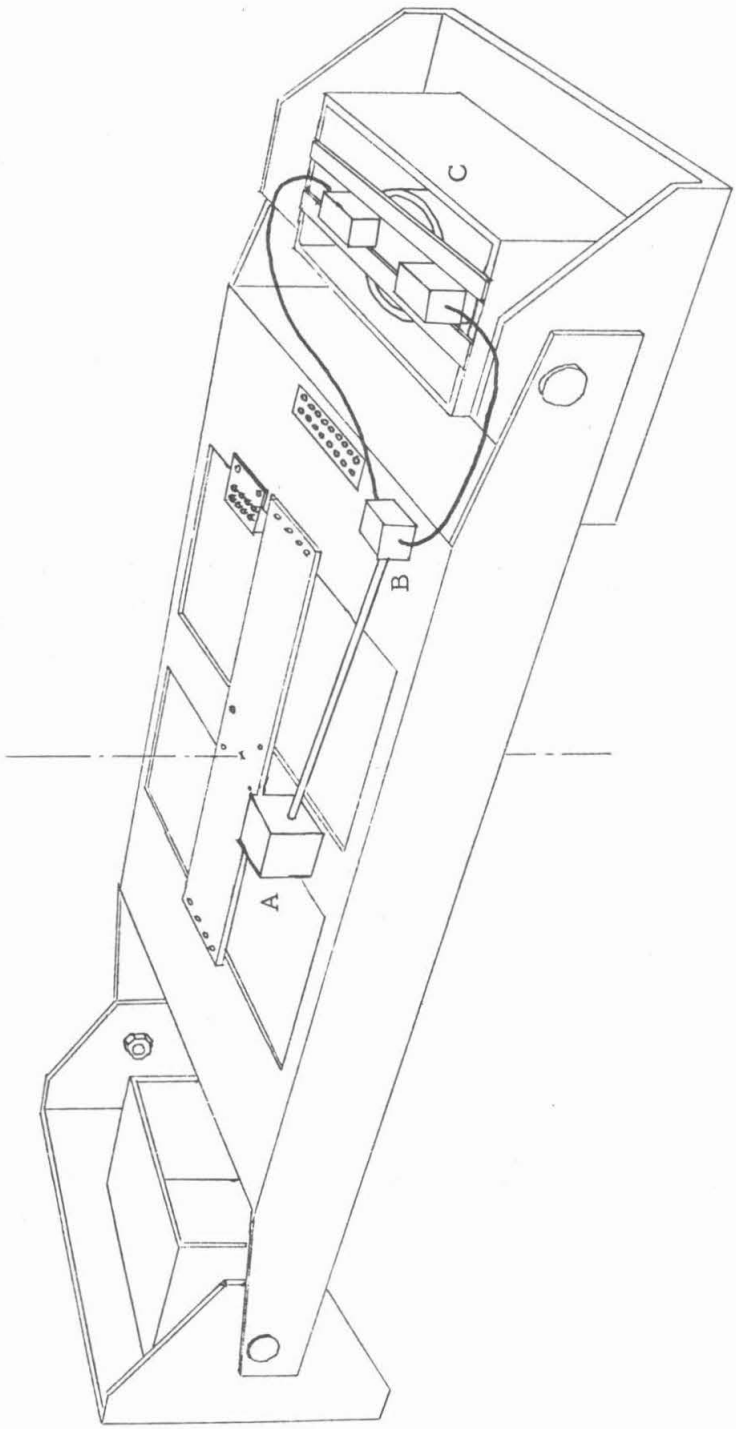

Fig. 4.1. Perspective of centrifuge arm showing schematic of pneumatic cyclic loading device (near end) and test container in flying position (far end)

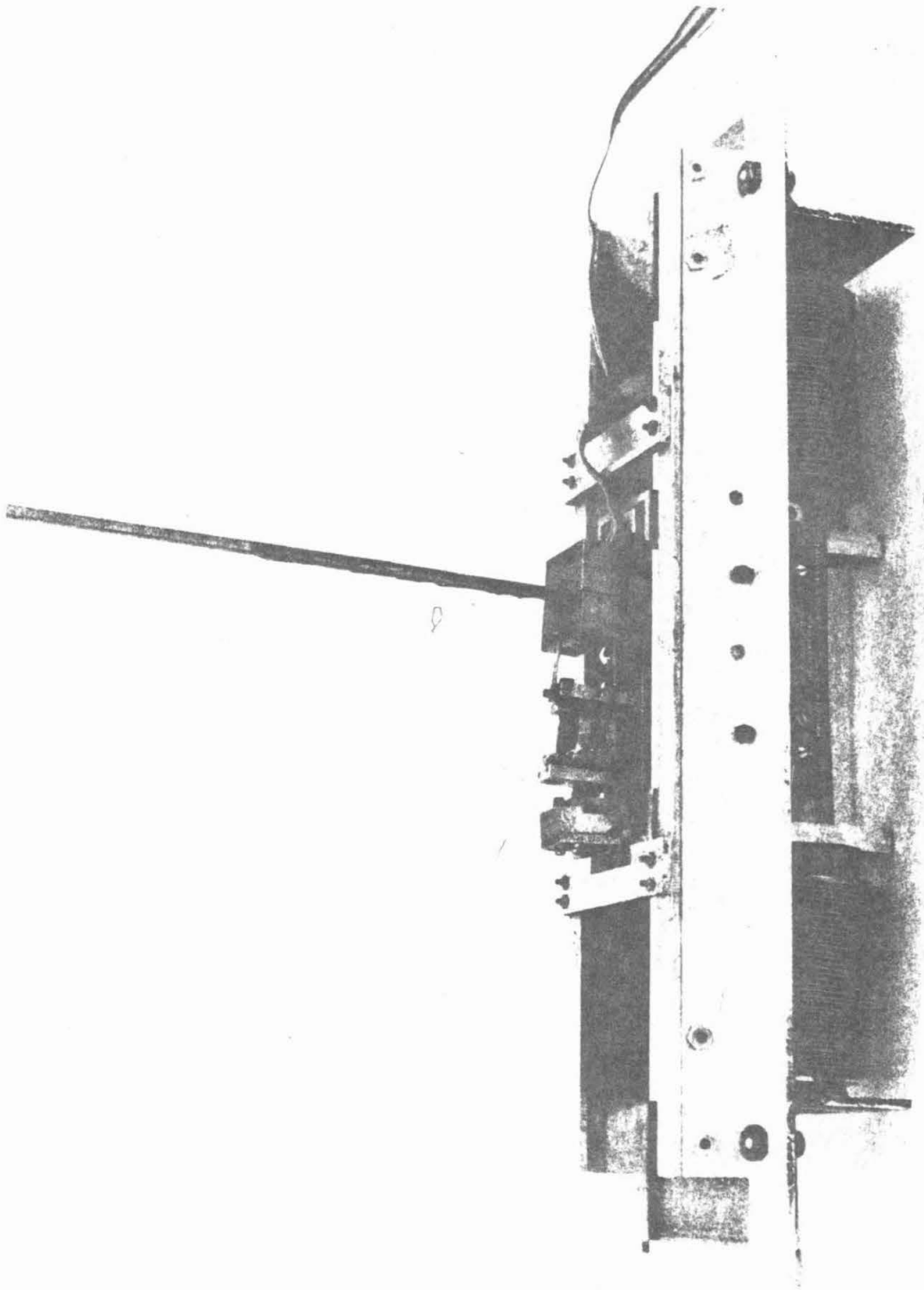

Fig. 4.2. Model pile cyclic loading bellows and load cell

is bolted atop an aluminum box (14.5" × 11.5" × 10" deep) which in turn is bolted to one of the acceleration arm mounting baskets. Within the aluminum box is contained a steel cylinder (8.0" I.D. × 8.5" depth) to hold the soil and pile. At the extreme ends of the framework the two bellows are positioned; interposed between them is the carriage assembly. The bellows are connected via 0.25" flexible tubing to a four-port valve mounted on the centrifuge cover. The valve allows air pressure to be applied to one bellows while the other is vented to the atmosphere. A 90-degree rotation of the valve applies the air pressure to the previously vented bellows while venting the opposing bellows. The valve is rotated through two universal joints and a shaft by a variable speed 1/50 hp Bodine motor (Model No. NSH-12R) which is remotely controlled by a Minarik motor control (Model SL-14). A rotating union (Deublin No. 1595-40) was mounted on top of the centrifuge housing to facilitate the application of air pressure to the control valve. The air pressure was remotely regulated in the control room by a Norgren (No. 11008118) pressure regulator and monitored with an Ashcroft (Amp 8317) pressure gauge with 0.25lb subdivisions.

The model pile was machined out of aluminum to the dimensions, 0.162" × 0.162" × 8.0" long. Five strain gauges (BLH FAE-12-35S6ET, G.F. = 2.01 ± 1%, Resistance = 350.0 ± .5, Ser. No. 7-DE-0A, Lot No. A 304) were bonded to one surface of the pile using an epoxy adhesive (BLH EPY-150). Measured from the top of the pile the strain gauges were located at: 1.25", 1.75", 2.25", 3.00", 4.00". Soldered to each gauge were two lengths of AWG 32 magnet

wire. These leads were then laid along the side of the pile and coated with a flexible protective coating (BLH Barrier J). To the top of the pile was clamped a pile cap of dimensions, 1.36" × 1.36" × 0.5" height, which weighed 105.1 gms and which could be moved up and down the pile. Atop the pile cap was bonded a terminal strip, which allowed the lead wires from the gauges to be soldered to a ten conductor AWG 26 ribbon cable.

The location of the centrifuge on the roof of Thomas Laboratory at CIT in close proximity to air conditioning units and elevator drive motors makes for a very noisy electrical environment. Efforts to minimize noise have included the installation of an amplifier (to be described later) mounted on the acceleration arm in order to increase the signal to noise ratio as close to the signal source as possible. The electrical configuration of this amplifier is such that one of the output leads from each signal source is common to ground. If a complete Wheatstone bridge circuit were to be constructed for each of the gauges on the pile, a total of five separate power supplies and ten sliprings would be needed. In order to circumvent this necessity a different circuit was used, namely the potentiometric circuit. This circuit is well-suited to dynamic strain studies, provided that ambient temperature fluctuations do not cause signals comparable in frequency to those from mechanical strain. This requirement is easily satisfied by the model pile, since it is well-insulated, by its imbedment in soil, from rapid changes in temperature.

The potentiometric circuit was designed as follows; two regulated DC power supplies were connected in series, with the connection between the two also serving as the signal input ground. The remaining two outputs of the power supplies were made available at the acceleration arm via two sliprings. The sliprings are constructed of coin silver and are imbedded in diallylphthalate plastic. The brushes (two per ring) are made of silver graphite. The current-handling ability of the rings varies, and the individual rings are selected according to function; i.e. signal out = 5A, DC power input = 10A, ground = 30A. A diagrammatic representation of the potentiometric circuit is shown in Figure 4.3.

The 500 ohm potentiometers shown in Figure 4.3 are used to null the input signal under zero strain conditions. The schematic amplifier in the same drawing was constructed by Electrical Engineering Services at CIT. It provides eight inputs and outputs which are switchable between 1x and 10x amplification and is located on the acceleration arm (see Figure 4.2). The circuitry of each of the eight channels is illustrated in Figure 4.4.

In addition to the measurement of strains in the model pile, load and deflection are recorded at the pile cap by a load cell and displacement transducer. So as to allow freedom of movement of the pile and to minimize off-axis load readings, the load cell was attached to the pile cap with a thin piece of metal which was essentially rigid in tension and compression, but was flexible in the direction perpendicular to the plane of the load. The load cell consists of a ring of stainless steel (1.0" O.D. × 0.5" height × 0.025"

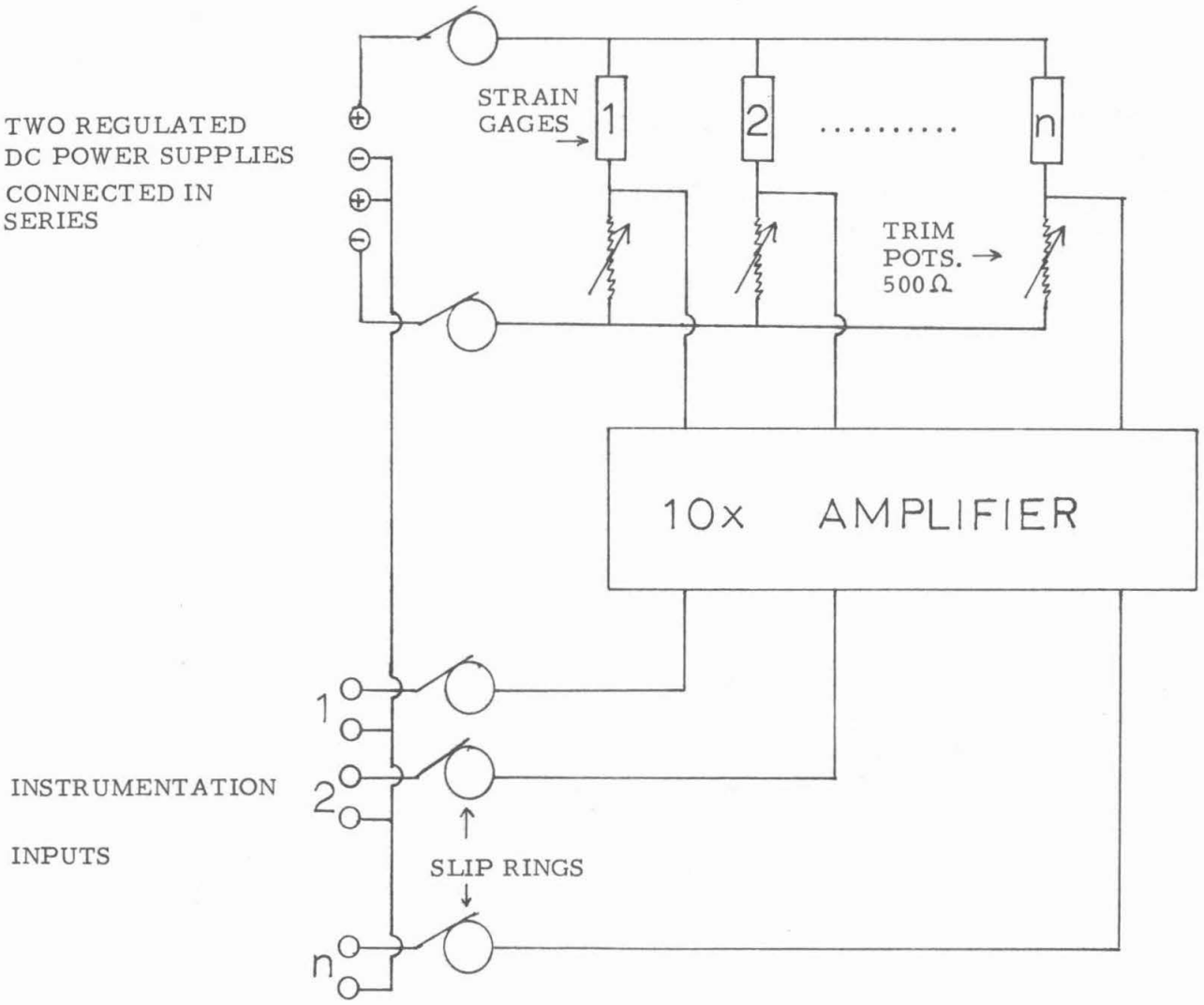

Fig. 4.3. Strain gauge circuitry

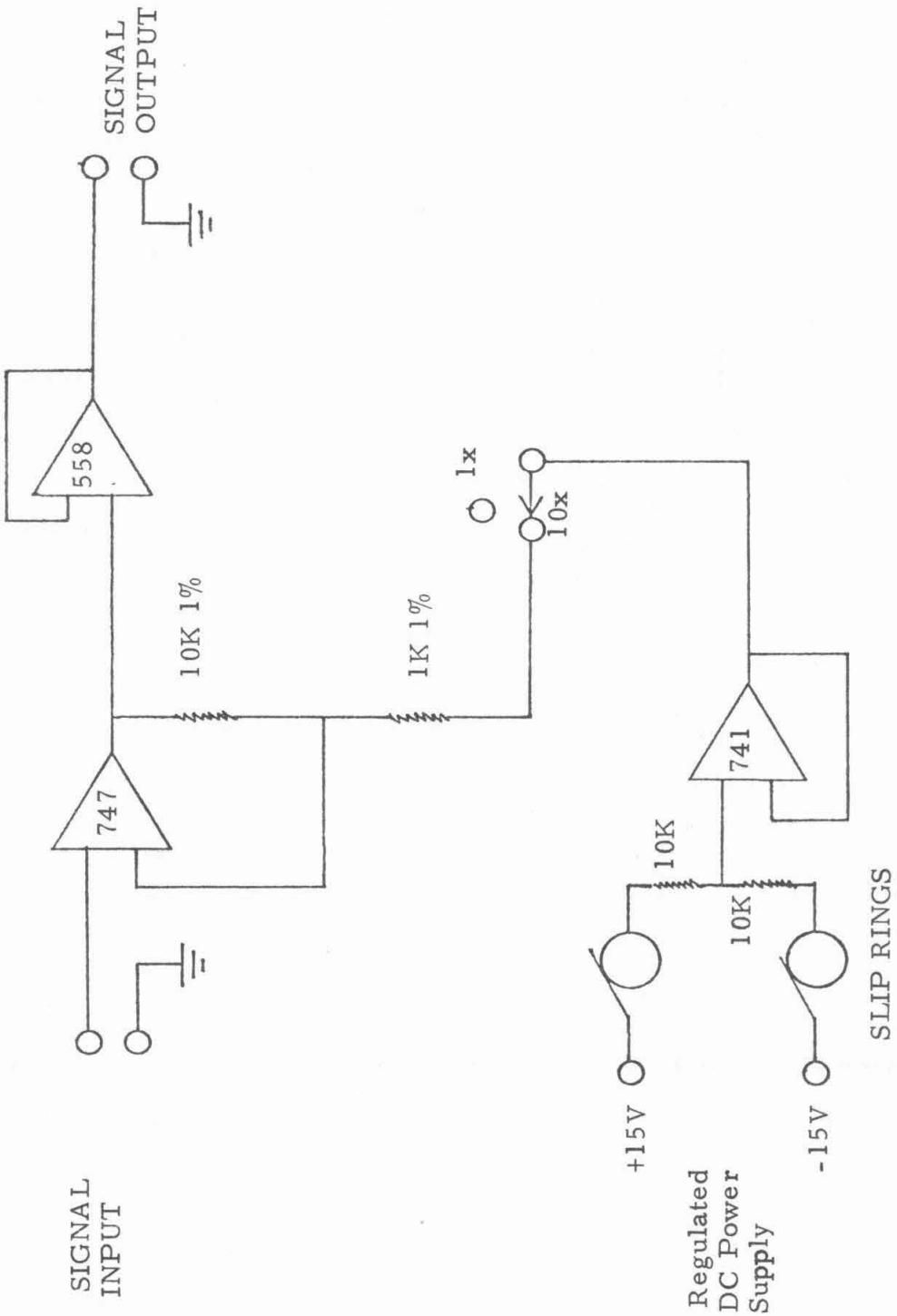

Fig. 4.4. Arrangement for amplification

wall thickness), to which were bonded four strain gauges (BLH FDE-06S-35ET, G.F. = 3.10 ± 1%, Resistance = 350.0 ± .5 ohms, Ser. No. 1-A-KH, Lot No. A-D-135) using an epoxy adhesive (BLH EPY-150). Two of the gauges were located on the outside of the ring diametrically opposite one another, while the other two gauges were placed in the same location, but on the inside. This arrangement provided reasonable output and good temperature compensation when wired into a complete bridge. A wiring diagram of the load cell is shown in Figure 4.5.

In order to minimize spurious lateral load readings generated by vertical movements of the pile, a ball joint system was used to attach the load cell to the carriage assembly. A 0.5" bronze ball was drilled and tapped, after which it was ~ 70% encapsulated in an epoxy resin in which it was free to rotate. This arrangement allowed the load cell to move several degrees in all directions with respect to the actuating carriage, without sacrificing rigidity in tension and compression. The layout of pile, pile cap, load cell and strain gauges is shown in Figure 4.6.

Also attached to the pile cap was a small strip of aluminum which made contact with the slider of a linear potentiometer (Bourns No. 8529139). The potentiometer was slightly spring-loaded to ensure intimate contact with the strip. This eliminated the need for a rigid attachment of the slider with the aluminum strip which would have compromised the pile's range of free movement. A wiring diagram of the potentiometer is shown in Figure 4.7.

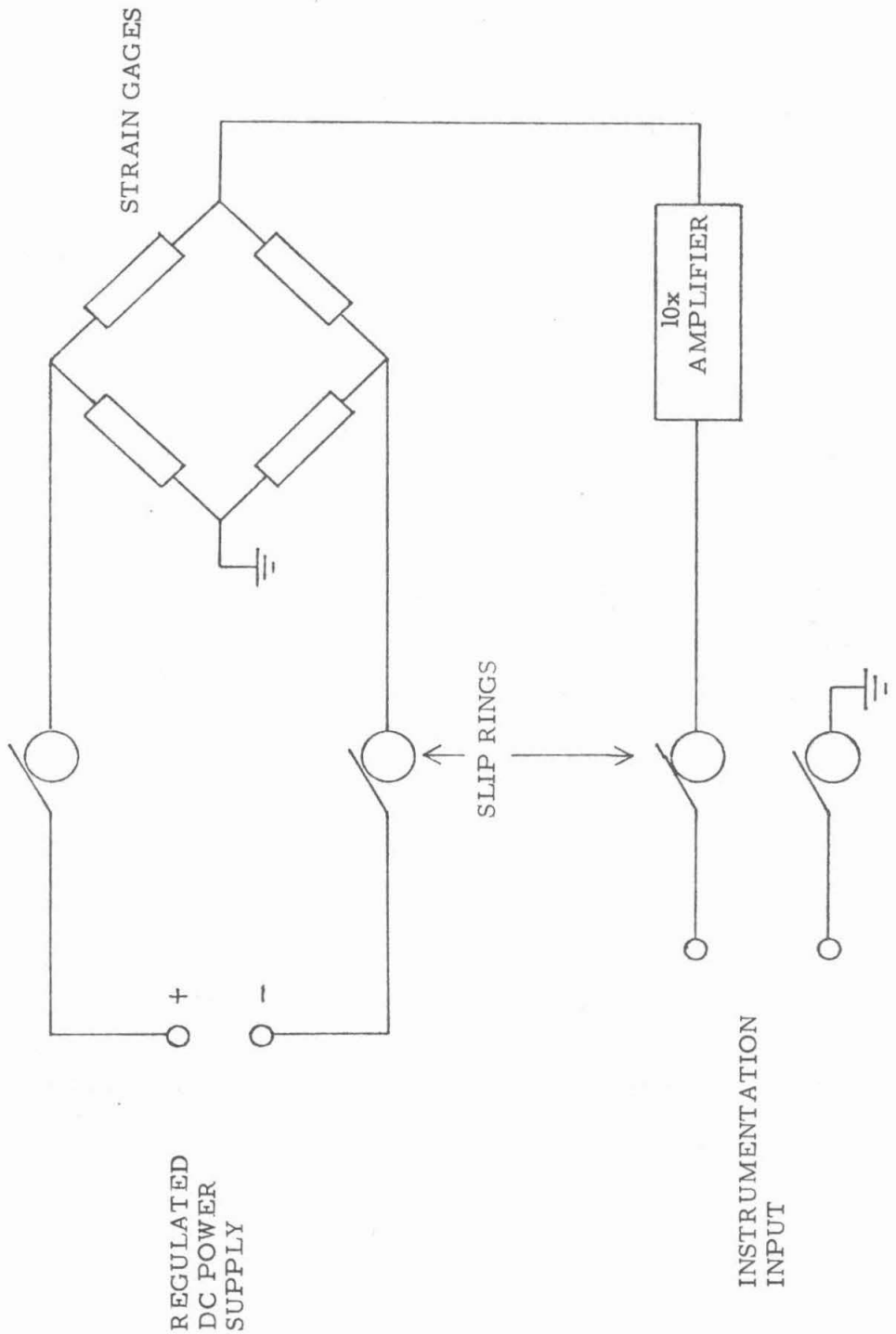

Fig. 4.5. Strain gauge bridge

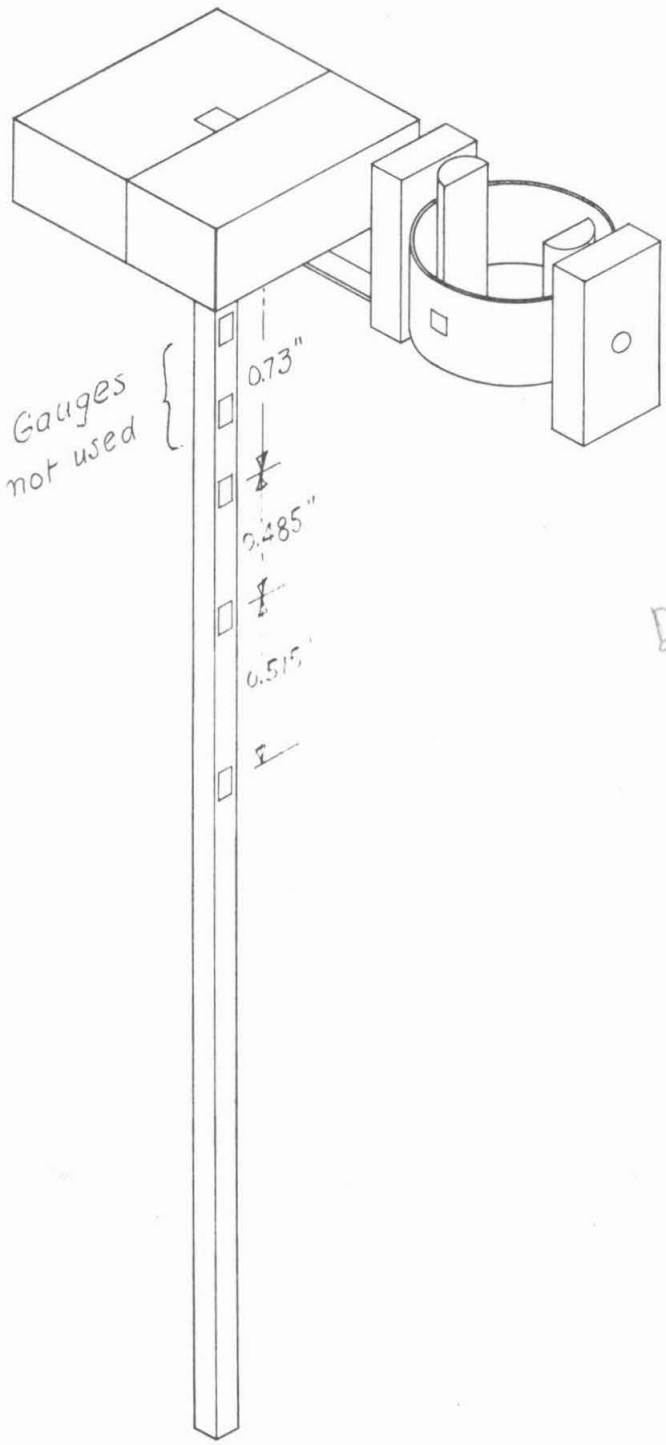

Dimensions?

measured EI? with gauges + protect. coating

Fig. 4.6. Model pile, pile cap and attached strain gauges

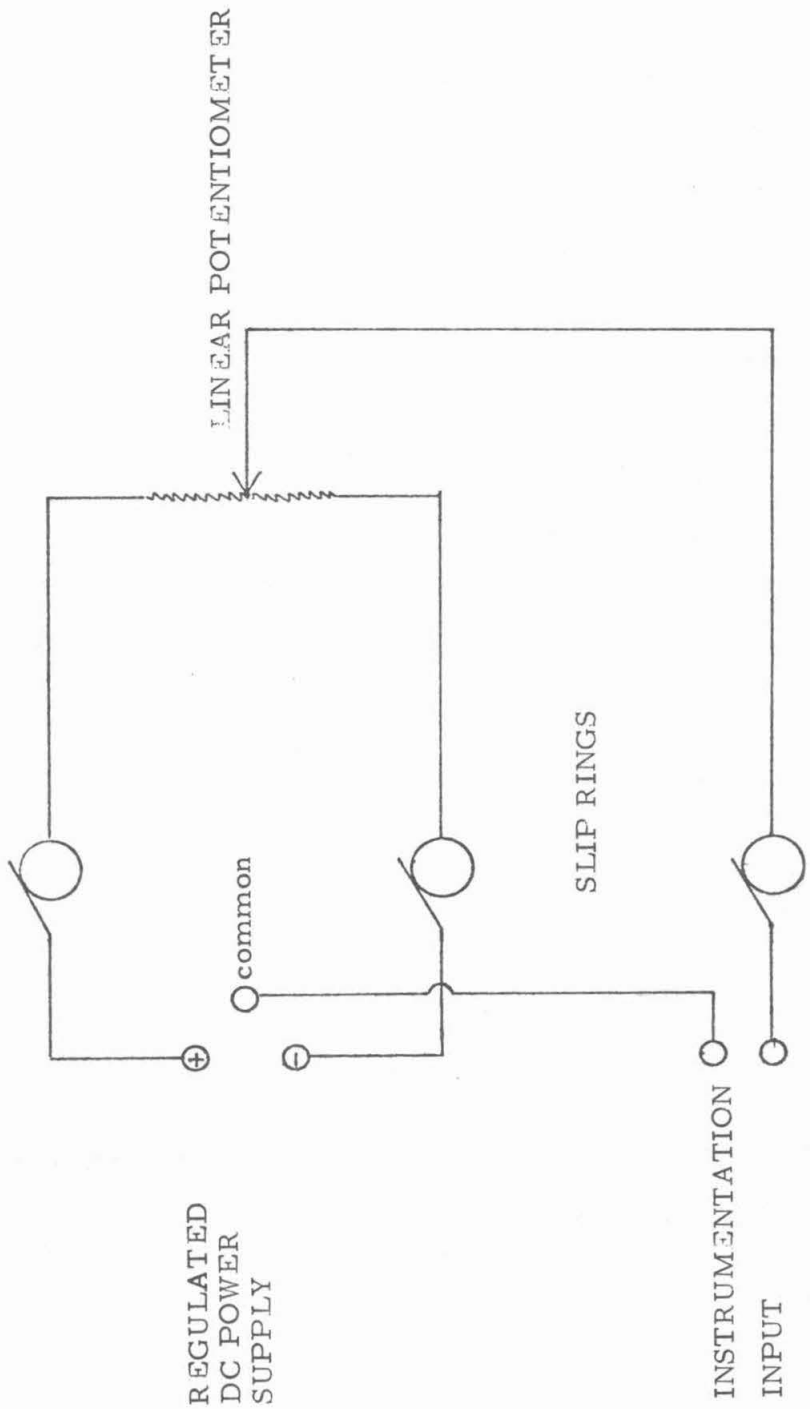

Fig. 4.7. Displacement measuring circuit

(c) Data Acquisition Systems

The recording instruments used were: (1) a Honeywell Model 1858 CRT Visicorder, which allows inertialess recording from DC to 5,000 Hz, (2) a Hewlett-Packard Model 7045A X-Y recorder. The X-Y recorder was used primarily to check that the tests were proceeding as expected; accordingly only the load and displacement at the pile cap were recorded on it. Via two T-connectors, the load and displacement were also recorded, along with the strain gauge signals, on the Visicorder.

All pre-test calibrations were carried out using the entire electronic circuitry, i.e. the calibration signals were routed through those terminals, amplifier channels, and sliprings which they would use during the actual testing. To calibrate the load cell, brass tester weights were suspended from the cell and the output recorded on both the X-Y recorder and the Visicorder. The calibration of the displacement transducer was accomplished with the aid of a Federal dial gauge accurate to 0.001 in. The output was again recorded on both the X-Y recorder and the Visicorder. In order to convert the voltage output of the strain gauges on the pile to a measurement of strain, it was necessary to suspend the pile in a horizontal position (by clamping the pile cap to a vertical surface) and to hang one, two and three pound weights on the end of the pile. The outputs recorded on the Visicorder were then converted directly to strain or moment measurements without use of gauge factors, since the exact locations of the gauges and load were known.

(d) Test Procedures

The Santa Barbara soil was thoroughly mixed with water, as described in Section 3, and placed in the prepared soil cylinder. The preparation consisted of placing 0.5" of saturated sand in the bottom of the container and covering both the sand and the vertical walls of the cylinder with blotting paper. This facilitates the drainage of water at 100g to maximize consolidation. Once the soil was introduced the centrifuge was brought to 100g acceleration and allowed to operate at this setting for several hours to consolidate the soil. After consolidation the centrifuge was stopped and the aluminum framework, which now included the load cell, the displacement transducer and the model pile, bolted to the top of the aluminum box which placed it directly over the soil. The depth of imbedment of the pile in the silt was 6.75". The electrical connections were reestablished and the centrifuge returned to 100g acceleration. The system was allowed to stabilize at this acceleration for 30 minutes, during which time the recording instruments were allowed to warm up, and the calibrated excitation voltages were set (Load cell = 6.00 Vdc; displacement = 1.57 Vdc; strain gauges = +10, -10 Vdc). After 30 minutes, the recording instruments were put into "record" mode and air pressure applied to the bellows (with the valve initially stationary) until the desired pressure was reached. The valve was then rotated until 100 cycles of pile loading had been completed.

(e) Data Reduction

The strip chart from the Visicorder was digitized onto punched cards (Benson-Lehner 099 Data reducer & 282E Telecordex

IBM 29 cardpunch) which were used with a computer program to yield plots of load versus displacement at the pile top and load versus strain at various levels down the pile. A typical portion of a Visicorder record is shown in Figure 4.8.

5. Tests: Description and Results

(a) Mustang Island Tests

Since so little work is evident in the geotechnical literature on the identification of centrifuge model with prototype test results, it was decided to do some preliminary work on this aspect, to give confidence in the technique. Suitable full-scale tests are required; only a few of these have been carried out to the detail required for comparison purposes. The tests at Mustang Island, Texas reported by Cox, Reese and Grubbs (3) and analyzed by Reese, Cox and Koop (7) were selected for simulation. In these field tests, the soil at the site consisted primarily of a dense uniform fine sand, with a water content of about 25% and a relative density in the range of 80 to 100% estimated from Standard Penetration Test blowcounts to a depth of 80 ft. In the top 10 ft, the relative density was somewhat lower, as shown in Figure 5.1. The sand profile was interrupted by a clay layer between depths of 40 and 50 ft; this would have had no effect on the lateral load-deflection behavior of the piles however. For the tests, the water table was above ground surface. Here and there in the profile there was evidence of clay or silt soil in the sand.

where was pile top ?

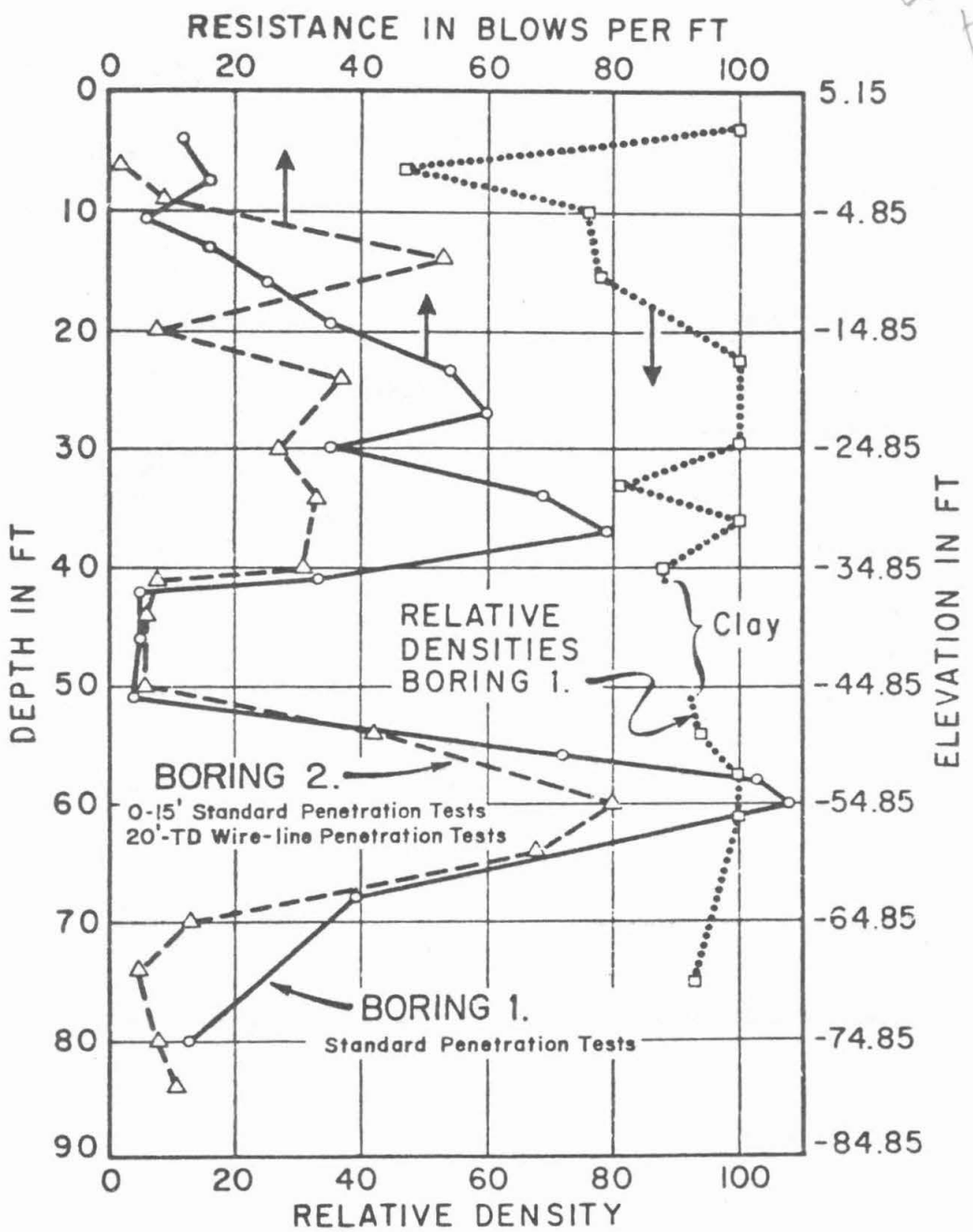

Fig. 5.1. Soil penetration resistance at Mustang Island site (from reference 7)

The two test piles were cylindrical A-53 grade B seamless steel tubes, 24 inches outside diameter, $\frac{3}{8}$ inch wall thickness and 79 ft long. The bottom 38 ft of the piles was not instrumented, since only lateral load tests were planned; inside the next 32 ft, 34 active and 6 dummy strain gauges were installed in 17 pairs, and the top 10 ft, protruding above ground surface, was again free of instrumentation. The embedded length was therefore 69 ft. Installation of the piles proceeded by driving the ungauged 38 ft length open-ended until the top was at ground level, then clearing the soil out before welding on the 32 ft long instrumented section which was sealed with diaphragms both top and bottom to protect the strain gauges from moisture. The paper does not give the extent of the soil plug formed in the 38 ft section. After welding of the two sections, driving was continued; when 69 ft of penetration had been reached, the top 10 ft section was bolted on. Driving records for the two piles were very similar. The distance between centers of the two test piles was 24 ft. Between them was installed a reaction frame for the horizontal load. It consisted of four 14WF78 piles 6 feet on axes, driven to 20 ft penetration, centered midway between the two test piles, and connected together at the top by the reaction frame.

A hydraulic ram reacting against the frame was employed to load the piles at the flange level one foot above ground surface. Load was measured by a load cell. Displacements were measured at two points on the unloaded uninstrumented 10 foot section above ground so that displacement and rotation could both be obtained. The paper does not describe the reference system for displacement measurements, which were apparently used to calculate the displacement

at the ground line,* as well as the slope of the pile. Since the load, acting 1 foot above the ground line generates a moment in the pile at ground surface, the pile deflection is slightly greater than would have been the case had the load been applied actually at ground surface.

The two test piles were subjected to static and cyclic lateral loads. The results of the static load tests on Pile 1 are reproduced in Figure 5.2 from the paper. In the cyclic tests, a greater load (by a factor of 3 or 4) was applied in one direction (major) than the other to simulate the effect of wave forces on an offshore structure, and cycles at increasing load levels were carried out. In Figure 5.2 are shown the results of the cyclic load tests on Pile 2, also. The load plotted is the major load, and the deflection, moment, etc. shown are those measured at the maximum number of cycles at each load level. The paper does not make it clear whether, for example, in the diagram of lateral load versus deflection at groundline, the deflection at each load is that occurring at the last cycle of the greatest load, at the different levels of load on the way to the peak, or is the deflection at each lower cycled load at the last cycle of loading at the lower level. It is assumed here that the first of these is intended. Unfortunately the residual moments remaining in the piles

---

*In the second of the two papers, figures are given of the deflection and slope "at groundline" versus load. The load was applied at 1 foot above groundline, so that there is some uncertainty as to whether the diagrams mean "groundline" or "load line." Presumably the measured load, 1 foot above the ground is plotted versus the calculated (from measurements), displacement at the groundline.

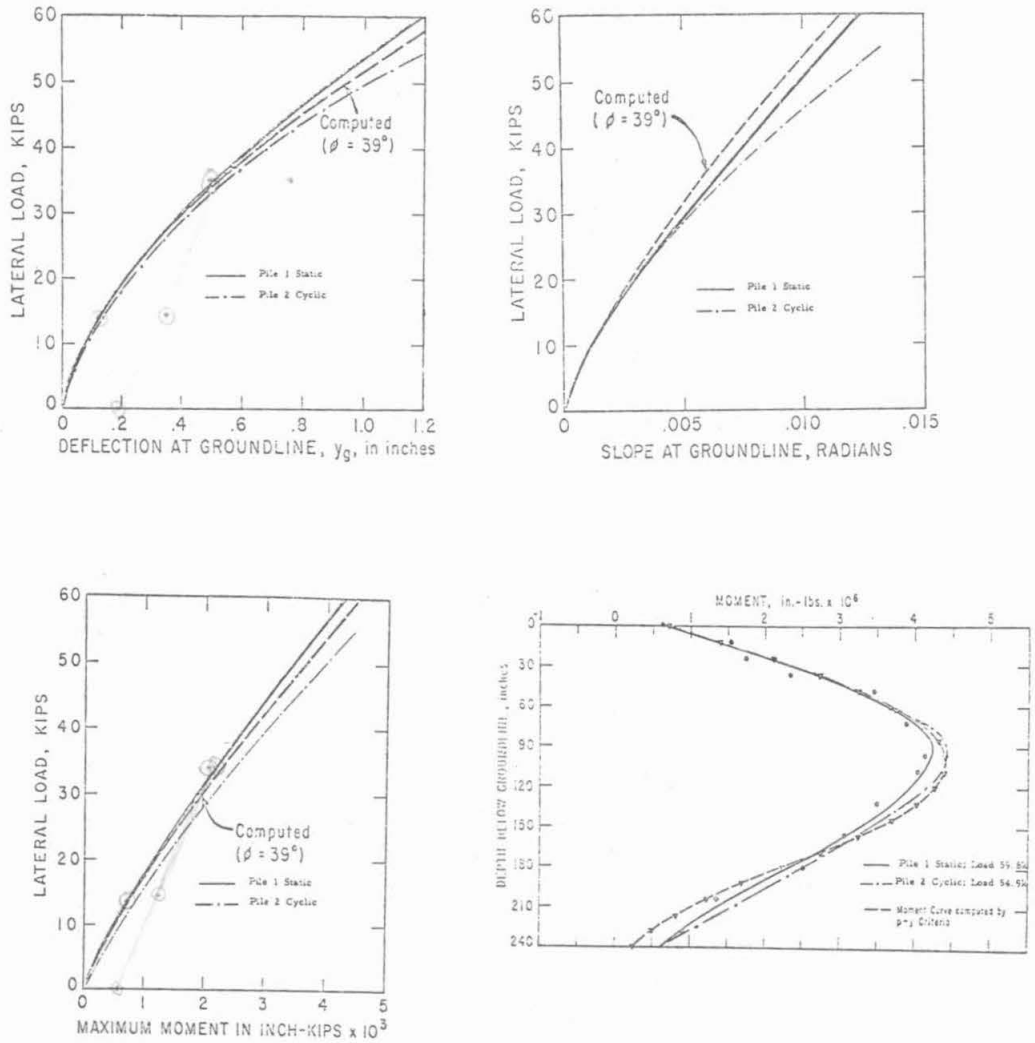

Fig. 5.2. Pile test results at Mustang Island site (from reference 7)

at the end of the first and Nth cycles, at zero ground line load, are not shown.

The product of the modulus, E, and moment of inertia, I, of the test piles, EI was approximately 6.0×10^{10} psi, as measured; the maximum stresses in the piles were limited to 27,000 psi compared to a measured yield stress of about 40,000 psi. By cone penetration tests a significant increase in soil density was observed to result from pile driving, particularly around the top of the pile. This was accompanied by surface settlements of up to 2 inches. Further changes of density occurred because of the cycling of pile loads, but this developed below ground surface.

(b) Centrifuge Model Tests; Mustang Island Simulation

The model pile described earlier was imbedded to a depth of 6.6 inches (55 ft prototype scale) in medium-dense Ottawa sand with a dry density of 105 pcf. Static lateral load tests at 100 g were performed on the pile with the sand both dry and saturated with water to the ground surface. The pile was pushed into the soil at 1 g, since equipment had not been built to simulate full-scale conditions by driving it at 100 g. Thus soil densification equivalent to that developed by the full-scale pile was probably not achieved in the model tests.

For these tests, the pile was loaded by a thread pulling laterally on the pile; the thread was tensioned by a cam loading device. Pile displacement was measured by an optical method. Neither of these measurement techniques was used in subsequent tests under this contract and are not described further in detail.

The outputs of strain gauges on the pile were not recorded in these tests, which were intended as a general test of the pile-load-centrifuge system and the simulation approach.

To obtain prototype quantities, pile loads and displacements were multiplied by factors of 100^2 and 100 respectively, as indicated by Table 2.1. The results are plotted in Figure 5.3 which shows the lateral load-deflection relationship for the two tests (dry and wet), as well as the curve for the full-scale static Mustang Island test on pile 1, reproduced from Figure 5.2. A number of useful observations can be drawn from the test behavior.

It will be observed that the model test curves are somewhat irregular; this is a consequence of the method employed to measure the displacements. A movement of 1 inch at the prototype pile cap is equivalent to 0.01 inches on the model so that 10 measurements of displacement in the 0 to 1 inch prototype interval represent model increments of 0.001 inch. The system was not accurate to this level (and is no longer being used) and the observed movements were therefore erratic. It is worth pointing out that <u>any</u> measurement system for use on the centrifuge has to have a capability of resolving movements of about 10^{-4} inch. Since it must be calibrated at 1 g and then utilized at 100 g, when the measuring instrument and its supports all deflect under the increased load, some difficulties have been encountered.

The full-scale test was performed in soil saturated to ground surface, and so should be compared with the wet model test. All the curves have the same general shape, which presumably indicates

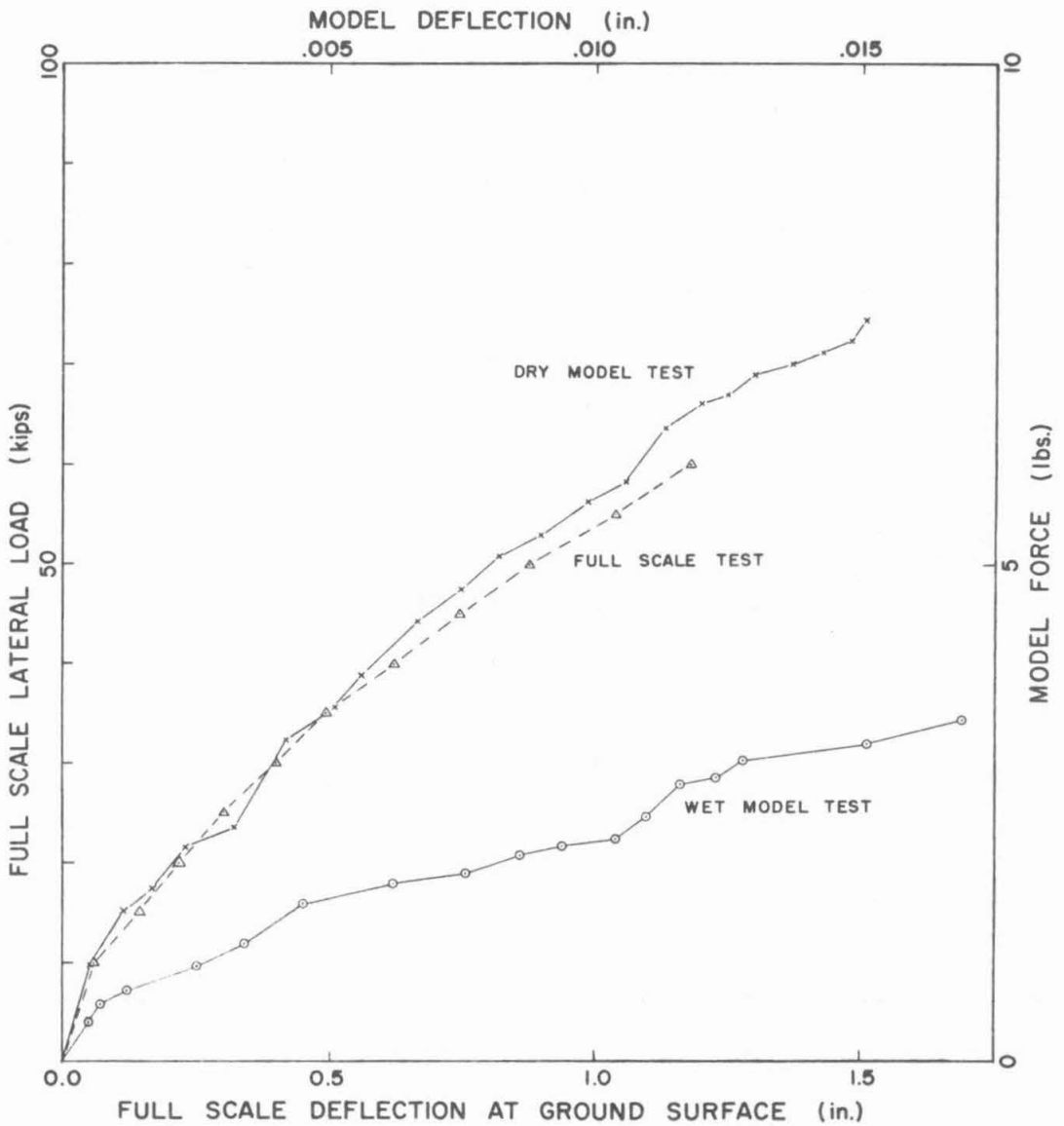

Fig. 5.3. Static lateral load-deflection behavior of single model pile in Ottawa sand compared to Mustang Island Pile 1 static test

that the same mechanical processes develop in model and prototype. The dry and wet model tests were both run on sand at a dry unit weight of 105 pcf. Assuming complete saturation of the wet sand, it would have had a wet density of 128 pcf and a buoyant unit weight of 65.7 pcf (with sand solids specific gravity of 2.67). Since effective stresses in the wet sand are generated by the buoyant unit weight of the material, it would be expected that the ordinates of the wet sand test would have been 65.7/105.0 = 0.626 of the ordinates of the dry sand test. They are in fact substantially (about 30%) lower than these values.

The reason for this is not known. The wet sand test was performed in the same sand as the dry sand test, except for a careful saturation process, and it is possible that the sand around the pile had been disturbed and loosened in the course of the previous loading. The test is, of course, quite sensitive to the state of relative density of the soil around the pile in the top two inches of the deposit. Because of the possibility of disturbance, the soil in succeeding pile tests was prepared afresh for each test. This had the advantage of avoiding the problem under discussion, but possessed the disadvantage that the material density around the pile was usually different in each test.

Regardless of these considerations, the model pile in saturated soil exhibited a resistance to lateral movement substantially smaller than that of the prototype pile. The prototype pile was driven into soil which was already close to 100% relative density in its natural state, and, as noted above, the pile-driving process densified it further. The soil in the model test was in a medium-dense state, and could have been

densified further, which would obviously have given an increase in lateral resistance. In addition, the model pile was made square in cross section, simulating the prototype EI correctly, but was too narrow in width, 16.2 inches in the prototype.

However, it is apparent that the model and prototype test results are qualitatively similar and that no special model effects are obvious which would invalidate the results. It was decided therefore to proceed to cyclic loading tests.

(c) Loading-Unloading Cyclic Tests; Sand

In a number of practical applications involving piles they may be subjected to loads which are applied and then removed back to essentially the zero lateral load condition without any subsequent application of load in the opposite horizontal direction. It was decided, because this type of loading condition was relatively easy to simulate with the existing equipment on the centrifuge, to perform such a test on the same pile in the same dry sand as previously employed. No particular quantitative evaluation will be made of the tests; instead the results will be presented and discussed as there are a number of interesting points in the pile load-displacement response, mostly having to do with experimental difficulties. The soil in these tests was prepared in a medium-dense condition again with a total dry unit weight of 105 pcf. Essentially the same mechanism was used as before, except that the optical displacement-measuring scheme was dispensed with. Instead a tectilinear potentiometer was attached to the displacing mechanism; the changing resistance of the potentiometer indicated movement. This also turned out to be a mistake for the following reason. The pile in these tests was pulled by a fine thread attached to the

load cell. At the beginning of a test, the thread was taut, the pile lateral load was essentially zero, and the displacement gauge was set at zero. With the centrifuge in flight, the pile was pulled laterally and load and displacement recorded during the first loading. The representation of this relation is believed to be correct. On unloading, however, the load gradually returned almost asymptotically to zero in the final stages, so that the no-load state was hard to detect. Since the pile retained a permanent lateral deflection after loading, it is inevitable that the unloading displacement overshoots and the thread goes slack. Consequently the permanent displacement cannot be determined, and the zero reading for the next loading cycle cannot be ascertained. In subsequent tests this technique was discarded and both load and displacement were measured directly at the pile cap. In Fig. 5.4, the dashed lines indicated the inferred load-displacement path, had the revised loading system been employed. The test results for a number of cycles of loading to different magnitudes of peak load are shown in Fig. 5.4. In these tests, which were carried out at 100 g, substantially greater peak loads were attained than in the former test. In the static test described above, the peak load was restricted to about 50 kips in order to simulate the prototype Mustang Island pile load and displacement. In the present tests, lateral loads were carried to the equivalent of about 140 kips in order to examine the pile behavior at these higher loads. Once again, no strains in the pile were recorded.

It should be pointed out that, in practice, the load applied to the level shown in Figure 5.4 would bring a real-life pile close to yield at ← line missing ? solid rod rather than the hollow tube of the real pile, the model pile did not yield at the maximum load indicated [see discussion in section 5(e)].

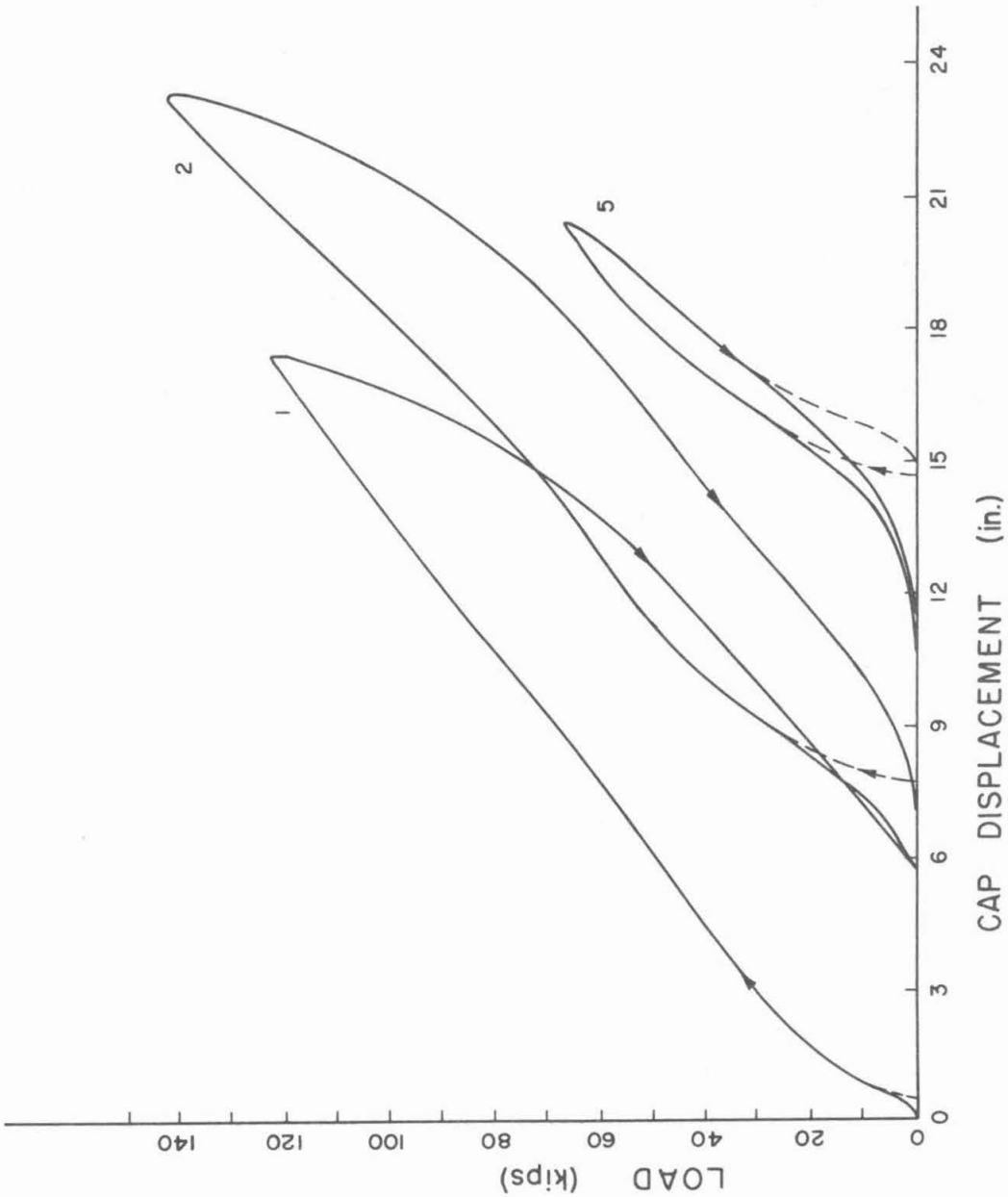

Fig. 5.4. Load-unload versus top deflection behavior of model pile in dry Ottawa sand

The first five cycles of loading are shown in Figure 5.4. In making this figure, the recorder was zeroed at zero load and displacement for the pile in its initial condition. The pile was then loaded up to a peak load of about 120 kips as shown on the diagram and unloaded back to zero load at which it showed a permanent displacement at the top of about several inches. This was not caused by yielding of the pile but rather by the yielding displacements in the soil, and the flow of soil into the cavity formed behind the pile by its lateral movement. Thus, when the load was removed, the pile was unable to return to its initial condition. It can be seen from the first cycle in Figure 5.4 only a small amount of softening was exhibited in the pile-soil behavior. The increased load at higher levels caused displacement to increase in almost linear fashion. The total lateral displacement of the pile was almost a pile diameter in contrast with the previous static lateral load test in which the maximum lateral prototype displacement was approximately one inch. In addition, the present pile-soil configuration is softer than the one tested before, in that here, in the first loading cycle, an inch or so of displacement was caused by a lateral load of only 15 to 20 kips instead of the 60 kips developed in the previous test.

This test illustrates one of the advantages of centrifuge testing, as compared with prototype or field tests. It is not difficult in the centrifuge to generate lateral loads of the magnitude shown in Figure 5.4 (in the range of 12 to 15 pounds for the peak loads shown) and, as can be seen at these loads, the pile is deflecting about a diameter at ground surface, which is an extreme condition in comparison with the values that might be used in the design of a real structure. Thus, the safety

of the pile or pile system can be investigated in the centrifuge readily. It would be very difficult in the field to arrange for loads of the equivalent magnitude of 100 to 200 kips required to achieve these deflections. It would not be difficult, after a testing program in a centrifuge had been completed, to subject the model pile to loads high enough to cause yielding in the pile, thereby effectively destroying it for future test purposes, but enabling an evaluation of its failure behavior to be made. The pile can be easily extracted for inspection after the test. For prototype critical structures this might be a useful test to give information on the limiting behavior of the system. However, in the field, the cost of building, instrumenting, and installing, and testing a pile is such that a testing agency would be extremely reluctant to destroy the pile at the end of a test sequence. Usually the analysis of a particular series of tests leads to a requirement for further testing which would not be possible were the pile damaged. Rehabilitation of the bent prototype pile would not be possible, but perhaps could be accomplished for a model pile, depending on where the hinge formed.

For the second cycle of loading shown in Figure 5.4 the recorder signal was not returned to zero so that the pile behavior during the second cycle cannot be compared directly with that of the first cycle. The permanent displacement, as discussed earlier, includes an unknown amount of slackening of the loading thread. It is apparent however from Figure 5.4 that behavior of the pile during the second cycle of loading is modified from that of the first cycle. Apparently the stiffness of the soil in front of the pile has been changed as a result of the strains developed during the first extreme cycle of loading. The initially soft

response is associated with the removal of slack in the loading thread, and is thus ignored in this discussion. At larger displacements the first cycle of load appears to have had the effect of densifying the soil, so that the load-displacement relation shown in Figure 5.4 for the second, and in fact, for the third and fourth cycles (not shown) is stiffer than that exhibited at large displacements for the first cycle of loading. For the same peak displacement obtained during the first loading, these cycles all required 10 to 15 percent greater load.

For the fifth and last cycle of loading an experiment was carried out to subject the pile to approximately half of the peak load obtained in the former cycles in order to see how much hysteresis was incorporated in the unloading sequence at the reduced load. The result of this is shown in Figure 5.4 as curve 5 which reached a peak load of about 65 kips at a peak displacement of almost 10 inches. It can be seen that the area underneath the fifth cycle of loading, which represents the energy dissipated in the load cycle, or the damping which such a pile would exhibit were it subjected to static cyclic loads, perhaps during long-period motion in an earthquake, is substantially smaller than the area under curves 1 through 4. Much more dissipation is developed by the increased loads. This point will be returned to in later test descriptions.

It was also discovered in this test sequence that the pile walked in the direction of the loading in the first few cycles.

After each cycle of displacement some residual lateral displacement was left in the pile before the next cycle of loading began. This effect was biggest in the first load cycle and was subtantially less between loads 4 and 5. The indication is that after a few cycles of loading in this soil the pile reached essentially a steady state condition and residual deformations did not increase further.

As no anomalies had been encountered during this test (except for the displacement measurement at low loads), and the general load application system had performed satisfactorily it was decided to proceed to complete cyclic loading tests including load reversals, carried out first on the same sand as before, and subsequently on the Santa Barbara silt. Tests once again were performed without measurement of the strains in the pile and these will be described first.

(d) Load Reversal Cyclic Tests; Ottawa Sand

Once again the sand used was prepared in a loose to medium-dense state. The same pile was used as in the previous tests.

Two different tests were performed. In the first test the effect of cycling the pile at different load levels was investigated and in the second test the behavior of the soil-pile system under a number of cycles of load at the same maximum value was studied. The cyclic load application device described in section 4(b) was utilized in these tests.

Figure 5.5 shows the results of load versus displacement in the first test series. The diagram was traced off the X-Y plotter record of the actual test. A number of interesting features are visible in the plot. When small loads were applied that gave rise to displacements of the top of the pile of about 4 inches in each direction at peak loads of approximately 50 kips in each direction the pile-soil behavior was relatively stiff. As the load was increased up to approximately 100 kips with peak displacement amplitudes of approximately 15 inches, the system was considerably softer and the amount of area underneath the load ("damping") was greater than for the tests at lower load. The largest load achieved, something in excess of 120 kips, at pile top displacements of the order of 20 inches, exhibited the softest behavior and the largest amount of dissipation in each cycle. The softening and increasing dissipation are to be expected at these loads with a soil in which yielding is occurring extensively around the pile top as the pile deflections are generated.

It can also be observed that the hysteresis loops are not symmetric about the origin in any of the three loading situations shown in Figure 5.5. In each case the displacement in the direction of the first load (in this case the positive load) is greater for all cycles than the displacement in the negative load direction. The shape of the unloading portion of the curve also appears to be different in the two loading directions. Since each of the curves shown in Figure 5.5 represents the load-displacement history during

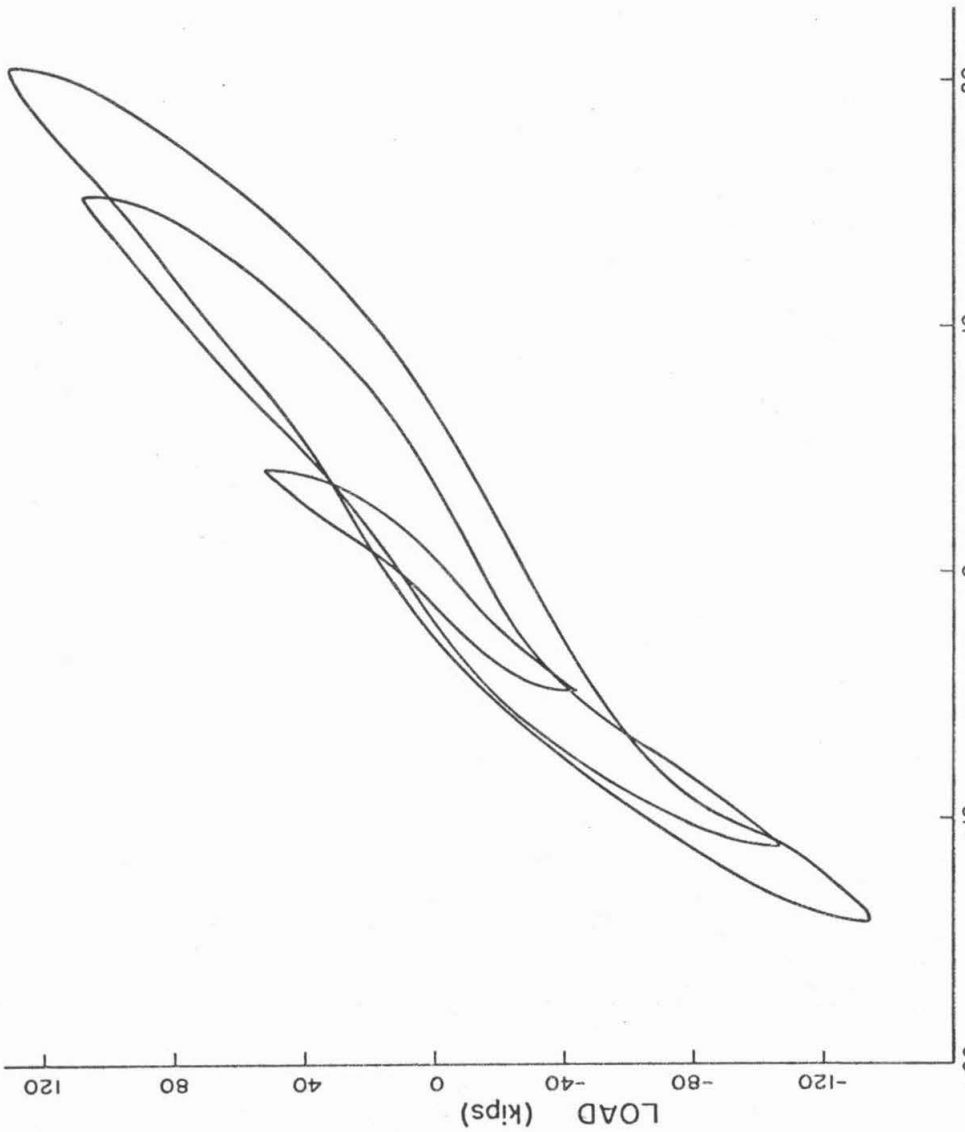

Fig. 5.5. Cyclic lateral loading test results for model pile in dry Ottawa sand at different maximum load levels

one cycle a few cycles after the load was initially applied, the behavior is approximately steady-state and is an interesting aspect of the pile response. From observation it appears that the direction of the first (positive) half-cycle of loading is important. It was seen from the uni-directional loading tests shown in Figure 5.4 that, at the end of a loading cycle, when the load was brought back to zero, a substantial deflection had been effected in the direction of load application. The pile remained deflected with a surface displacement of several inches after unloading.

This means that for the reverse half-cycle of loading the pile's initial condition was different from that in the previous half-cycle; in effect the pile and surrounding soil were pre-stressed. Thus the response of the pile to a half-cycle of reversed loading would not be expected to be the same as for a first half-cycle of loading in that direction. Since on first loading the pile moves away from the soil permitting some soil to fall into the cavity formed or tending to form behind the pile, it is necessary in the reverse half-cycle of loading for the pile to deform this soil in addition to the material originally in place around the pile. Thus the pile-soil system is stiffer for the reverse half-cycle than for the half-cycle in the positive direction. Consequently, none of the displacements in the reverse direction reach as large values as those in the positive direction. The effect is greater the larger the applied load. On each reverse half-cycle since the pile does not move as far in the reverse direction not as large a cavity is formed behind the pile as in a positive half-cycle, less soil falls in, and therefore the resistance in the positive direction is relatively less altered.

In loading-unloading tests on material deforming plastically, the initial slope of the unload-rebound displacement curve (the elastic rebound) should be equal to the initial slope of the curve of the first load application. This was observed to be the case in these tests, although the initial loading curve does not appear in the figures.

A brief study of the effect of repetitive cycling at a single load level in sand was also undertaken and the results are shown in Figure 5.6. In this figure cycle 1 refers to the first complete cycle, and cycle 6 is the sixth cycle in the sequence. The initial load application is not shown. It will be observed in this test that the loading device which is intended to apply an equal load at the two ends of the loading cycle did not achieve this. The peak reverse load on cycle 6 is somewhat smaller than the peak load on cycle 1. This may have been due to a change in the air pressure in the system which went undetected at the time. However, what the test does show is that the peak displacement has drifted or walked during the cycles from 1 through 6.

It was found in subsequent cycling (not shown) that most of this effect occurred in the first five or six cycles in this soil, and was considerably diminished thereafter. Little change in the extent of dissipation in the soil is evident in the two cycles shown. Once again a difference in the positive and reverse load behavior is apparent. Following this test, preparations were made for carrying out tests on the pile in the Santa Barbara silt.

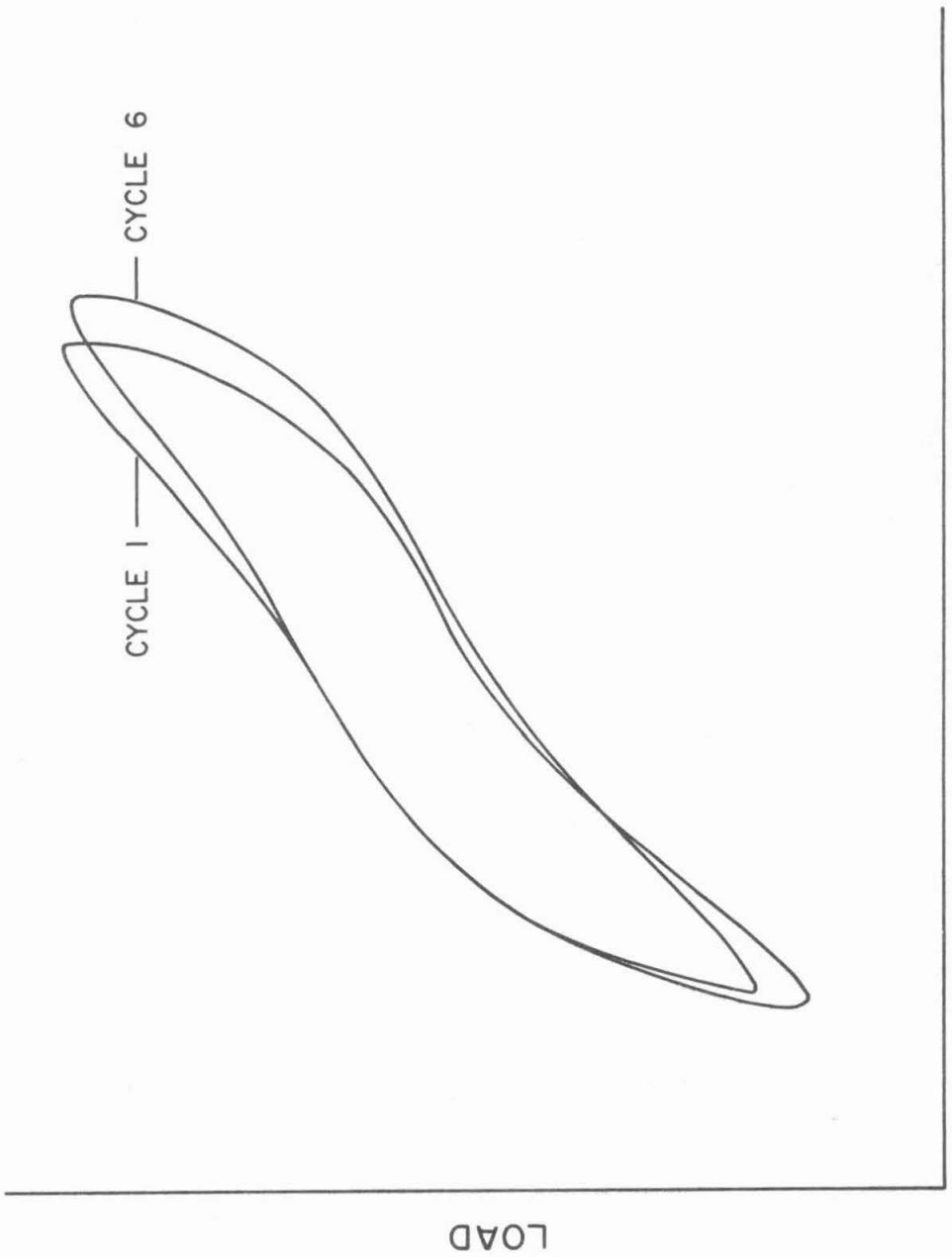

Fig. 5.6. Effect of number of cycles of lateral loading on behavior of pile in Ottawa sand

(e) Load Reversal Cyclic Tests; Santa Barbara Silt

A number of preliminary cyclic tests were carried out on the pile installed in the Santa Barbara silt, and are not reported here since a number of operational problems developed. For example, the previous pile tests had resulted in punctures developing in the plastic coating covering the strain gauges so that, when the pile was installed in the wet silt, one or two of the gauges shorted. As described in the previous section, some difficulties had also emerged in the employment of the bellows loading system. Apparently at the 100-g level the carriage loads cause the ball bearings to deform the supporting rail locally. This resulted in an excessive amount of friction in the system. The problem was not completely overcome before the tests reported in this section were carried out. However, in each of the tests, load and deflection were measured at the pile cap and are therefore independent of what the loading system did. The result of the malfunction was that the loads in the positive and negative directions were not necessarily equal and varied from cycle to cycle.

The test reported was carried out for approximately 70 cycles of loading and the results have been sampled for detailed analysis at cycles 1, 17, and 68. Load and displacement at the pile cap were recorded on the X-Y plotter and load, displacement, and strains were also plotted simultaneously on the Honeywell oscillograph. In order to prepare the figures shown here, the Honeywell traces were digitized at equal times, as described in section 4(e), and the resulting plots are shown in Figures 5.7(a,b,c) and 5.8(a,b,c). The condition of the Santa Barbara silt for these tests has been described in section 3.

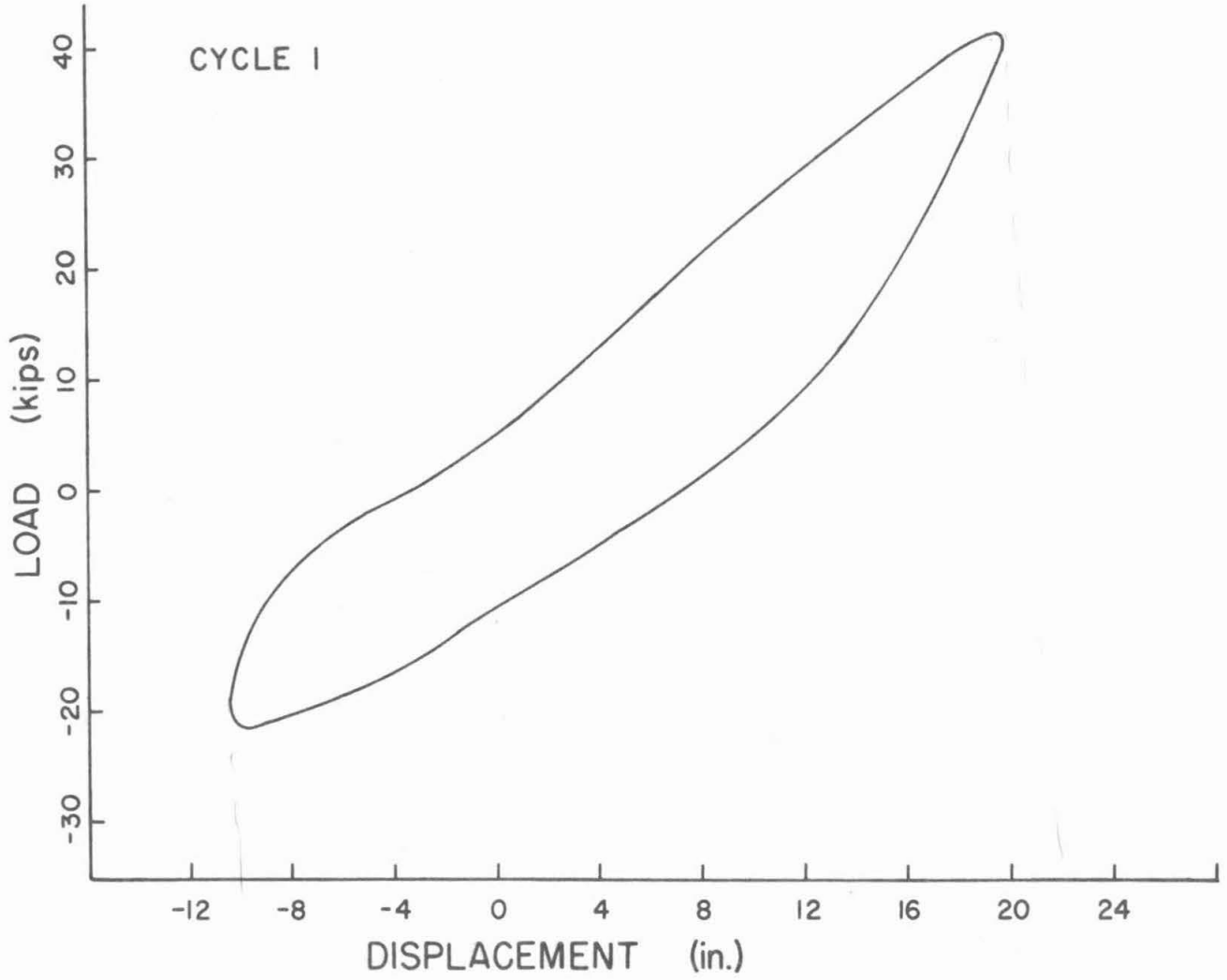

Fig. 5.7a. Cyclic lateral load versus displacement of top of model pile in saturated Santa Barbara silt; Cycle number 1

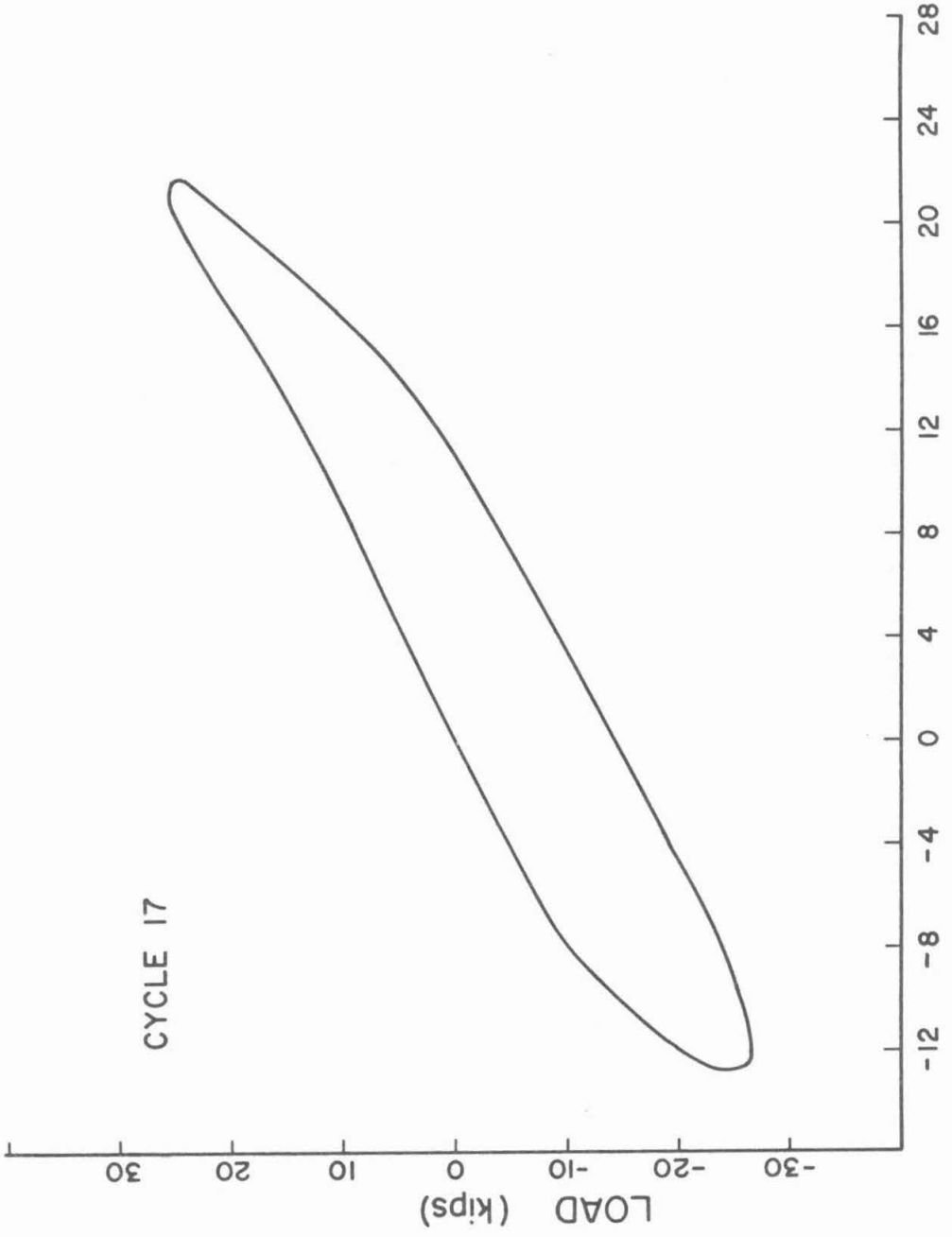

Fig. 5.7b. Cyclic lateral load versus displacement of top of model pile in saturated Santa Barbara silt; Cycle number 17

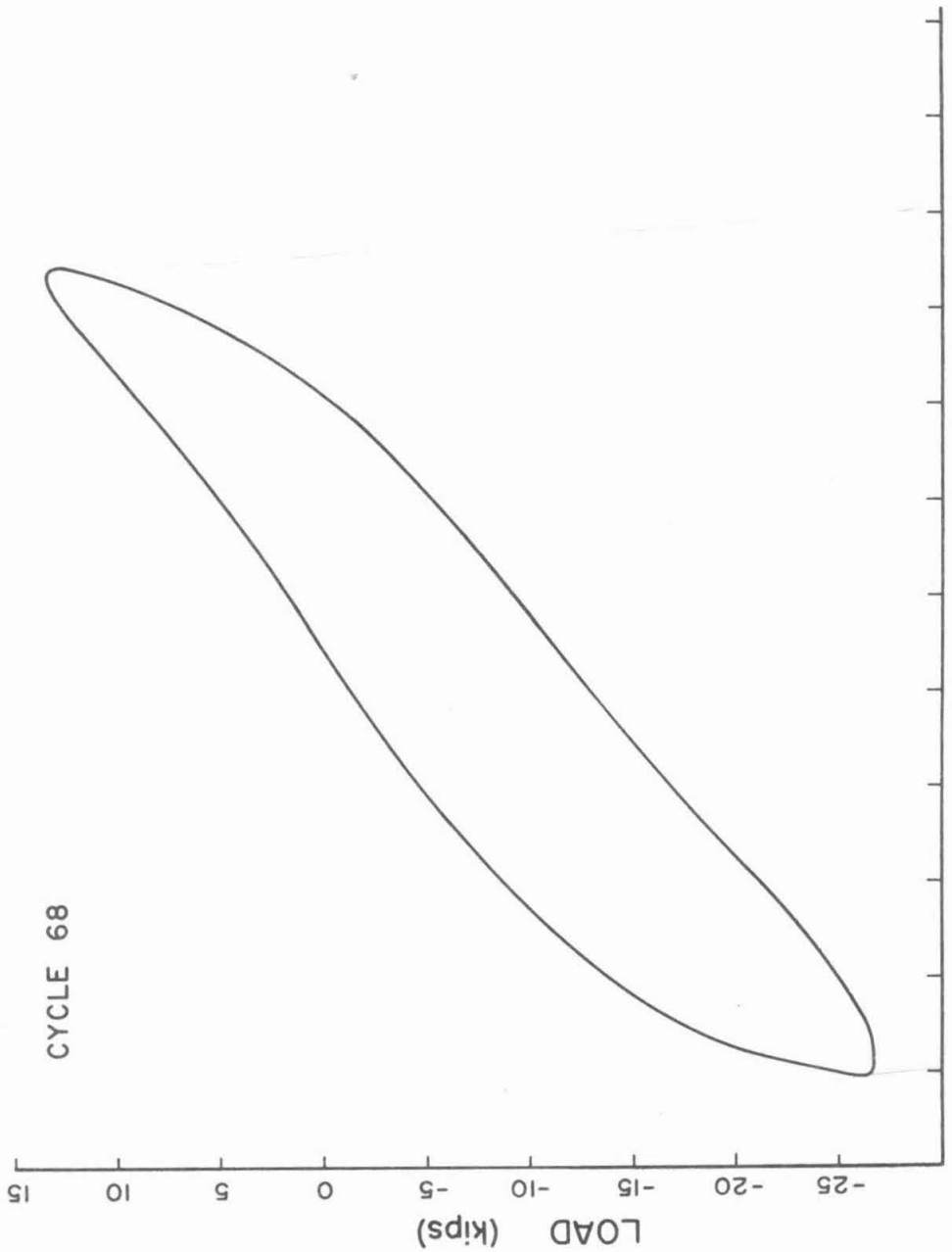

Fig. 5.7c. Cyclic lateral load versus displacement of top of model pile in saturated Santa Barbara silt; Cycle number 68

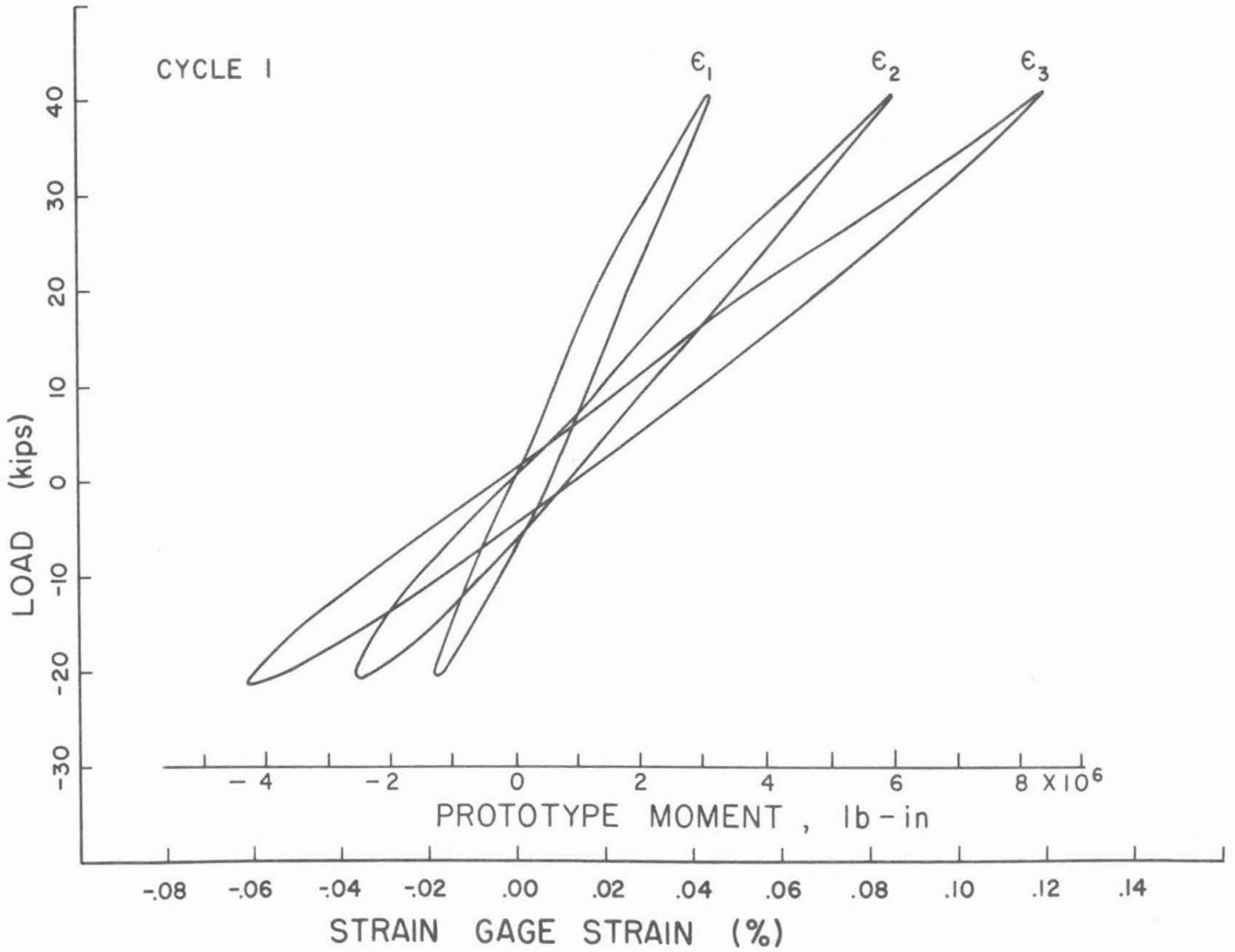

Fig. 5.8a. Strains and moments in model pile during cyclic lateral loading test in saturated Santa Barbara silt; Cycle No. 1

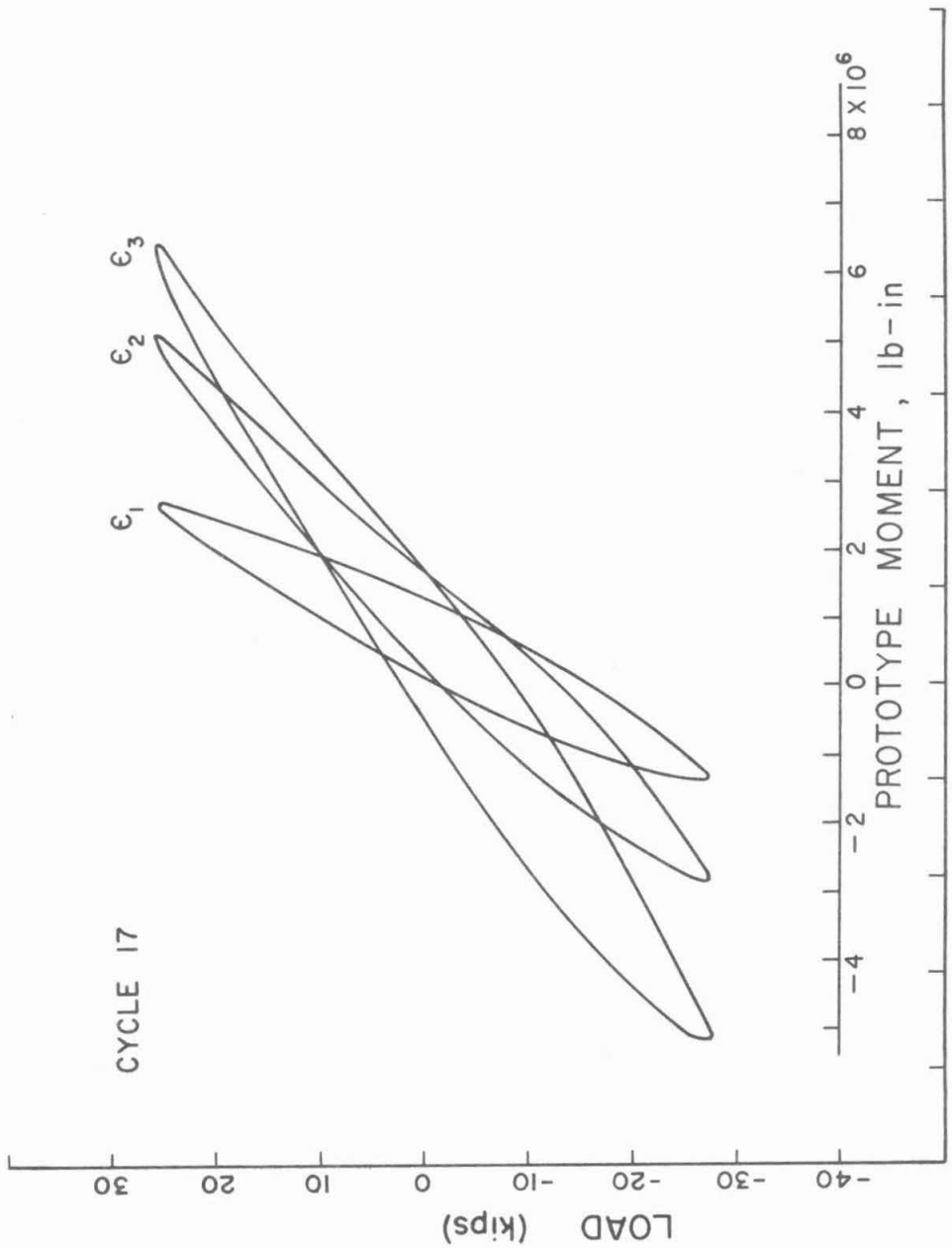

Fig. 5.8b. Strains and moments in model pile during cyclic lateral loading test in saturated Santa Barbara silt; Cycle No. 17

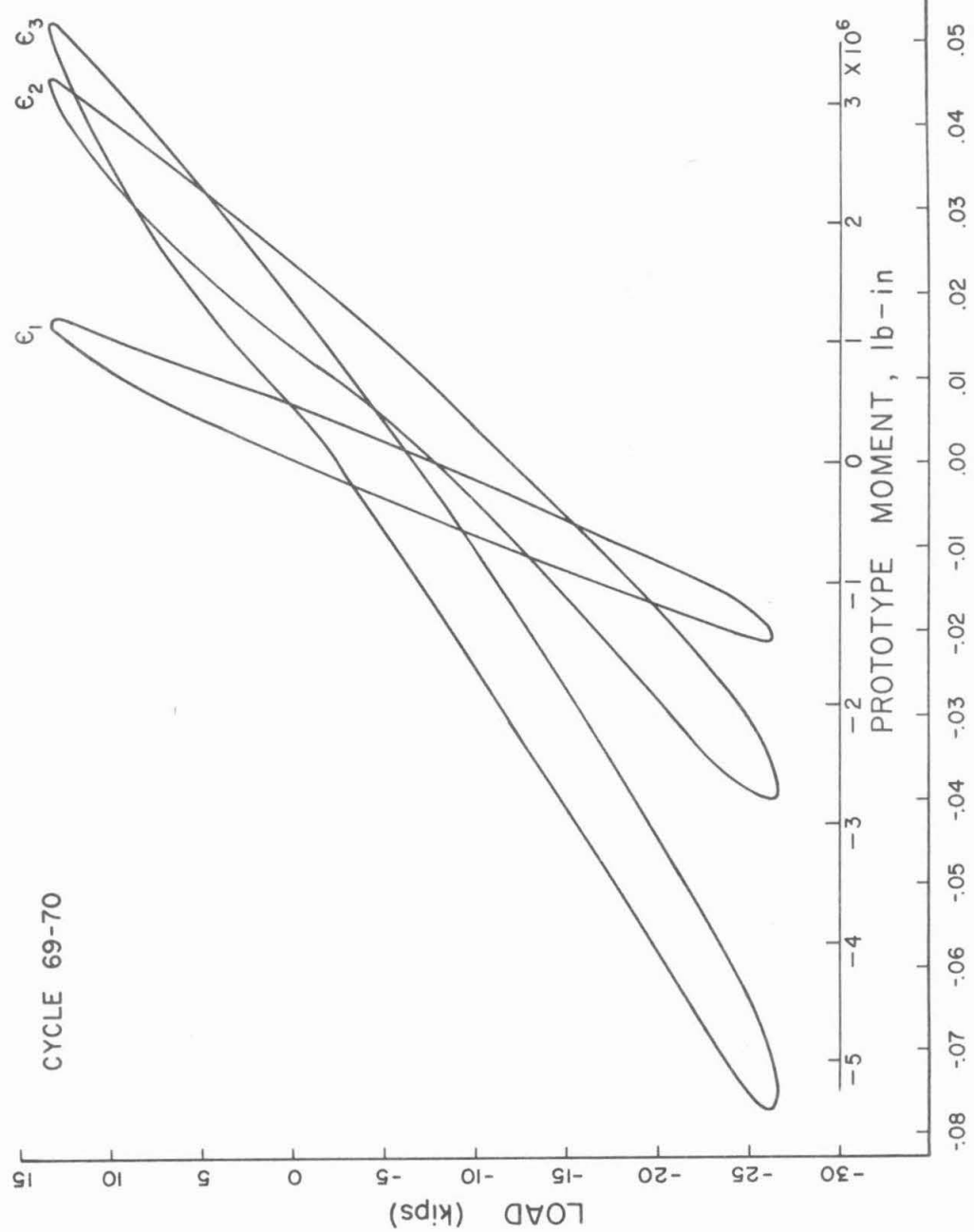

Fig. 5.8c. Strains and moments in model pile during cyclic lateral loading test in saturated Santa Barbara silt; Cycle No. 69-70

As prepared, the silt was considerably softer than the sand tested previously. Thus the peak load achieved in the Santa Barbara silt tests at displacements of about a pile diameter in each direction was only in the region of 20 to 40 kips (prototype scale). In addition, the softening effect of cyclic reversal loading in the Santa Barbara soil was much more apparent than in the dry sand, as can be seen from Figure 5.7. The average slope of the cap load versus displacement curve flattens considerably between cycles 1 and 68. There was no indication with this material that a steady state condition was reached; by cycle 68 softening behavior was still continuing. The stiffness of the pile system at the pile cap decreased from approximately 2.0 kips per inch at the first cycle through 1.5 at the seventeenth cycle, to a value of 1.2 at the sixty-eighth cycle. This effect may be related either to pore pressure effects in the soil, or to reworking and mixing of the near-surface soil with water as the pile moved back and forward. The water level in these tests was kept slightly above the soil surface in order to prevent the soil from drying out, and to simulate a sea-floor condition. Consequently, in the course of moving the pile back and forward, the tendency to alternate formation of cavities in the soil at front and back of the pile was accompanied by a flow of water up and down the pile. The water mixed with the soil during the cyclic motion and contributed to the softening of the soil adjacent to the pile. As the soil softened, the deflection of the pile at shallow depths increased and proceeded further down the pile. This effect was due to the presence of water and was absent in the case of dry soil.

It will be noticed in Fig. 5.7 that the negative load stayed fairly constant at approximately 20 to 25 kips during all cycles, but the positive load varied from about 40 kips at the start of the test through 25 kips at cycle 17 to only 15 kips by cycle 68. Apparently, the bellows system was encountering increased frictional resistance in the positive load direction as the test proceeded. This is unfortunate since it complicates interpretation of the results, but it could not be corrected while the test was running. In cycle 17, the most symmetric of the tests as far as load conditions were concerned, the displacement in the positive load direction (that is the direction of the first application of load) was greater than the displacement in the negative direction. This was noticed in the pile-sand tests.

The variation of strains in different cycles is shown in Figures 58(a) through (c). The positions of these strain gauges are shown in Figures 4.6 (and 5.9) from which it can be seen that, unfortunately, they were not spaced far enough apart to catch the maximum moment existing in the pile at any stage of the loading. Since the load was applied slightly above and parallel to ground surface, it would be expected that the moment in the pile would increase with depth to a maximum value and then decrease. From the strain information in Figure 5.8, it can be seen that the maximum strains in the three strain gauges increase from strain gauge 1 through 3. The position of the gauges was decided from preliminary calculations in which the Santa Barbara silt was assumed

to be stiffer and stronger than it eventually turned out to be. Thus, it was estimated that the maximum moment would be higher in the pile than was the case in the test. The recording system at the time of the test only permitted three strain gauges to be used on the pile. It is unfortunate that either the gauges were not placed lower or another one or two gauges further down the pile could not be included. This will be remedied in future tests. However, it is apparent and may be assumed that the third strain gauge was not far from the position of maximum moment.

If this assumption is made, some conclusions can be drawn from the data obtained. The peak strain observed is of the order of 10^{-3} and this value together with the pile properties and dimensions gives rise to an indicated moment of 7 lb-in in the model pile. Since the scaling factor for moment is 10^6 at 100 g, the equivalent moment in the equivalent prototype pile is 7×10^6 lb-in.

If a yield stress of 40,000 psi is assumed for the model pile, then the yield moment required to initiate a hinge in the model pile is approximately 50 lb-in. For the same yield stress the moment required to develop a hinge in the prototype pile is about 7×10^6 lb-in. Thus, the maximum moment recorded in the model pile is close to the equivalent yield moment in the prototype pile. It can be seen from Figures 5.8 that as the number of cycles develops, the strain in the second strain gauge approaches more closely the strain in the third gauge in the positive loading part of the cycle. This indicates a changing distribution of displacement and moment down the pile as the cycle progresses, again reflecting the progressive deformation of the pile due to changing soil properties in the cycling process.

In each cycle of loading the load passes through zero twice, and it can be observed on Figures 5.8 that residual strains and therefore moments are left in the pile at these points. Selected moments from Figures 5.8 are plotted versus depth in Figure 5.9 at different levels of loading,* +13K, zero, and -20K. To the right of the axis the moments in the pile obtained from strain gauge readings are shown at a lateral load of +13 kips equivalent prototype value. This value was selected because it is the maximum positive loading achieved at cycle 68 as shown in Figure 5.8(c), and thus both the previous cycles 1 and 17, selected for examination, passed through this value. The moments are not zero at the ground surface since the horizontal loading passed through a point on the pile two feet (prototype scale) above the surface.

It can be seen from Figure 5.9 that the strain gauge at the deepest location (ϵ_3) apparently indicates approximately the maximum moment in the prototype pile for various load cycles at a depth of about 150 inches below ground surface. The moments at depth generally increase as the number of cycles increases indicating progressive softening of the soil.

The peak moment in the prototype pile was indicated by the deepest strain gauge at the highest lateral load achieved, which occurred during the first cycle. It had a value of approximately 8.5×10^6 lb-in as can be seen from Figure 5.8 a. If the prototype pile is considered to be the Mustang Island pile of 24 inches

---

* Because slight variations in the traces have significant effects on the indicated strains, Figure 5.9 was drawn from measurements made by hand from the original Honeywell record. The curves thus differ slightly from those that would be obtained directly from Figures 5.8.

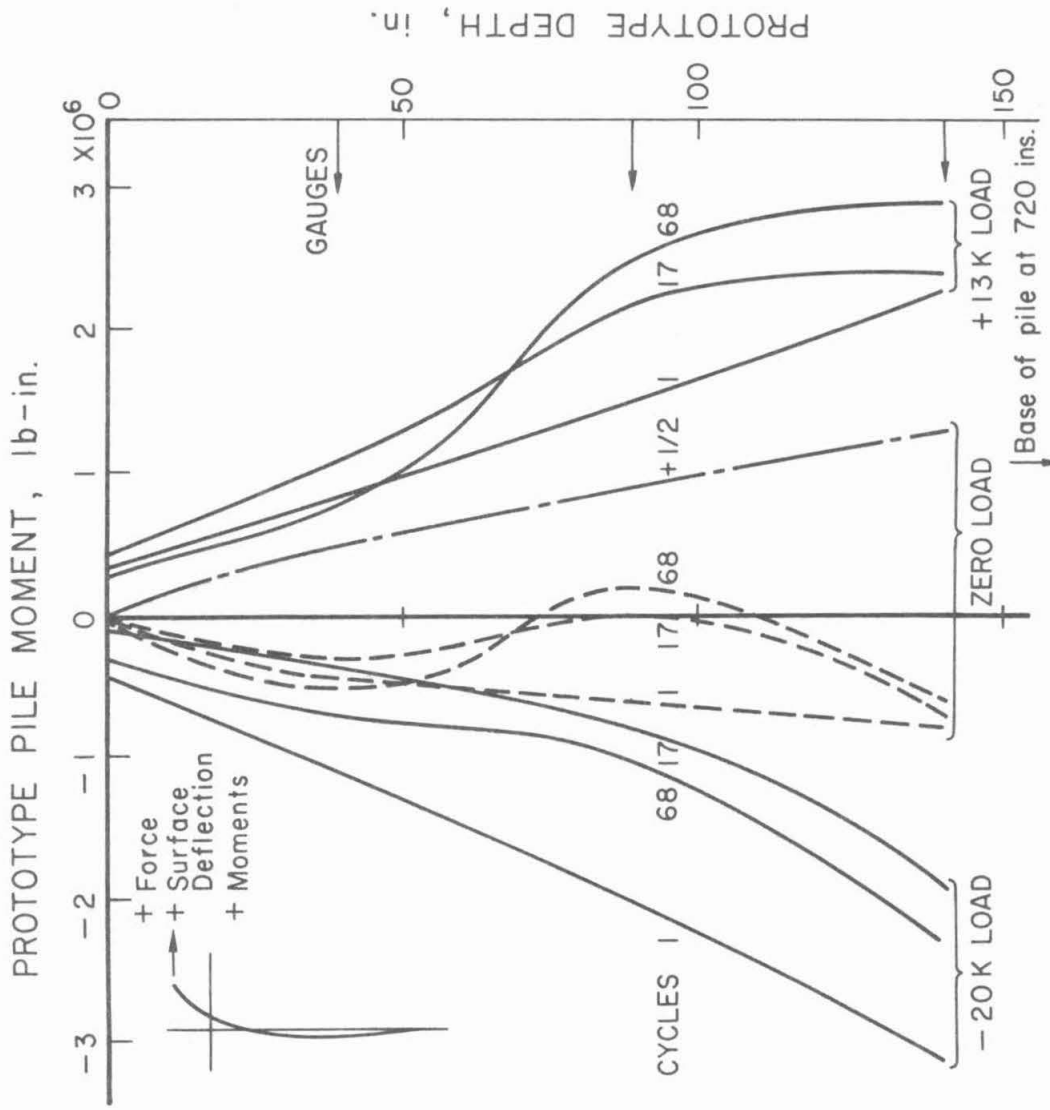

Fig. 5.9. Moments in model pile as a function of depth during cyclic lateral loading test in saturated Santa Barbara silt

diameter and $\frac{3}{8}$ inch wall thickness, this moment would have slightly exceeded the yield value. It might therefore be considered an extreme moment on which to base a safety factor for pile behavior; it developed at a horizontal load of about 42 kips and pile top displacement of 20 inches. It should be repeated that the Santa Barbara silt is much softer and gives a much lower resistance than the sand in the Mustang Island pile tests.

On Figure 5.9 is also shown the distribution of moment in the pile at the end of the first positive cycle of loading ($+\frac{1}{2}$) when the horizontal load was zero. This is moment remaining in the pile after application and removal of the 42 kip horizontal load. It can be seen that at depths in excess of 150 in a considerable moment of perhaps 1.5×10^6 lb-in remains in the pile. When the load is next applied in the opposite (negative) direction, the moments generated must be added algebraically to this existing residual positive moment state. It is apparent that repeated cycles of loading of varying magnitude in realistic field conditions will give rise to complicated pile moment-depth distributions.

The negative moment developed by the first -20 kip load is therefore less than it would be were the load the first to be applied. On the left side of Figure 5.9 are plotted the moments generated in the pile at a value of -20 kips lateral load. The highest moments were generated by the -20 kip load during its first cycle of application; with subsequent load reversals the negative moments gradually decreased until, apparently, little change developed between the seventeenth and the sixty-eighth cycle. The values shown for cycles

17 and 68 are probably not particularly accurate, as the curve drawn through them has a questionable shape. However, it is thought that the indication of maximum negative moments decreasing with number of cycles is correct.

In the first positive loading, the moments in the pile increase almost linearly with depth, and it is apparent that the maximum moment must be at a depth of 150 to 200 inches for the +13 kip load. The load was increased to a maximum of about +40 kips and removed. When it was zero, the residual moments shown by the curve $+\frac{1}{2}$ were left, showing almost the same depth pattern as the +13 kip load. Subsequently, the load direction was reversed to a maximum of -20 kips, and the distribution of moments at this load is similar to that at the +13 kip load. On removal of the negative load to zero, a residual negative moment was left in the pile, with a maximum value of about -1×10^6 lb-in at an indicated depth greater than 150 inches. The moments were smaller than those left at zero load after the first positive half-cycle ($\frac{1}{2}$ curve).

On subsequent cycling, the moment pattern changed substantially from cycle 1 to cycle 17, and to a lesser extent at cycle 68. It might be considered that a steady state was being approached, except for the evidence from pile top deflections, which will be discussed later. The moments due to the +13 kip load after repeated cycling are larger than those developed by the -20 kip load. Although the positive load 17 and 68 cycle moments appear to indicate a maximum moment about the -150 inch level, the measurements at the -20 kip load point to a maximum moment

at greater depth. The moment distributions for zero load at the end of the 17th and 68th cycles are similar to each other and also bear a resemblance to the negative load moment curves at the same cycles. The shape of these moment diagrams at zero load is strange with a maximum negative moment at a depth of about 40 inches and another maximum apparently indicated below 150 inches. Since the gauges did not malfunction and had the same calibration in checks before and after the test, the distributions must be accepted as shown. They indicate a greater complexity of pile-soil behavior than was anticipated, but on the other hand, the test was carried out at greater equivalent prototype displacements than have previously been attempted.

The pile-top displacements after an increasing number of cycles have also been plotted and are shown in Figure 5.10. Three curves are presented, at zero load, and at the two loads of +13 kips and -20 kips for which the moments were displayed. It can be seen particularly in the figure that the zero load displacement moves in the direction of positive load until in fact the top of the pile is so far displaced that even the -20 kip load does not return it to its originally zero location. In terms of the logarithmic scale of cycles, the lateral displacement (sway) is developing at an increasing rate. It appears that the initial large movements at the top of the pile mix the adjacent soil and water, and may also develop liquefaction further down the pile as a consequence of the associated cyclic shearing strains. Thus the soil weakens, so the deflections increase, and more soil weakening ensues and progresses down the pile. The process

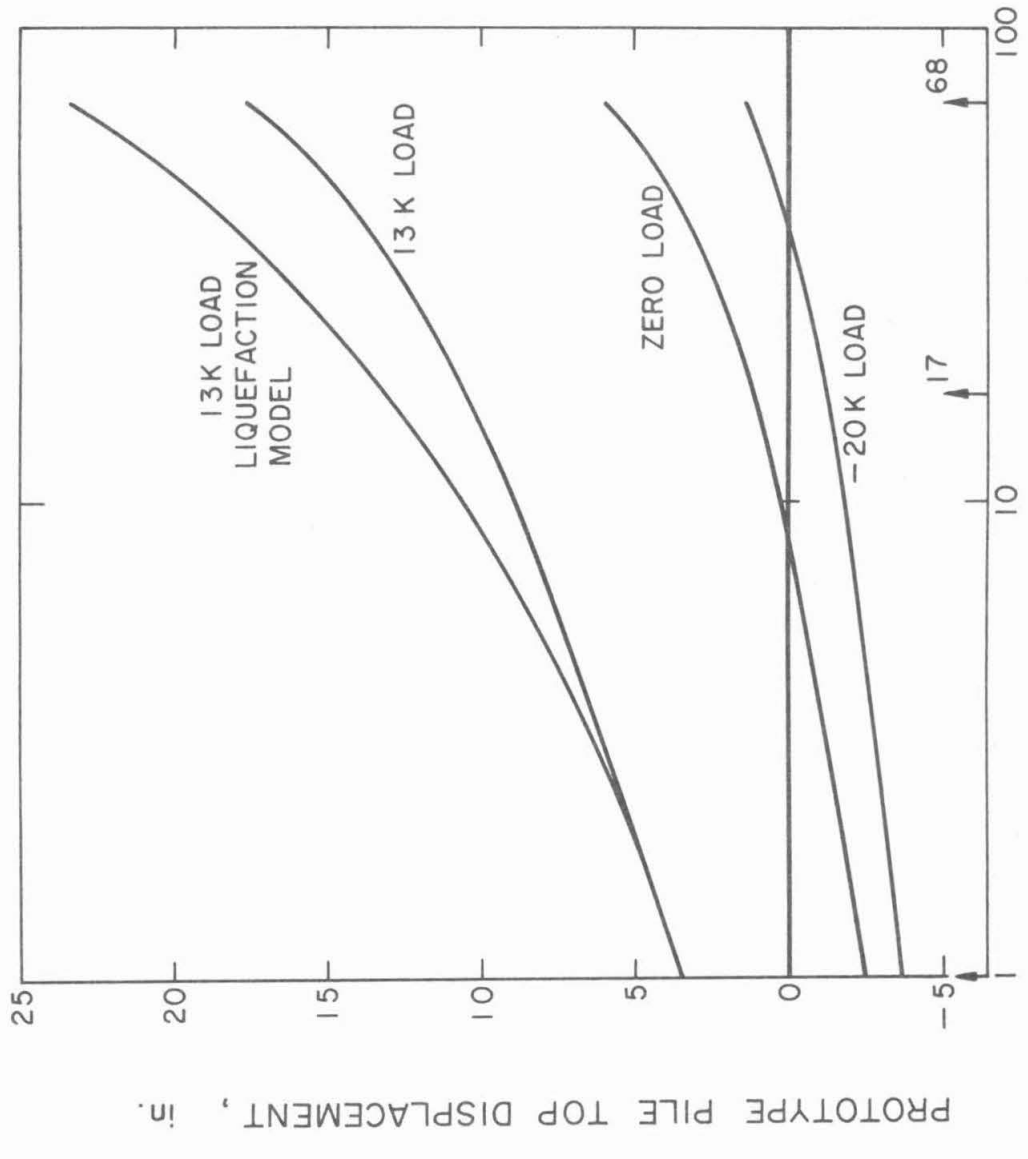

Fig. 5.10. Drift of model pile top during cyclic lateral loading test in saturated Santa Barbara silt

is apparently an unstable one, and the question arises naturally: Is it arrested at some depth? To try to answer this, an attempt at an analysis of the process was made.

6. Liquefaction Analysis

It is obvious that an exact analysis of the stresses developed around a pile subject to cyclic lateral loading under conditions whereby the stresses cause changes in the soil properties is impossible, and probably will remain so. Approximations are necessary and must be selected carefully to maintain the important features of the phenomena involved. The analysis presented here is very rough, but gives some representation of the processes believed to be at work during the pile movements. The assumptions will be clearly stated, and may be altered if a different view of the events is taken, or as more information becomes available.

Firstly, the three-dimensional nature of pile-soil interaction near ground surface will be ignored; instead, stresses will be estimated on the basis of a two-dimensional plane-strain model, representing conditions on a horizontal plane including the pile. In this plane, the pile will be taken to be a circular rigid inclusion in an elastic incompressible soil medium, whose modulus, however, will be taken to be given by the slope of a secant on the soil's stress-strain curve. An alternative soil model in the horizontal plane would be one with rigid-plastic behavior, in which the stresses would be given from a plasticity analysis. However, it is believed that the elastic or reversible component of soil behavior is

important for the pile reactions and is needed in the vertical view of the pile-soil interaction; on this basis, the elastic model was selected. A logical development would be to represent the soil behavior as linearly elastic-plastic in both the horizontal and vertical interactions, but this is computationally more complex. It may be worth examining at a later date, because of its increased realism. In the vertical direction, the pile-soil interaction is given by the usual beam on a Winkler foundation analysis. The coefficient of subgrade reaction in this analysis is assumed to be constant with depth. This is clearly a poor assumption for the sands or Santa Barbara silt on which the pile tests were performed, but it simplifies the mathematics for the present and permits the principal features of the analysis to develop with the least complication. It would not be difficult to extend the method to the case where the subgrade reaction coefficient, more realistically, is taken to vary with depth linearly, or in some other fashion.

The cyclic load liquefaction behavior is taken to be that of the Lee-Seed model (9), in which the cyclic shearing stress, the vertical effective stress and the number of cycles of loading determine whether or not liquefaction will occur. In a separate report (5) Lee describes the behavior of the Santa Barbara silt in this respect. His results will be used in this analysis, which particularly employs the data from the simple shear test configuration.

The analysis is based on the following mechanistic model of what happens as the pile is moved cyclically to and fro in the soil.

Under lateral load, the displacements are greater at ground surface and diminish more or less exponentially with depth. Adjacent to the pile shearing stresses are generated on vertical planes in the soil, which are greatest at the surface, and near the pile. [This holds obviously for the model adopted herein of a soil with "elastic" properties constant with depth. It is probably also the case for the soil whose modulus increases with depth, but is not patent there, and would have to be demonstrated mathematically]. Effective normal stresses on horizontal and vertical planes in the soil are assumed to increase linearly with depth, so that the important ratio of shearing stress to normal effective stress on the vertical surfaces on which distortion is taking place is greatest at ground surface. It is important to note that, in this model, it is the effective normal stress on the vertical plane which is important. Thus the pile behavior is affected by both the in-place stress state -- as characterized by the ratio of lateral to vertical effective stresses -- and the change in the effective lateral stresses caused by the method of driving or inserting the pile. In the analysis here the effective stress on the horizontal plane caused by the buoyant unit weight of the soil is employed to save on the assumptions.

At the appropriate number of cycles for the stress ratio at ground surface, as determined by Lee's results (5), the soil liquefies. It is then assumed that in the liquefied zone, the subgrade reaction coefficient drops to 1/16 of its value in the unliquefied underlying soil. [The value of 1/16 is chosen because in the subsequent mathematics, the subgrade coefficient appears in the form

of its fourth root, and it makes things numerically simpler to choose the ratio as $1/2^4$]. Any other value could be chosen, preferably based on tests, such as Lee (5) performs on the residual resistance of the soil at large strains following liquefaction. A variation in the analysis is made by assuming the liquefied soil resistance drops to zero. This is applied later to the model pile tests in the Santa Barbara silt, since the assumption simplifies the analysis considerably.

The pile at this and subsequent stages is imbedded in a layer of weak soil overlying a stronger material. Cyclic displacements and shearing stresses at the surface of the stronger layer are calculated. Since the Lee-Seed liquefaction model uses the initial effective stress as the reference state, the stress ratio of the stronger material is obtained by dividing the calculated pile-generated shearing stress by the in-place vertical effective stress. After the relevant number of cycles, the surface of the stronger layer liquefies, and the liquefaction zone moves down.

In actuality the process takes place continuously, with a steadily-growing zone of liquefied soil. However, it is found in this analysis that the process is convergent as a result both of the diminishing lateral load and moment in the pile and of the increasing vertical effective stress with depth. In consequence, the result of the analysis is the prediction of depth of liquefaction, given the number of cycles of loading, and, of course, the soil and pile properties. For the required number of cycles, the known depth of liquefaction, together with the resistance properties of the liquefied and unliquefied

material, enables the pile top load-deflection relation to be calculated. The deterioration in this spring constant with number of cycles can be tracked. From a design point of view, the ultimate spring constant can be established for the design storm or earthquake loading. The details of the analysis follow:

Considering the pile first as a circular (or other shape) rigid inclusion of radius a in an elastic plane [Fig. 6.1(a)], a solution was sought in the technical literature. The problem has not been solved, and there are, in fact, mathematical difficulties in obtaining it. However, the results of a photo-elastic analysis of a loaded pin in a flat plate are reported by Coker and Filon (2). From their values, it appears that the peak shearing stress at the pin-plate interface was approximately equal to half the average stress applied by the pin (pin load divided by hole diameter times plate thickness). Unfortunately, they do not report the displacements of the pin, a value which is convenient for subsequent developments. Consequently (another approximation) the problem was compared to that of the expansion under pressure p of a cylindrical cavity in an elastic medium of modulus E, Poisson's ratio ν in plane strain [Fig. 6.1(b)]. Here, the radial displacement of the cavity wall u is given by the equation

$$u = \frac{pa(1+\nu)}{E} \tag{6.1}$$

We equate the pressure p to the average pressure produced by the load on the pin and, from the previous conclusion about the shearing stress $\tau(a)$ at the pin-plate interface, obtain the result

$$\tau(a) = \frac{P}{2} = \frac{Eu}{2(1+\nu)a} = \frac{Gu}{a} \qquad (6.2)$$

However, in the expanding cavity problem, the stresses diminish with the square of radial distance, and it would not be fair to take into account only the highest shearing stress at the pile-soil interface. Assuming the same variation in the pin problem, therefore, at a distance of one radius away from the pile surface (one diameter from pile center) the shearing stress would be only $\frac{1}{4}$ of the above value in equation (6.2), but this is probably too low. Consequently in subsequent developments, a value of τ will be used equal to <u>half</u> that of equation (6.2). Thus

$$\tau = \frac{Gu}{2a} \qquad (6.3)$$

To evaluate this expression requires calculation of the lateral displacement of the pile; we obtain this from the Winkler model of beam-soil interaction. In general, the situation to be considered is that shown in Figure 6.2, in which a lateral load P (maximum value of cyclic load, to generate maximum value of τ as used in liquefaction tests) at some stage has developed a liquefied zone of soil surrounding the pile to a distance of some fraction of a radius, (for normal lateral deflections of the order of an inch), and to a depth s. (A combination of load and moment can be introduced at the top of the pile, but this is also left out for simplicity). Below this depth s, the undisturbed soil properties prevail. This is an unrealistic assumption since there would be a transition zone, in practice, between fully liquefied and originally solid material. However, the

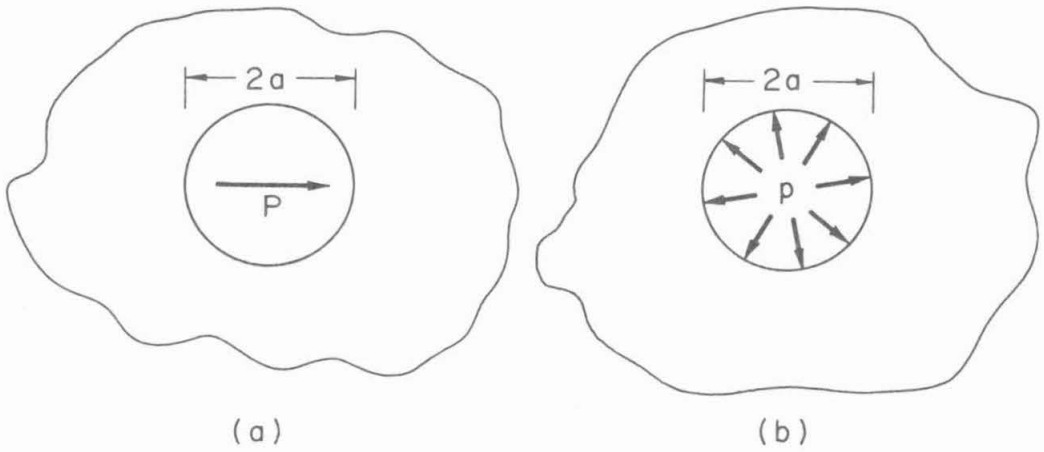

Fig. 6.1. Horizontal section through pile and soil as model for analysis: (a) idealized; (b) approximation

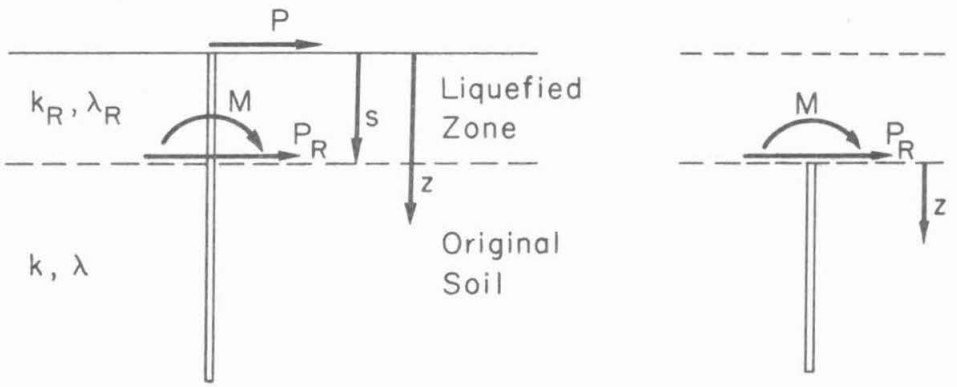

Fig. 6.2. Vertical section through pile and soil as model for analysis including presence of liquefied zone

latter represents a modification which can be made later. In the original soil the subgrade reaction coefficient is k, which together with the pile properties, gives the reciprocal of the characteristic length of the system

$$\lambda = \sqrt[4]{\frac{k}{4EI}} \tag{6.4}$$

Above, in the liquefied zone, the properties in the first model are k_R, λ_R (R-Reduced) where, as mentioned before, in this analysis we will take

$$k_R = k/16 \quad \text{and thus, by (6.4)} \quad \lambda_R = \lambda/2 \tag{6.5}$$

As a result of the presence of the liquefied zone, the load P generates a reduced shearing force P_R and a moment M at the level s. From the Winkler analysis (4), these forces have the values

$$P_R = Pe^{-\lambda_R s}(\cos\lambda_R s - \sin\lambda_R s) \tag{6.6}$$

and

$$M = \frac{P}{\lambda_R} e^{-\lambda_R s} \sin\lambda_R s \tag{6.7}$$

However, in the general case we wish to know the displacement at and below the surface s (so that we can calculate the shearing stresses there and follow the development of liquefaction). In this case, we will consider the pile as if itwere imbedded in the original soil below level s, and subjected to a force P_R and moment M at the

interface s. This is an approximation, but it avoids more algebraic complexity than the analysis justifies, and probably gives results good enough for our present purpose. Once again, if it proves worthwhile, the approximation can be removed later.

For $z > s$, the Winkler analysis (4) gives

$$u(z) = \frac{2P_R\lambda}{k} e^{-\lambda(z-s)}\cos\lambda(z-s) + \frac{2M\lambda^2}{k} e^{-\lambda(z-s)}\left[\cos\lambda(z-s) - \sin\lambda(z-s)\right] \tag{6.8}$$

After substituting for the loads from equations (6.6) and (6.7), this becomes

$$u(z) = \frac{2\lambda P}{k} \overbrace{e^{-(\lambda z-\lambda s)-\lambda_R s}\cos(\lambda z-\lambda s)\sin\lambda_R s\left\{\cot\lambda_R s - 1 + \frac{\lambda}{\lambda_R}\left[1 - \tan(\lambda z-\lambda s)\right]\right\}}^{A} \tag{6.9}$$

We will call the last part of this equation A, as shown, where

$$A = f(\lambda_R s, \lambda s, \lambda z) \tag{6.10}$$

Substituting equation (6.9) in equation (6.3) gives

$$\tau = \frac{G\lambda P}{ak} A \tag{6.11}$$

At this stage, we need to make another approximation. The subgrade reaction coefficient k is related to the elastic properties of the soil. A good deal of work has gone into obtaining expressions for k, and these usually involve both pile (beam) and soil properties. However, studies of some laterally loaded piles by the author (unpublished)

show that for a flexible pile (usual case) a simple expression gives useful values of deflection, moment, etc. For a pile, the k used in the above equations is the product of the basic subgrade reaction coefficient k_0 and the pile diameter 2a. The studies referred to above indicate that, approximately

$$k_0 = \frac{E}{2a} = \frac{2(1+\nu)G}{2a} = \frac{3G}{2a} \qquad (6.12)$$

where E is the Young's modulus, G is the shearing modulus of the soil, which is taken to be incompressible (undrained). Thus

$$k = k_0 2a = 3G \qquad (6.13)$$

which is substituted in equation (6.11) to give

$$\tau = \frac{P\lambda}{3a} A \qquad (6.14)$$

However, the parameter of interest in liquefaction studies is τ/σ_{vc}, where σ_{vc} is the effective stress in the soil at the level of interest. Assuming, as described previously, that this is just the vertical effective stress in the present problem, gives

$$\sigma_{vc} = \gamma' z \qquad (6.15)$$

where γ' is the buoyant unit weight of the soil. Dividing equation (6.14) by (6.15) has the final result

$$\frac{\tau}{\sigma_{vc}} = \frac{P\lambda}{3a\gamma'} \frac{A}{z} = \frac{P\lambda^2}{3a\gamma'} B \qquad (6.16)$$

where

$$B = \frac{A}{\lambda z} = g(\lambda s, \lambda z, \lambda_R s) \tag{6.17}$$

for convenience in keeping all the variables in one function. Equation (6.16) is now the operating or control equation for this problem.

It can be used to calculate the stress ratio at and below the interface s as a function of z, for any desired load P. However, it is apparent that the worst stress conditions for liquefaction always occur at the interface, that is, where $\lambda s = \lambda z$. Consequently, if the stress ratio is obtained for a selected value of number of loading cycles, this stress ratio will dictate through equation (6.16) the value of s (= z) to which liquefaction will progress in the stated number of cycles. Thus, although the full form of equation (6.9) has been obtained, since it may be of use for some future calculations, we need only concern ourselves, in this simple analysis, with the special form of the variable B in equations (6.9) and (6.16) in which $\lambda z = \lambda s$. This can be obtained as

$$B = \frac{e^{-\lambda_R s} \sin \lambda_R s}{\lambda s} \left[\cos \lambda_R s + \frac{\lambda}{\lambda_R} - 1 \right] \tag{6.18}$$

Equation (6.16) with equation (6.18) for B is used in the following way: The pile properties and diameter are known or assumed, and the soil properties are estimated from soil tests, previous pile behavior, or judgment. With these values, the parameters λ and λ_R are obtained for a particular trial computation. Next the design pile load is chosen from the design wave or earthquake motions. From the

same motions, the number of cycles of application of this load is also estimated. Reference is then made to a simple shear cyclic liquefaction test on the site soil at an appropriate range of σ_{vc} (usually at small values, since we are dealing with near-surface conditions), and the value of τ/σ_{vc} picked off the τ/σ_{vc} versus number of cycles to liquefaction curve at the appropriate number of cycles. Then equation (6.16) with B from equation (6.18) is solved for the value of λs, or s for that τ/σ_{vc} value. The equation is transcendental and has to be solved for λs or s by trial and error. A plot can be made of τ/σ_{vc} or number of cycles versus depth s, and this shows the progress of liquefaction with depth around the pile. Finally, the changing deflection or spring constant at ground surface can be tracked through the Winkler equations, as a function of number of cycles, or liquefaction depth.

This last stage will not be treated further here; it is not a difficult extension of the results. It should be noted that this analysis does <u>not</u> predict the pile lateral <u>drift</u> under cyclic load indicated by the experiments.

A numerical example will illustrate the first method. In the load versus deflection curve of the Mustang Island tests, (Figure 5.2) it is seen that a load of about 30 kips produced a lateral deflection of about 0.5 inches. These values, with EI of the Mustang Island pile equal to 6×10^{10} lb-in^2, can be used with the Winkler pile-soil model, using an assumed subgrade reaction coefficient uniform with depth (not, of course, correct) to calculate a value of 8×10^{-3}

inches^{-1} for λ for this case. The pile diameter is 24 inches and the buoyant unit weight of the soil, γ', is assumed to be 60 pcf. Putting these values into equation (6.16) gives

$$\frac{\tau}{\sigma_{vc}} = 1.54B \qquad (6.19)$$

With B given by equation (6.17), equation (6.19) is solved first for the case s equals zero, and various values of z, since loading begins on the pile in the initially undisturbed soil. The curve of τ/σ_{vc} versus depth resulting is shown in Figure 6.3, which indicates very high stress ratio values, as would be expected with this model, at shallow depths.

These values may be compared with Figure 6.4, which is reproduced from Lee's report on the cyclic simple shear behavior of Santa Barbara silt, and is assumed to represent a typical soil response of this kind at low values of σ_{vc}. It is seen from Figure 6.4 that a stress ratio of 0.5 would cause liquefaction in <u>one</u> cycle. Down to a depth of $\lambda z = 0.85$ ($z \approx 106$ inches) the calculated stress ratios are all higher than this, and it is therefore assumed that the soil would liquefy to this depth approximately during or on the first cycle. However, the consequence of this liquefaction is to increase the shear stress and stress ratio at greater depths, so that liquefaction propagates further in the next one or two cycles.

Consequently, equation (6.16) employing the short form for B from equation (6.18) comes into play. It can be solved for the value of s (or λs) corresponding to various stress ratios, or,

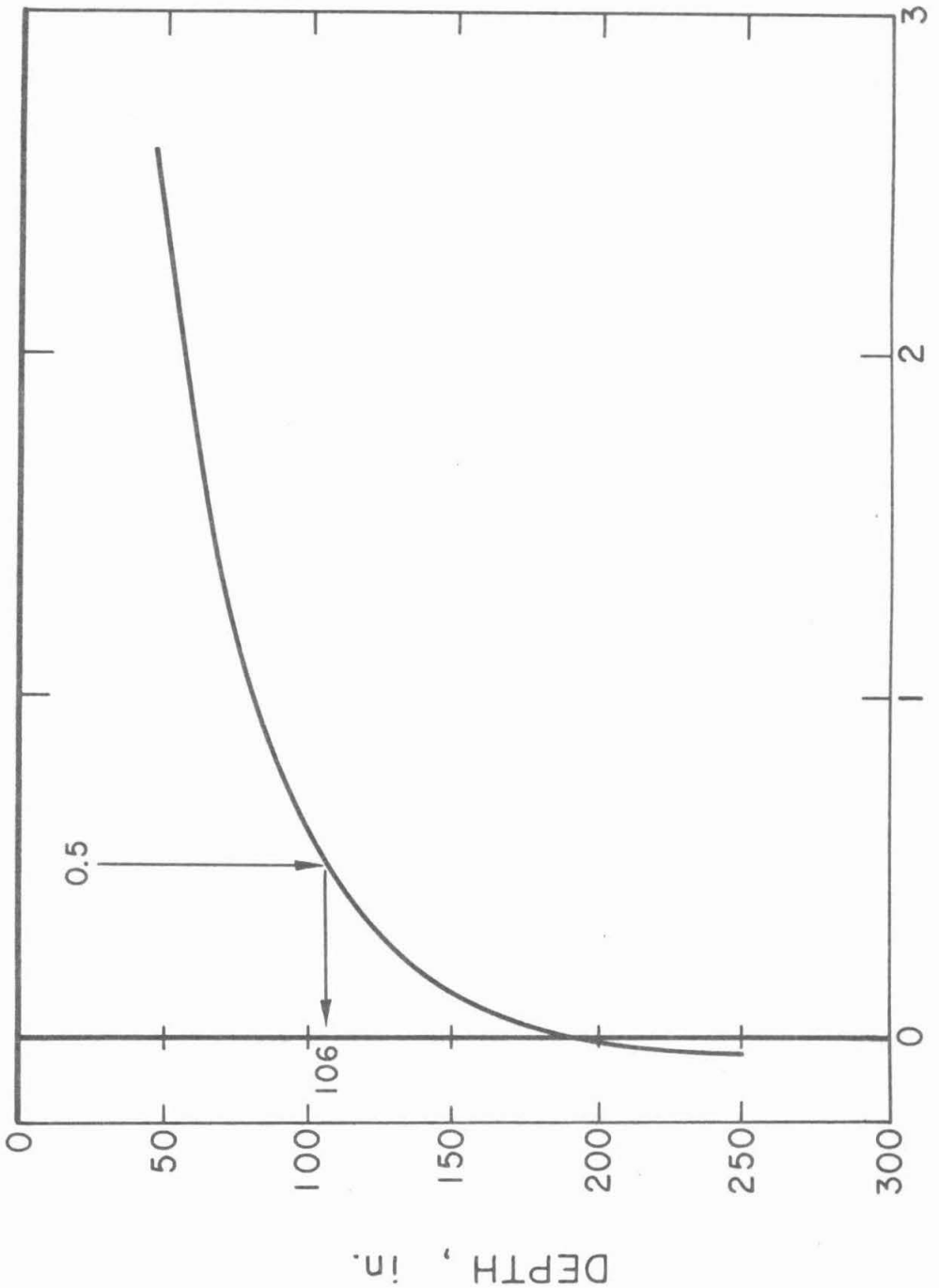

Fig. 6.3. Variation of stress ratio versus depth as obtained from analysis

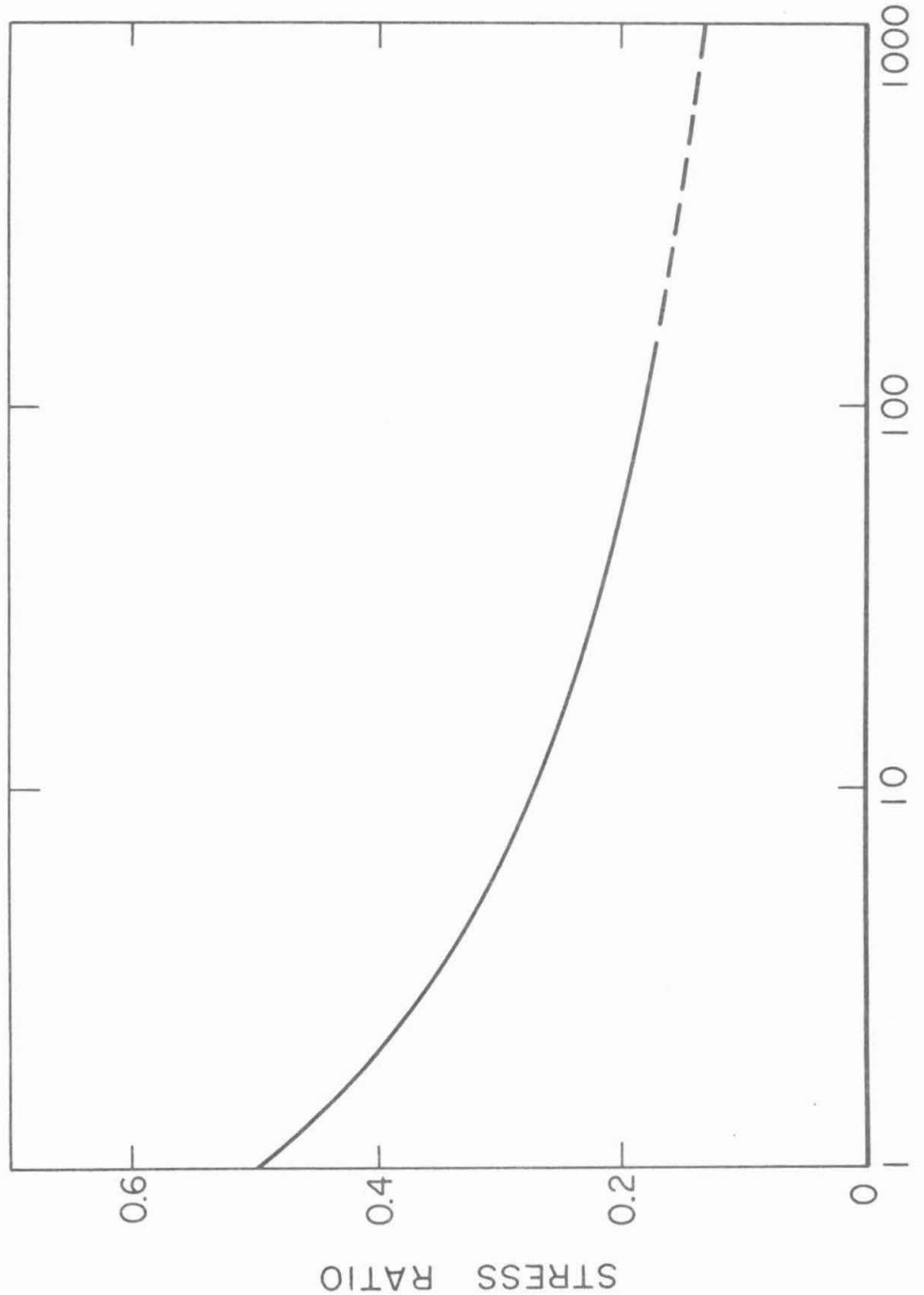

Fig. 6.4. Stress ratio versus number of cycles to failure for Santa Barbara silt (from reference 5)

alternatively and move conveniently, the stress ratios can be calculated for different values of s (λs). This has been done and the result is plotted in Figure 6.5. Figure 6.5 answers the question: after liquefaction has commenced, how far must it progress down the pile before the stress ratio at the pile-soil interface is 0.5, 0.4, etc? By reference to Figure 6.4, each level of liquefaction can be associated with a number of cycles of the applied load, as shown in Figure 6.6. Since liquefaction begins at the surface during the very first cycle, the associated cycle numbers in Figure 6.6 are labeled 1+, 2+, etc., meaning liquefaction progresses to the noted depth in somewhat more than 1, 2, etc., cycles. The liquefaction depth is apparently approaching a limiting value at 1,000 cycles in Figure 6.6.

In Figures 6.5 and 6.6 dashed curves have been drawn showing the equivalent behavior for a 10 kip cyclic load on the same pile-soil system. The actual values for liquefaction depth indicated on these figures should not be taken too seriously because of the number of arbitrary assumptions made in the model. It would be interesting to repeat the calculations, for example with a soil subgrade reaction coefficient increasing linearly with depth.

An alternative and simpler analysis, which can also easily give the increasing pile top displacements as liquefaction progresses down the pile, is to assume that the soil has a specified lateral resistance in the liquefied zone, but still follows the Winkler model below it. The specified soil resistance may be obtained from the residual shearing strength of the soil , or may derive from the strength exhibited at the end of a cyclic liquefaction test. In either case the strength is

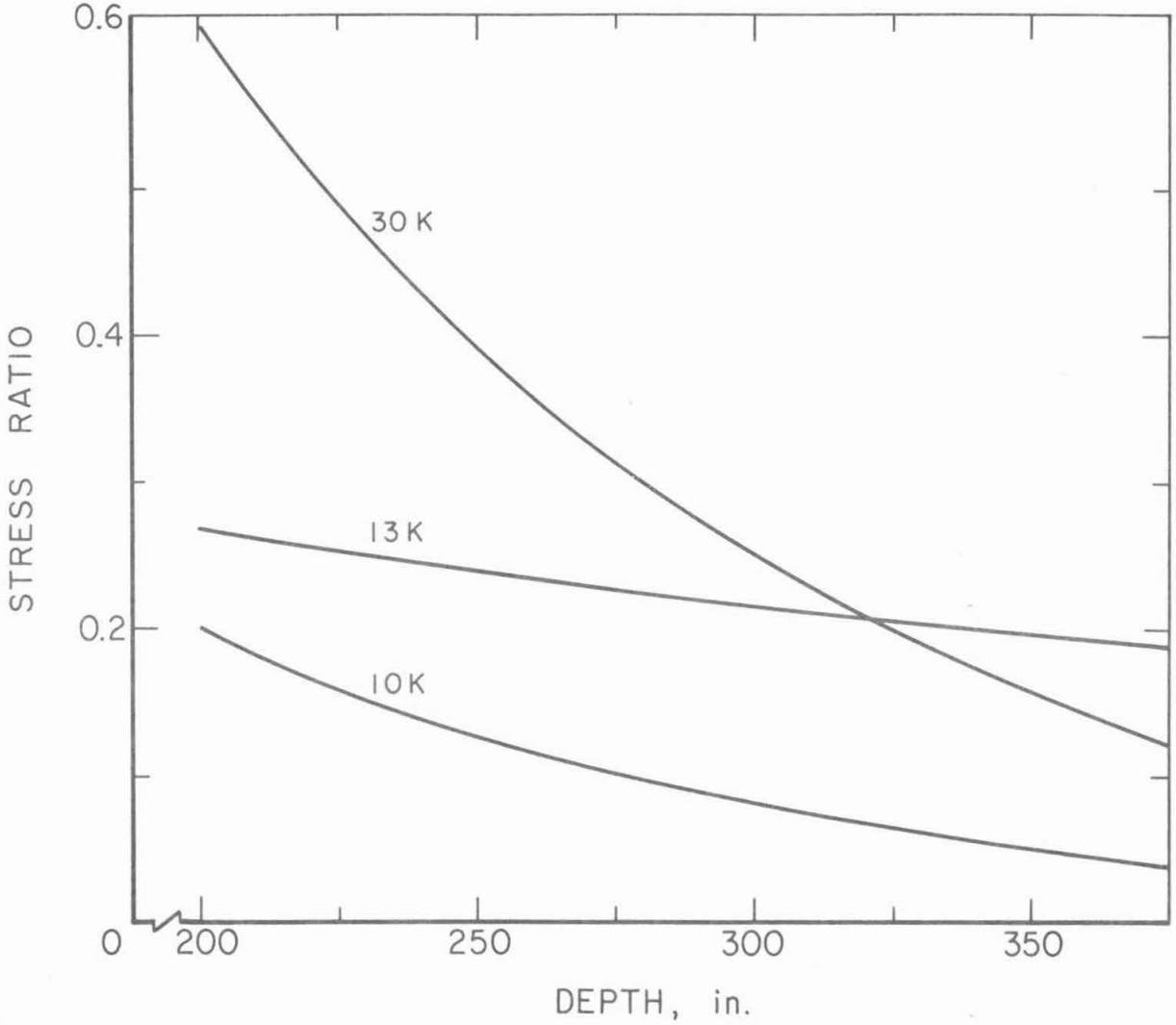

Fig. 6.5. Variation of stress ratio with depth for two soil models:
(a) Mustang Island conditions, 10K and 30K load;
(b) Santa Barbara silt test conditions, 13K load

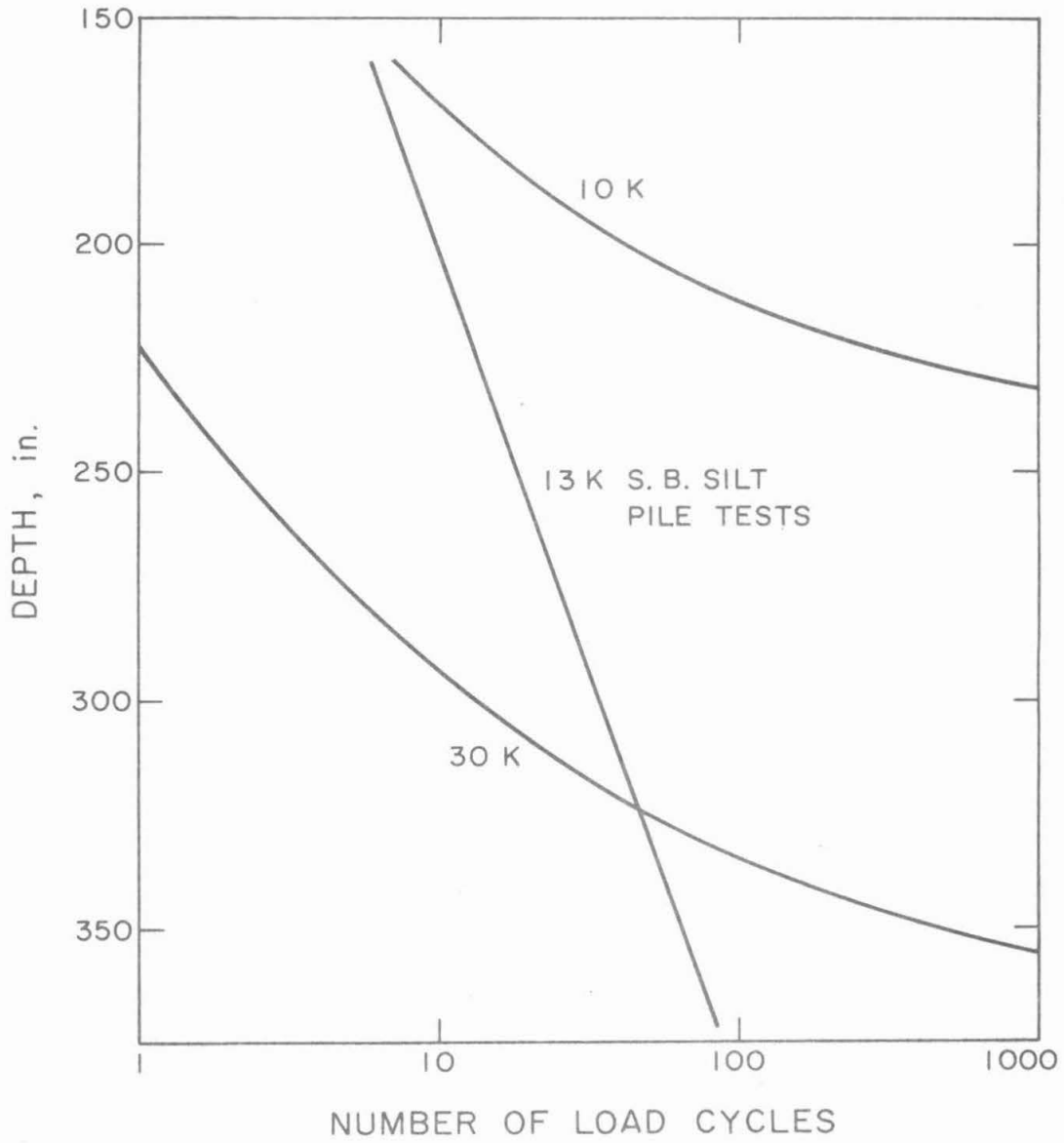

Fig. 6.6. Number of cycles required to develop liquefaction to indicated depth for (a) Mustang Island case, 10K and 30K loads, and (b) Santa Barbara silt test properties, 13 Kip load

multiplied by some factor involving the geometry of the pile in lateral soil yielding. It may be constant with depth, or more probably it increases more-or-less linearly reflecting the pre-cyclic consolidation state.

The simplest condition to use for a speedy analysis is that of zero soil strength in the liquefied zone. All the equations are considerably simplified in this case.

At the interface between liquefied and solid soil, depth s, the pile is subjected to horizontal load P and moment load Ps. The displacement u(s) at this level is given by Winkler theory to be

$$u(s) = \frac{2P\lambda}{k}(1+\lambda s) \qquad (6.20)$$

With the same considerations as before, the interface stress ratio can be calculated from this equation to be

$$\frac{\tau}{\sigma_{vc}} = \frac{P\lambda^2}{3a\gamma'}\frac{(1+\lambda s)}{\lambda s} \qquad (6.21)$$

and this can be compared with the stress ratio required to cause liquefaction in a certain number of cycles. This equation can be solved for s, if desired. In addition, the deflection at the pile top can now be readily calculated. This deflection is the sum of the deflection u(s), the deflection gradient at s, times the distance s, $(du/dz)_s$, and the deflection of the cantilever beam, length s, under the load P.

The deflection due to the slope is given by the equation

$$s\left(\frac{du}{dz}\right)_s = \frac{2P\lambda}{k}(1 + 2\lambda s)\lambda s \qquad (6.22)$$

and from the cantilever beam

$$u_P = \frac{Ps^3}{3EI} \qquad (6.23)$$

Thus

$$u(0) = u(s) + \left(\frac{du}{dz}\right)_s s + u_P \qquad (6.24)$$

For an example, we will take as a basis the results of the model pile test in Santa Barbara silt, réported above. In that test, in the first positive half-cycle, a lateral load of 13 kips produced a deflection of 3.5 inches. Representing this behavior by a Winkler model of uniform spring constant gives a value of 3.14×10^{-3} inch^{-1} for λ. Substituting this value for λ in equation (6.21) gives the 13 kip curve shown on Figure 6.5. Comparison with the Santa Barbara silt liquefaction behavior produces the 13 kip line on Figure 6.6. It is seen that liquefaction progresses much faster with depth with this model, due to the lack of load attenuation in the liquefied zone. Equations (6.22) through (6.24) can be employed to give pile top deflection at different numbers of cycles equivalent to differing depths of the liquefaction zone, and the results are shown on Figure 5.10 for this liquefaction model. The zero deflection line is taken as a base for these deflection values, so they are not strictly comparable with the experimental point. In addition, the deflections obtained are too large, indicating that the assumption of zero strength is too

conservative. Figure 5.10 could be used in a trial-and-error process to obtain for the shearing strength of the soil a value which would give deflections closer to those observed. However, the trend of deflection expressed by the analysis compares favorably with that of the experimental data.

The analysis represents a first attempt at a liquefaction determination for a single, laterally-loaded pile. As such, in line with usual empirical liquefaction procedures, it contains a number of coefficients which could be adjusted to suit particular centrifugal test results or field observations.

7. Conclusion

Although the tests and analyses carried out and reported herein are far from satisfactory, they represent the initial stages of static and cyclic loading of piles in a small centrifuge and have yielded results which possess some features of interest. A number of deficiencies were observed in both the apparatus and recording system used to determine the behavior of the pile during tests. It proved difficult to perform the tests at 100 g, which is apparently a distressing environment for electrical motors, wiring, actuating systems, and instrumentation. As a result of these tests, a number of improvements has been effected in the equipment and tests are being continued in the hope of obtaining considerably better results than are reported here. Most of the major features expected to be associated with laterally loaded pile response in sands and

saturated silts have been indicated from the tests. In particular the strain and displacement softening evidenced by the Santa Barbara silt during repeated cycles of load at large displacements appears to be of interest. It will be useful to carry out such tests at the different load levels and possibly with unsymmetric loading configurations to much higher numbers of cycles in order to simulate the loading conditions which may be experienced by a platform during storm conditions at sea. Although the tests to date have included only static cyclic effects, apparently pore pressure and remolding phenomena in the soil have played a part.

It is intended to subject such piles to dynamic vibratory loads at frequency ranges of interest in the earthquake excitation of offshore structures. Similarities and differences in the performance of the piles in these dynamic loading situations as compared with the static cyclic behavior reported here will be of interest. There seems to be some possibility that design parameters of use for the prototype can be obtained from such tests.

A preliminary analysis of progressive liquefaction around a cyclically laterally loaded pile has produced results bearing some similarity to those observed with the model pile. Further analysis efforts appear warranted.

In the case of a pile imbedded in soil below the water table, where the water level is above the soil surface, it is not certain that the process of cyclic liquefaction as currently described is the appropriate one to invoke in analysis. As described earlier in this report, the lateral movement of the pile alternately opens cavities

in both front and back of the pile, and these constitute channels through which the water is pumped. The water mixes with and softens the adjacent soil. Consequently, a combination of liquefaction at greater depths and mixing near the surface may develop.

8. References

1. Bucky, P. B., "Use of Models for the Study of Mining Problems," AIMME Tech. Pub. No. 425, 1931.

2. Coker, E. G., and L.N.G. Filon, "Photoelasticity," Cambridge Univ. Press, 1931.

3. Cox, W. R., Reese, L. C., and B. R. Grubbs, "Field Testing of Laterally Loaded Piles in Sand," Proc. 6th Annual Offshore Technology Conf., Paper No. OTC 2079, Houston, Texas, May 1974.

4. Hetenyi, M., "Beams on Elastic Foundation," Univ. of Michigan Press, Ann Arbor, 1946.

5. Lee, K. L., "Characterization of Soil Behavior Under Cyclic Loading as Applied to the Foundation Design of Offshore Structures," UCLA-ENG-7735, Final Report to API, March 1977.

6. Polshin, D. E., Rudnitski, N. Y., Chizhikov, P. G., and T. G. Yakovleva, "Centrifugal Model Testing of Foundation Soils of Building Structures," Proc. 8th Int. Conf. Soil Mech. and Found. Eng. 1.3, 203-208, Moscow, 1973.

7. Reese, L. C., Cox, W. R., and F. D. Koop, "Analysis of Laterally Loaded Piles in Sand," Proc. 6th Annual Offshore Technology Conf., Paper No. OTC 2080, Houston, Texas, May 1974.

8. Scott, R. F., Liu, H.-P., and J. Ting, "Dynamic Pile Tests by Centrifuge Modelling," Proc. 6th World Conference on Earthquake Engineering, Paper 4-50, New Delhi, January 1977.

9. Seed, H. B., and K. L. Lee, "Liquefaction of Saturated Sands during Cyclic Loading Conditions," Proc. ASCE, 92, Jour. Soil Mech. and Found. Div., SM6, 105-134, November 1966.

9. Acknowledgments

The tests and instrumentation were setup and operated by John Lee, research engineer at California Institute of Technology. Mr. Lee also digitized the records and prepared the computer plots presented with this report. The author would like to acknowledge with appreciation the attention and interest paid to this research project by the API OSAPR advisory committee, particularly J. D. Murff, J. H. Sybert, R. S. Crog, J. A. Klotz, and J. C. Pearce.

APPENDIX A

HISTORY OF STRESS AND STRAIN IN CENTRIFUGE MODEL AND PROTOTYPE

The objective of centrifuge testing in regard to structures that are to be built on or to be composed of soils is to test the same soil in the model as that which is to be used in the prototype, at the same stress and strain conditions throughout. In practice, there are a number of difficulties in producing the same soil in the centrifuge as in the full-scale configuration. If, as is usually the case, the prototype soil is in its natural state and the structure is to be built on or in it, the soil will possess inhomogeneity and anisotropy to a varying and probably unknown degree. No naturally deposited materials are ideally homogeneous. The natural materials may, in addition, be fissured or cracked. Because the model scale is in the order of one-hundredth of the prototype, it will generally be impossible to obtain a field sample of the prototype soil with dimensions of a meter or so which accurately reproduces the layering and stratification existing in the equivalent full-scale hundreds of meters. Thus, the fabric or structure of the prototype in the large cannot be represented. Cracks and fissures represent the middle scale of fabric and may or may not be represented in the model soil sample, depending on the dimensions of the fissure intervals. Presumably, with carefully taken samples, the microstructure of prototype soil will be maintained in the model.

The fidelity of model tests will depend in some part on the homogeneity of the prototype soil; the less homogeneous, the less likely it is that the model results will follow those of the prototype. In addition, the nature of the test to be performed plays a part. The presence of cracks and fissures in the prototype, unreproduced in the model, will strongly affect correlation of failure tests, such as failures of embankments or cuts. They will probably be less important in cases where deformation of the soil under generally increasing compressive stress loading paths is concerned. In either case, little can be done if fissures or marked inhomogeneity is present in the prototype. The question of identity of model and prototype stress- and strain-paths remains.

Since the behavior of soils is nonlinear and hysteretic and is therefore stress- and strain-path dependent, it follows that correspondence between model and prototype results will only be achieved, in general, if the stress-paths of all elements of the model reasonably closely duplicate those of the homologous elements in the prototype. To see if this is even possible, it is useful to examine the history of stress on a soil element in a few cases of practical interest. A convenient way of doing this is to employ the principal stress space diagram of Figure A-1. Here, the axes are the principal stresses applied to a soil element. A point in the space represents the stress state at a point in soil. It is important to understand that, since soil is saturated with water in many cases of practical interest, two stress systems in soil have to be distinguished: total stresses and effective stresses. Since the water component can take only

hydrostatic, not shearing, stresses, total and effective shearing stresses are identical. However, total and effective normal stresses, σ, differ by the pressure in the pore water, p, thus

$$\sigma_{Total} = \sigma_{effective} + p$$

The importance of this is that the soil responds to the effective stress system only. That is to say, two samples of the same soil at different total stresses will behave identically if their pore pressures are also different such that the effective stresses are the same in the two samples. Their strains will be identical under identical changes in effective stress, and in particular, they will yield or fail at identical effective stress states. For example, if the total stress and pore pressure are both increased or decreased on a soil sample, so that the effective stresses are unchanged, no deformations will be experienced by the sample. In Figure A-1, therefore, the axes may represent either principal total or effective stresses depending on how the stress paths are specified. In the diagram, there is an axis which makes equal angles to all three principal axes; it is the hydrostatic axis. All hydrostatic stress components, in particular pore pressure, in the figure are parallel to this axis. If a point A exists in the figure representing a total stress on a soil element, which is also subject to a pore pressure p, then the effective stress on the element is given by point B separated from A by the line AB parallel to the hydrostatic axis and of length $\sqrt{3}$ p (the $\sqrt{3}$ comes from the geometry of the figure). A line CD connecting two points in principal stress space represents a stress path (total or effective) which shows how a soil element has been loaded.

Since many soil tests are performed on axially symmetrical cylindrical test samples, and soil in the ground below a level surface is in an axially symmetrical stress state, it is convenient to specialize Figure A-1 to its axially symmetric plane, as shown in Figure A-2. In axially symmetric stress states, the stress state points lie on the plane, including the major principal stress σ_1-axis and, since the minor σ_3 and intermediate σ_2 principal stresses are equal, the line making a 45° angle to the σ_2- and σ_3-axes. It is necessary to point out that many, even the majority of, prototype loading situations cause plane strain stress states (the intermediate strain ϵ_2 is zero) which plot on surfaces in principal stress space other than the axially-symmetrical plane of Figure A-2. This will be ignored in the following discussion, for clarity in the representations.

It is necessary to bring out three other points in soil behavior before the figures can be used. The first is that, under certain combinations of effective stress, soil yields or fails (for this discussion, no distinction is made between the two), as a shearing stress reaches a maximum value equal to the strength of the soil. When the failure effective stress states are plotted on Figure A-2, they form two traces on the intersection with the plane of Figure A-2, of a failure surface or envelope surrounding the hydrostatic axis of Figure A-1. One of these lines describes failure in axial compression, the other in axial extension. A sample fails when the point representing its effective stress state reaches one of these lines. These failure lines diverge from the hydrostatic axis at increasing hydrostatic effective stress.

The second important aspect of nonlinear soil behavior is that its volume changes under not only hydrostatic effective stress changes, but also under shearing stress changes. Points representing equal hydrostatic effective stresses lie on planes or lines at right angles to the hydrostatic axis, the hydrostatic plane of Figure A-2. Were soil behavior linear, an effective stress path lying along the hydrostatic plane would cause no volume changes; therefore, for a linear material, hydrostatic planes represent constant volume contours. Soil behavior is not linear, soils generally (not always) decrease in volume as they are sheared, and in consequence, constant volume contours for soils appear as lines curved as shown in Figure A-2. The volume described by each contour decreases with increasing hydrostatic effective stress. Lastly, for saturated soils, the water component is essentially incompressible compared with the soil structure. Consequently, if water is not permitted to drain from the soil element during stressing, the soil specimen will deform at constant volume. In a test specimen in the laboratory, drainage is usually controlled by valves in drainage lines. In a model or prototype situation, however, the extent to which the soil drains depends on the rate of loading with respect to the permeability of the soil.

Coarse soils such as sands and gravels have high permeabilities, and pore pressures dissipate rapidly, usually essentially simultaneously with the application of load. On the other hand, clays are very impermeable, drain very slowly, and the pore pressures developed by surface or other loads require months or years to decay. In all cases, as the pore pressures go down to hydrostatic values, the soil elements decrease in volume, and thus time-related displacements of the soil region occur. Settlements of buildings constructed on clays may go on for many years. In summary, applied stresses cause changes in both effective stresses and pore pressures in excess over hydrostatic in a soil mass. In time, short or long, the excess pore pressures dissipate and the effective stresses undergo further changes. In a dry or partly saturated soil, the effective stresses develop immediately as the load is applied, and there are essentially no time-related displacements.

It is relevant to the centrifuge testing question to consider various stress paths, which, for simplicity, will be drawn on Figure A-3, the plane of axial symmetry. The soil considered will be a cohesive one. The first of these, for interest, is that undergone by a soil element after deposition on the floor of a lake or ocean, and subsequent lowering of the water or uplift of the soil until the water table is just at or close to ground surface. Soil is deposited on the lake or ocean floor very slowly, over thousands to millions of years, so that the total stresses on an element gradually buried to greater depths build up slowly, drainage takes place concurrently and the total and effective stresses are separated at all times only by the hydrostatic water pressure. In Figure A-3, the total stress path is O'A'B', while the corresponding points on the effective path are O, A, B, during deposition. When deposition stops and the water level is lowered, the total stress falls from B' to B", and the hydrostatic pore pressure is decreased (to $\sqrt{3}$ BB") but the effective stress remains unchanged at B.

Two cases of loading will be considered for a comparison of centrifuge model and prototype stress paths. In the first, (1) a circular concrete footing will be placed directly above the soil whose stress state is represented by B" and B, and loaded until failure occurs in the soil, whose behavior on the average will be represented by developments proceeding from point B. In the second, (2) an excavation will be made adjacent to the soil element represented by B and B" in Figure A-3, and will be made deep enough until the soil fails. The prototype situation is described first.

1. FOOTING

The load may be applied slowly (with respect to drainage or pore pressure dissipation) or rapidly. If it is applied slowly, the total and effective stress paths proceed parallel to one another from points B" and B, respectively; they are separated only by the pore pressure component. Both axial and lateral stresses will increase, so the stress paths proceed along lines B"C' and BC. Failure will occur when the effective stress state reaches the failure line at C, where the total stress state is at C'. For a load applied rapidly (by definition of "rapid", no drainage occurs), the total stress point proceeds along the line B"C' as before, but, since no volume change can occur in the element, the effective stress point moves along the constant volume contour through B to point D at failure. Since the total and effective stress states are separated only by a pore pressure, the total stress state at failure in this case is represented by point D' different from D by the line DD' drawn parallel to the hydrostatic axis. It is apparent that the load which the footing can take under this rapid loading condition is much less than it can sustain when stressed slowly. At failure, a large positive excess pore pressure ($\sqrt{3}$ DD') exists in the rapid load case.

For the centrifuge model test, it is assumed that a sample of the field soil will be obtained, placed in the centrifuge and brought up to the correct g-level to simulate the experiment scaling, and then the surface of the block loaded by a model circular footing. A problem immediately is evident. The stress condition at BB" in the prototype soil represents the stresses in an element of soil some distance below the natural ground surface. Nearer the surface, the in-place stresses are 1-1', 2-2' etc., and at greater depths they are 3-3' in Figure A-4. The real footing will cause stress changes to be initiated from all these points, but a sample block for the centrifuge can only involve essentially one depth in comparison with the prototype scale. The stress in the sample block will be taken for the illustration to be that at B-B". When the block is extracted, the total stresses become zero. Probably during excavation, the vertical total stress goes to zero first, then the lateral stresses, so that the total stress path followed might look like B"C'D'O' in Figure A-4. Assuming the sample to be obtained relatively rapidly, the effective stress path will be (at constant volume) BCDO. Depending on the details of the total stress path, the sample may even reach failure under low vertical and high lateral effective stresses. The axial compressive shearing stresses therefore decrease initially from B, then increase in axial extension

to D, and ultimately diminish again until the final effective stress state is hydrostatic at O, with the total stresses being zero at O'. Since the total stresses are smaller than the effective values, it follows that the pore pressure is tensile. That is to say, the soil sample would like to expand under the relief of stress, but cannot because of the restriction imposed by the almost incompressible pore water. If a high enough tension exists in the sample, the pore water may cavitate.

However, as soon as stress relief is initiated during sampling, the sample begins to expand as pore water pressures increase (from below atmospheric to atmospheric). Assuming that at least a few hours to a few days intervene between sampling and centrifuge, swelling will be complete for most soils by the time the centrifuge test is ready to be begun. The effective stress path in this time will be OO', and the effective stresses will be small before test initiation.

When centrifuging begins, the total stresses will not follow along the former path OO'A'B' in Figure A-3, since the hydrostatic water pressure increases during centrifugation along with the soil stresses. Instead, the total stresses move along the proportional path O'1'2'B" etc. in Figure A-4. In comparison with the permeability conditions of most fine-grained soils, centrifuge accelerations build up quite rapidly (in a few minutes) so that the soil block may be undrained during centrifugal loading. Partial drainage may occur in some soils. If no drainage takes place, the effective stress path will be along the constant volume contour through O in Figure A-4. (The contour curvature is different from that through B because of the unloading of the soil sample.) Once again, the failure surface may be approached at B_1, and this will have the effect of constraining the total load path (the lateral stresses will be forced to increase at a higher rate, since the effective stress point cannot go outside the failure surface). Although different elements of soil in the block at different depths will be subjected to different total stresses, it is convenient to consider the depth at which the total stresses get back to the field value of B". It is obvious that, were the load to be suddenly applied to the footing at this stage in the centrifugation process, before the soil had drained and consolidated under the centrifugal acceleration, failure would occur at a smaller (scaled) value of the load than in the prototype, since the effective stress starts close to the failure surface at B_1.

Obviously, the soil must first be allowed to equilibrate under the centrifugal acceleration. Then the effective stress path for this element ideally would be B_1B, and the soil's effective stress state would end up at B. If the soil element's behavior had been unchanged by its excursion BODOO'B_1B, the loading stress paths from here on would duplicate those of the prototype of Figure A-3. It is more likely, though, that the soil would have been somewhat disturbed and weakened by its adventures, and that the failure envelope for the disturbed material might now be somewhat closer to the hydrostatic axis than that of the natural material. Failure, drained or undrained, would therefore develop at lower stresses in this element.

On the other hand, the surface layers of the model block, having been obtained at some depth below the ground surface, will be considerably

stronger than the material at the same scaled depth in the prototype. This effect would be expected to outweigh the first, and overall, the centrifuge test would give a scaled bearing capacity higher than that which a prototype test would exhibit.

One way of avoiding the stress path discrepancies which the use of natural block samples involves is to obtain the soil from the site and to remold it with the addition of water to bring it to a fluid consistency. The medium is then placed in the centrifuge container and drained or consolidated by bringing the centrifuge up to the test acceleration level before the model structure is placed or built on the soil. While avoiding some difficulties, this approach generates others. The soil is the same as that to be loaded by the prototype structure, and the stresses and stress gradients are the same. However, any bonds or cementation which may have developed between the soil particles in the geological time during which the soil accumulated in nature will be destroyed by this process. Layers, fine or coarse, will also be eliminated as the sample is homogenized. Whether or not these aspects are important in comparison with stress path considerations will depend on the soil type and the test contemplated.

2. EXCAVATION

The prototype situation is described first. As in the first example, the excavation may be made slowly or rapidly with respect to pore pressure dissipation. Again, if the soil removal occurs slowly, the total and effective stress points move along stress paths from points B" and B, respectively in Figure A-3. However, in this case, the soil element represented by B"-B is being unloaded by the excavation on adjacent earth. The total and effective principal stress will decrease, as will also the lateral principal stresses. Failure develops in the soil element when the effective stress path reaches point E on the failure envelope, with total stress at point E'. It would be possible to remove soil only to form an excavation filled with water to the original water level at the ground surface, but it is assumed in this example that both soil and water are removed from the excavation to refer to a more practical application. In that case, the lines BE and B"E' will not be parallel to one another, but will converge, so that E' might be separated from E by only a small hydrostatic pore pressure when failure occurs.

When the excavation is made so rapidly that no drainage can occur, effective stresses in the element follow the no volume change path from B to failure at D again, at the same time as the total stress path duplicates the slow unloading path B"E'. However, since total and effective stresses are always separated by the hydrostatic component, the total stress path must go beyond E' to D" at the time failure occurs. At this stage, it is seen in Figure A-3 that the total stresses are smaller than the effective stresses, so the pore pressure is negative, that is, below atmospheric pressure. Since soil is much stiffer in unloading than loading, an unloading condition such as is generated by an excavation must proceed faster than a loading process to maintain the undrained condition. The total stress unloading path in the rapid

case is longer than that in the slow excavation situation and this means that a deeper excavation can be made before failure occurs if it is done quickly than if it is done slowly. In effect, the negative pore pressures impart increased strength to the soil (for the same total stress, negative pore pressures require greater effective stresses to balance the effective stress equation).

An interesting development arises in the rapid excavation case in practice. If material is dug out quickly until the total stress path reaches point E', the corresponding effective stress point will be at point E_1, so that a small tensile stress ($\sqrt{3}$ E'E_1) exists in the water. Now the excavation is stopped, and the soil begins to take up water (swelling, to diminish the negative water pressure). The effective stress diminishes as the negative pore pressure decreases algebraically, so that the effective stress point moves along the hydrostatic path E_1E'. Swelling and drainage will continue until the effective and total stresses are separated by the previous hydrostatic positive pressure (equivalent to $\sqrt{3}$ B"B for example). This will occur only when the effective stress arrives at point E, which is on the failure surface. When this happens, the soil element fails. Consequently, if the excavation proceeds rapidly to such a depth that total stresses move along the path B"E' to a point at or beyond E', but short of D" the excavation will be stable as completed, but will collapse at some time after construction. The time is set, in this model where the stresses in the element represented by points BB" are taken to be representative of those in the severely stressed region immediately adjacent to the excavation, by the dissipation of pore water following the end of excavation until the effective stress state, following a hydrostatic path, reaches the failure envelope.

For the centrifuge model test, two cases must be distinguished as follows. The block of soil has been obtained as before from the field site, and both total and effective stresses will be represented as being close to point O' in Figure A-4, as described previously for the footing case. However, it is assumed for the present that it would be very difficult to excavate the soil in the centrifuge model, after it had reached its design value of acceleration. If this is, in fact, possible, the argument will in large part, follow the previous discussion. In tests described in the literature, the excavation has been made at one g acceleration. It can be made as quickly as possible after centrifuging the sample block to the design acceleration, and then stopping the centrifuge. The centrifuge is brought up to speed again after the excavation is made to the full intended depth. Ideally, it may be assumed that the soil block drains and consolidates during the first acceleration so that the stress state at the appropriate point reaches the values described by points BB" in Figure A-4, and then deceleration and excavation proceed so rapidly that swelling cannot occur.

In this case, at the start of acceleration of the excavated block, the total stress is essentially at point O', effective stress is at O, and a large negative pore pressure exists in the soil. The centrifuge is assumed to be brought up to speed again rapidly so that no drainage occurs, and the effective stress path proceeds along the

constant volume line OB in Figure A-4 to failure at point G. It is not known what the total stress path is in this case, except that it seems fairly likely that all the principal stresses increase during centrifugation, with the major principal stress outstripping the others. The total stress path, then, might look like O'G'. At failure, a small negative pore pressure ($\sqrt{3}$ GG') is indicated. Whether or not failure occurs in the centrifuge model at the same excavation depth as in the prototype depends on how close the total stress points D" in Figure A-3 and G' in Figure A-4 are to each other. As shown in the figures here, the distance B"D" in Figure A-3 is greater than B"G' in Figure A-4, and this would imply that the prototype excavation could be taken to a greater depth than that in the scaled model. That is to say, the acceleration required to bring the total stress to point G' in Figure A-4 is less than that required for proper scaling of the excavation.

As a second condition in this problem, it may be assumed that the excavation is made in the soil block in its expanded one-g condition before any centrifuging. Both total and effective stresses lie at point O' in Figure A-4, and the centrifuge is brought up slowly enough to speed that drainage is complete at all stages of stressing. Assuming that the total stress path starts out along the line O'G' in Figure A-4, in this case, the pore pressures are likely to remain at small positive values, and the effective stress path is, say, O'H. Failure occurs at an effective stress represented by point H, and at a total stress given by H'. The degree of correspondence between the final total stress locations H' in Figure A-4 and E' in Figure A-3 represents the correlation between centrifuge model result and that of the prototype. As shown in these figures, again in the fully drained excavation case it appears that the model will predict failure at too-low values of acceleration. This result depends largely on the assumption of the centrifugal loading path O'H' in Figure A-4 which may not represent the correct path.

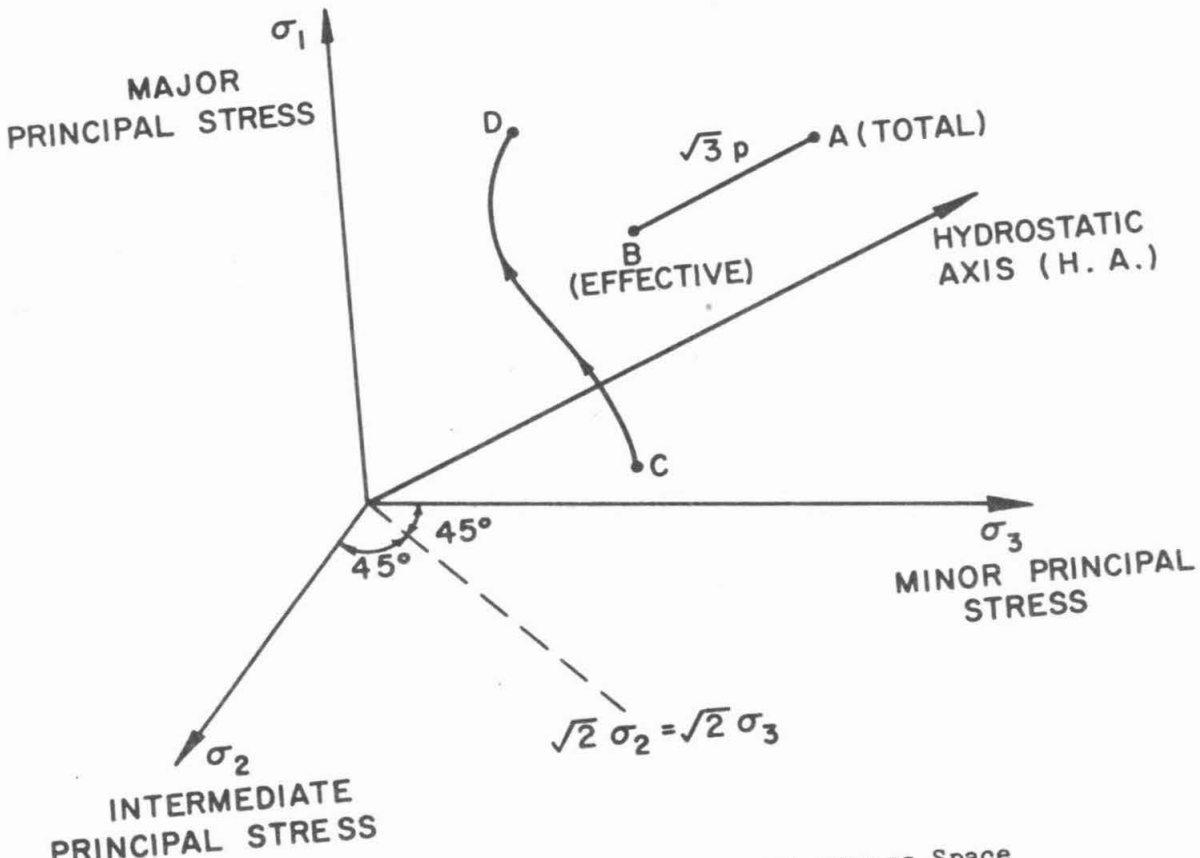

Figure A-1. Principal (Compressive) Stress Space

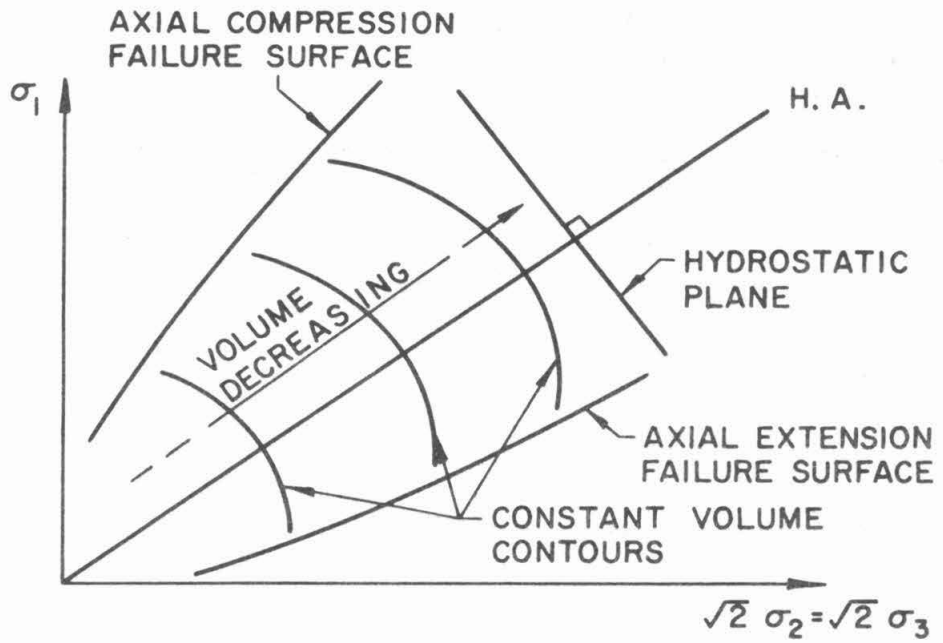

Figure A-2. Plane of Axial Symmetry in Principal Stress Space

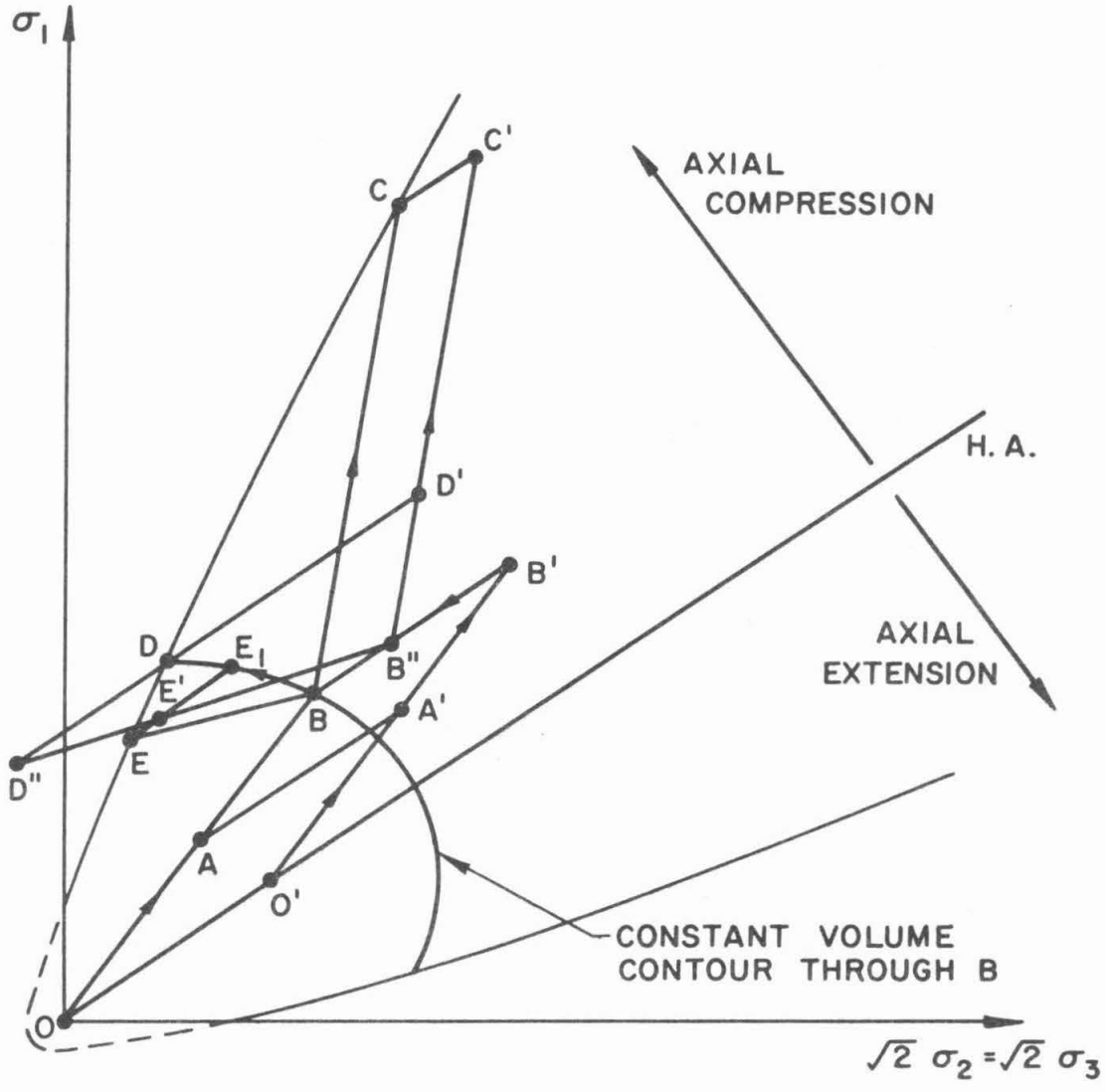

Figure A-3. Prototype Stress Paths

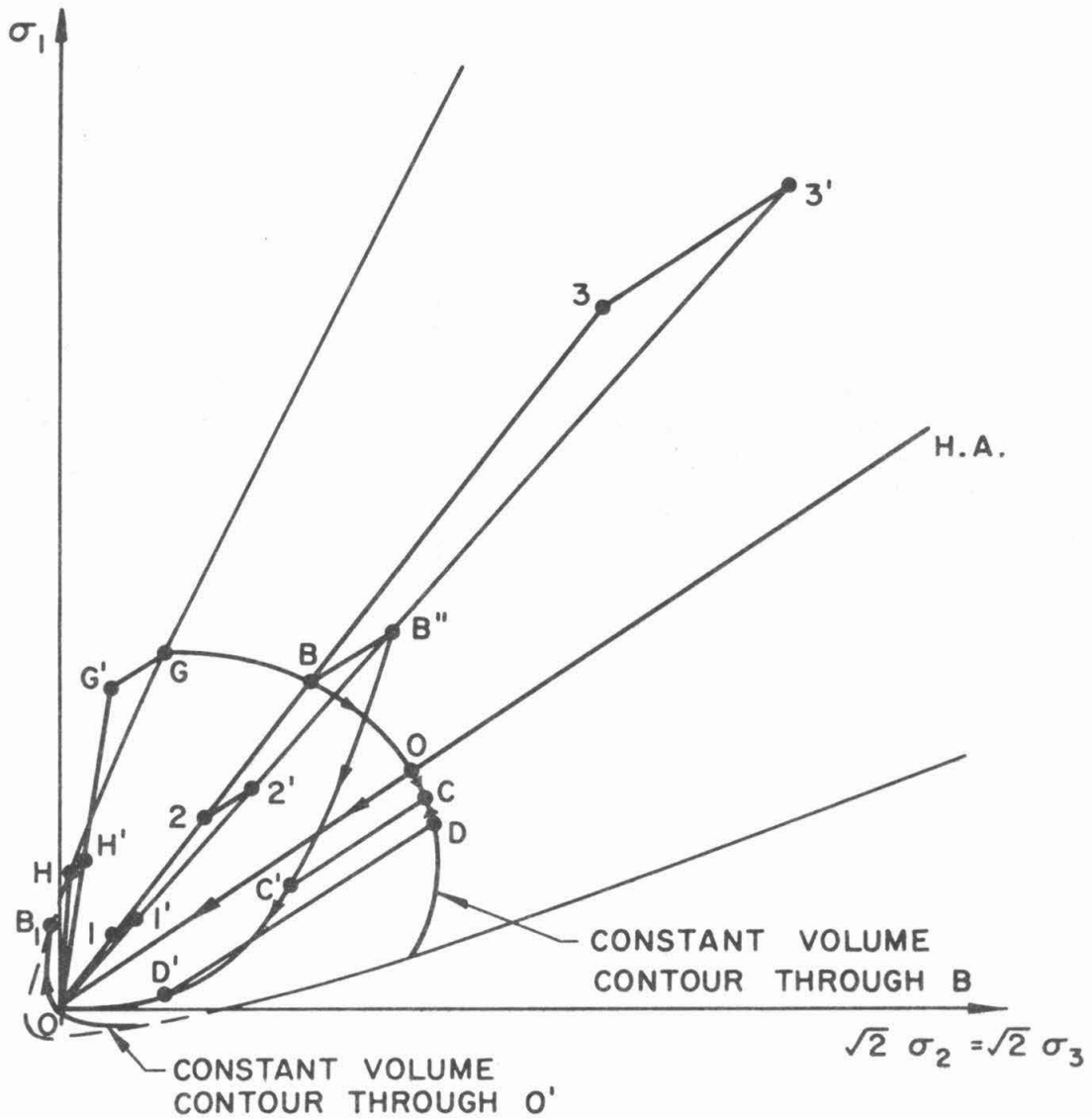

Figure A-4. Centrifuge Model Stress Paths